Copyright Warning & Restrictions

The copyright law of the United States (Title 17, United States Code) governs the making of photocopies or other reproductions of copyrighted material.

Under certain conditions specified in the law, libraries and archives are authorized to furnish a photocopy or other reproduction. One of these specified conditions is that the photocopy or reproduction is not to be "used for any purpose other than private study, scholarship, or research." If a, user makes a request for, or later uses, a photocopy or reproduction for purposes in excess of "fair use" that user may be liable for copyright infringement,

This institution reserves the right to refuse to accept a copying order if, in its judgment, fulfillment of the order would involve violation of copyright law.

Please Note: The author retains the copyright while the New Jersey Institute of Technology reserves the right to distribute this thesis or dissertation

Printing note: If you do not wish to print this page, then select "Pages from: first page # to: last page #" on the print dialog screen

ABSTRACT

NANOCARBON MODIFICATION OF MEMBRANES FOR ENHANCED WATER DESALINATION AND WATER TREATMENT

by
Worawit Intrchom

Water scarcity is foreseen to be one of the great global issues in the coming decades. The challenges are not only in providing water supply to cope with the growing public demand, but recovering clean water to natural resources. Clean water supply, from brackish and seawater is attractive. Membrane distillation (MD) is an emerging thermal membrane-based process that has been used for desalination and other pollutant separations from water. MD can be operated at low temperature, so low-grade energy sources are a good alternative heat source for MD. High salt rejection and low membrane fouling also make MD interesting for sea water desalination and wastewater treatment. In this dissertation, three major challenges related to water treatment are addressed. Approaches to enhance the MD performance by modifying the commercial membranes with different carbon-based nanomaterials are explored. These are the basis of this dissertation.

In the first application, graphene oxide (GO) is immobilized on the permeate side of a polytetrafluoroethylene (PTFE) membrane for desalination via direct contact membrane distillation (DCMD). The hydrophilicity of the permeate side of the membrane is enhanced by immobilizing the GO to facilitate fast condensation and withdrawal of the permeate water vapors. The graphene oxide immobilized membrane on the permeate side (GOIM-P) improves the performance of DCMD. The water vapor flux of the modified membrane is higher than that of the unmodified membrane for all operating parameters; temperature, feed flow rate, and concentration.

In the second application, the raw carbon nanotubes (CNTs) and the more polar carboxylated carbon nanotubes (referred to as f-CNTs) are employed to create carbon nanotube immobilized membranes (CNIMs) for ammonia separation via direct contact membrane distillation (DCMD). The ammonia removal by both CNIMs are markedly superior to that of the original PTFE membrane, while functionalized CNIM (CNIM-f) shows the best performance in terms of flux, mass transfer coefficients, and selectivity. The enhancement in ammonia removal with f-CNTs is attributed to the favored chemisorption of ammonia with the carboxylic groups of the f-CNTs.

In the third major application, functionalized carbon nanotube immobilized membranes (CNIM-f) and graphene oxide immobilized membranes (GOIM) are applied to separate methyl tert-butyl ether (MTBE) from its aqueous solution via sweep gas membrane distillation (SGMD). CNIM-f provides the best performance in terms of flux, removal efficiency, mass transfer coefficients and overall selectivity. The immobilization of functionalized CNTs (f-CNTs) alters the surface characteristics of the membrane and enhanced partition coefficients, and thus assists MTBE transport across the membrane. The fast adsorption-desorption of organic moiety on f-CNTs results in activated diffusion and lead to high flux enhancement.

This dissertation shows that the modification of the membranes with carbon-based materials namely CNTs, GO and their derivatives is an effective alternative to enhance the performance of MD and the membrane modified by CNTs and GO has the great potentials for water purification and solvent removal from aqueous solution using MD technology.

NANOCARBON MODIFICATION OF MEMBRANES FOR ENHANCED WATER DESALINATION AND WATER TREATMENT

by
Worawit Intrchom

A Dissertation
Submitted to the Faculty of
New Jersey Institute of Technology
in Partial Fulfillment of the Requirements for the Degree of
Doctor of Philosophy in Environmental Science

Department of Chemistry and Environmental Science

May 2020

.

APPROVAL PAGE

NANOCARBON MODIFICATION OF MEMBRANES FOR ENHANCED WATER DESALINATION AND WATER TREATMENT

Worawit Intrchom

Dr. Somenath Mitra, Dissertation Advisor — Date
Distinguished Professor of Chemistry and Environmental Science, NJIT

Dr. Tamara Gund, Committee Member — Date
Professor of Chemistry and Environmental Science, NJIT

Dr. Robert B. Barat, Committee Member — Date
Professor of Chemical Engineering, NJIT

Dr. Edgardo T. Farinas, Committee Member — Date
Associate Professor of Chemistry and Environmental Science, NJIT

Dr. Yong I. Kim, Committee Member — Date
Assistance Professor of Chemistry and Environmental Science, NJIT

BIOGRAPHICAL SKETCH

Author: Worawit Intrchom

Degree: Doctor of Philosophy

Date: May 2020

Undergraduate and Graduate Education:

- Doctor of Philosophy in Environmental Science,
  New Jersey Institute of Technology, Newark, NJ, USA, 2020

- Master of Science in Environmental Management,
  Chulalongkorn University, Bangkok, Thailand, 2005

- Bachelor of Science in Public Health,
  Khon Kaen University, Khon Kaen, Thailand, 1996

Major: Environmental Science

Publications:

Intrchom, W., Roy, S., and Mitra, S., Removal and Recovery of Methyl Tertiary Butyl Ether (MTBE) from Water Using Carbon Nanotube and Graphene Oxide Immobilized Membranes. *Nanomaterials*, 2020, 10(3), 578.

Intrchom, W., Roy, S., and Mitra, S., Functionalized Carbon Nanotube Immobilized Membrane for Low Temperature Ammonia Removal via Membrane Distillation. *Separation and Purification Technology*, 2020, 235, 116188.

Intrchom, W., Roy, S., Humoud, M.S., and Mitra, S., Immobilization of Graphene Oxide on the Permeate Side of a Membrane Distillation Membrane to Enhance Flux. *Membranes*, 2018, 8, 63.

Intrchom, W., Thakkar, M., Hamilton Jr, R.F., Holain, A., and Mitra, S., Effects on Growth and Photosynthesis Activities of Metal-Carbon Nanotube Composite Exposure to Fresh Water Algae C.reinhardtii. *Scientific Reports*, 2018, 8, 15301.

Intrchom, W. and Mitra, S., Analytical Sample Preparation, Preconcentration, and Chromatographic Separation on Carbon Nanotubes**.** *Current Opinion in Chemical Engineering*, 2017, 16:1-13.

Azizighannad S, Intrchom W, Mitra S. Raman Imaging of Membrane Fouling. *Separation and Purification Technology*, 2020, 242, 16763.

Humoud, M.S., Intrchom, W., Roy, S., and Mitra, S., Reduction of Fouling in Microwave Induced Membrane Distillation on Carbon Nanotube Immobilized Membrane. *RSC Environmental Science Water Research and Technology*, 2019, 5(5), 1012-1021.

Roy, S., Humoud, M.S., Intrchom, W., and Mitra, S., Microwave-Induced Desalination via Direct Contact Membrane Distillation. *ACS Sustainable Chemistry and Engineering*, 2018, 6(1), 626-632.

Presentations:

Intrchom, W., Thakkar, M., and Mitra, S., Toxicity of Carbon Nanotube-Metal Hybrid Particle on Freshwater Algae C.reinhardtii. *ESGSA/A&WMA Student Poster Competition*, Rutgers, New Brunswick, NJ, Feb. 27th, 2019.

Intrchom, W., Roy, S., and Mitra, S., Graphene Oxide Immobilization on the Permeate Side of the PTFE Membrane to Enhance Flux in Membrane Distillation. *ACS* National Meeting in Orlando, FL, Mar. 31st – Apr. 4th, 2019.

To my beloved parents: Dad Taweep and Mom Somlim, and family; your unconditional love and your continued support have encouraged me to step forward so far and in the future. This success is dedicated to all of you.

(แด่พ่อทวีปและแม่สัมลิ้มอันเป็นที่รักยิ่ง รวมถึงน้องสาววราภรณ์ น้องสาวรวิวรรณ น้องเขยเวโรจน์ หลานชายนิติภูมิและหลานสาวจอมธนา ความรักอันปราศจากข้อแม้ใดๆและการสนับสนุนในทุกๆเรื่องตลอดมาของทุกคน เป็นแรงขับเคลื่อนให้ข้าพเจ้าเดินไปข้างหน้าจนมาถึงวันนี้ และจะเป็นเช่นนี้ต่อไปในอนาคต สำหรับความสำเร็จในครั้งนี้ข้าพเจ้าขอมอบให้แด่ทุกคนดังที่ได้กล่าวมาข้างต้น)

ACKNOWLEDGMENTS

I came to NJIT on a long journey overseas to pursue my PhD degree. Generous support came from many kind persons. Without this support, my dream might not have come true. I would like to acknowledge these persons here to express my heartfelt gratitude to them and to remind them that every support is imprinted on my memory forever.

First, I wish to express my profound gratitude to my advisor, Professor Somenath Mitra for his unqualified support from my application to my graduation. My study has been closely followed and my research fully supported by both his academic guidance and budget. Many things about conducting research have been clearly explained because of his expert guidance. Good opportunities to broaden my academic knowledge and valuable experiences have been afforded by his generosity. It has been an honor and pleasure to be a student under his supervision.

Next, I would like to sincerely thank Professor Tamara Gund, Professor Robert Barat, Dr. Edgardo Farinas, and Dr. Yong Kim for their time serving as my dissertation committee members and providing valuable advice and useful comments.

Of special importance, I would like to acknowledge Naresuan University for sponsoring my PhD scholarship, and my colleagues at Department of Environmental Health, Faculty of Public Health, Naresuan University, Thailand for sharing the workload during my study. The Chemical, Bioengineering, Environmental, and Transport Systems Division, National Science Foundation, USA (Grant no. CBET-1603314) is also gratefully acknowledged for the research funding.

In addition, I wish to thank Dr. Jeong Seop Shim, Dr. Larisa Krishtopa, and Dr. Xueyan Zhang for their technical support, I would also like to recognize Dr. Chaudhery Hussain, Genti Price, Silvana Brito, Leslie Williams and gratefully thank Yogesh Gandhi for their invaluable assistance.

I would like to thank my previous research group members Dr. Kun Chen, Dr. Megha Thakkar, Dr. Smruti Ragunath, Dr. Xianyang Meng, Dr. Zheqiong Wu, and Dr. Madihah Humoud for their suggestions and assistance. For my current research group members—Dr. Zhiqian Wang, Oindrila Gupta, Indrani Gupta, Mitun Chandra Bhoumick, Sumona Paul, Samar Azizighannad, and Mohammad Saiful Islam—I offer my warm thanks them for their friendship, assistance, and all the fun we have had together. My special thanks also goes to Dr. Sagar Roy, who is both my friend and my laboratory supervisor, for his technical guidance, mutual assistance, and close supervision. In addition, my sincere thanks goes to my friends in Thailand: Pechrung, Nipawan, and Kitiluk for their love and encouragement when I was down and felt lonely.

Last and foremost, I am profoundly grateful to my parents—Dad Taweep and Mom Somlim—for their unconditional love, great looking after, positive encouragement, and continuing support for my life and all studies. I am also very thankful to my sister, Rawiwan; brother-in-law Veroj; nephew and niece, Nitibhum and Jomthana, for their complete support. With all of these supports, my PhD degree has now been completed successfully.

TABLE OF CONTENTS

TABLE OF CONTENTS
(Continued)

Chapter **Page**

TABLE OF CONTENTS
(Continued)

Chapter **Page**

TABLE OF CONTENTS
(Continued)

Chapter **Page**

LIST OF TABLES

LIST OF FIGURES

LIST OF FIGURES
(Continued)

LIST OF FIGURES
(Continued)

CHAPTER 1

INTRODUCTION

1.1 Background

The world population has rapidly and continuously increased from 1.65 billion in 1900 to 7.6 billion at the present (2019) and it is projected to be 9.8 billion in 2050 and 11.2 billion in 2100 [1]. The increase in world population not only results in industrialization and urbanization, but also simultaneously stimulates the development of sciences and technologies. Although these advancements promote the quality of life and the growth of economy, they exploit a lot of resources and generate several types of environmental pollution at the same time. A variety of environmental issues arising in many counties around the world have continually been reported [2-6], these include water pollution. Water pollution is caused by releasing and leaking of different kinds of pollutants from municipality, industry, and agriculture into the water body. These pollutants deteriorate the water quality, restrict water use, and can harm human health [7]. Therefore, to protect the water quality, preserve the water resources for human use, and consequently promote human health, the appropriate water treatment technologies are of significant importance.

Water is a basic human need. Human use water for drinking, cooking, and cleaning in everyday life, so clean water is of vital necessity for human health [7, 8]. In fact, the amount of water in the world is available for all populations, but most of the water (~ 97%) is saline water in the seas and oceans that must be treated for consumption, and the rest (~3%) is fresh water that only 1% of this amount or 0.03% of all water can be accessed by human [9] as the detail shown in Figure 1.1. Furthermore, not everybody can use or access

fresh water reservoirs because of limitations such as the unmatched distribution of these reservoirs with world population distribution, long distance from water reservoirs [10], and poor quality of water [11-13]. As a result, there is only the small amount of fresh water that humans can use to fulfil human needs and people in some areas still face with the scarcity of water [14, 15]. As mentioned before, brackish and sea water are the largest water resources in the world that can supply water for all people; therefore producing clean water from this resource is attractive. However, purification technologies called desalination are necessary to treat these waters [16].

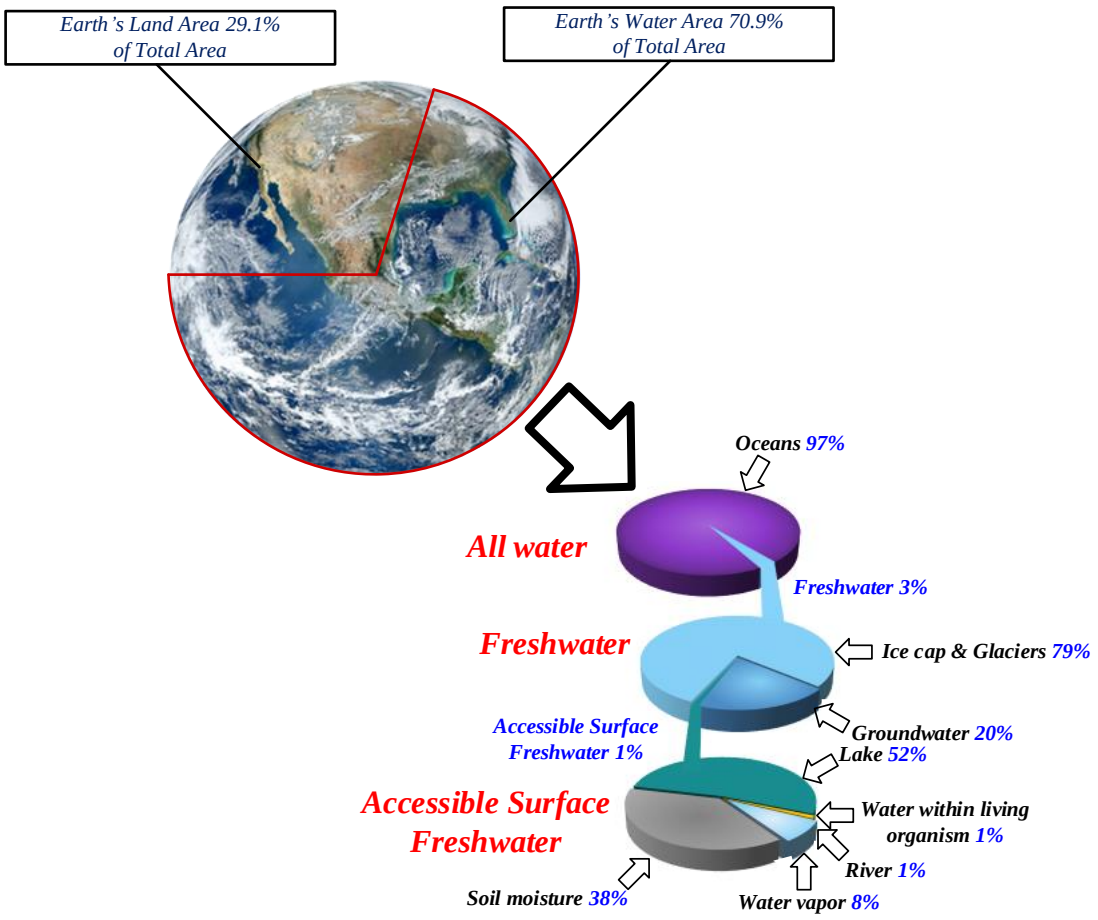

Figure 1.1 The world's water distribution.

Water and wastewater treatment technologies have been continuously studied, developed, and exploited from small households to big firms [17]. Among these technologies, membrane separation process has gained attention from several sectors, especially the industrial [18-21], since membrane process offers many advantages over other wastewater and water treatment technologies. In membrane separation, a variety of the membrane with different pore sizes can be chosen and used to screen the mixture at the molecular scale step by step up to the level determined by the standard or to the scale of what we desire [22]. With different polymer membranes and further modification [23], membranes can have high selectivity for the specific matter [24]. Simple concept and easy operation with low maintenance process is a key advantage of membrane technology. In addition, less chemical and energy consumption compared to other technologies make this technology more friendly to the environment [25].

Membrane technology such as reverse osmosis (RO) and other filtrations—like microfiltration (MF), ultrafiltration (UF), nanofiltration (NF), and forward osmosis (FO)—have played a key role as the main membrane processes in water and wastewater treatment [26]. Although these processes offer many outstanding merits, they still have inherent limitations. As MF, UF, NF, and RO are pressure-driven membrane processes, membrane fouling is one of their impediments [27, 28] especially for RO. RO process is sensitive to fouling that can occur when the high concentration formed or concentration polarization happens at the boundary layer [29]. Therefore, pre-treatment of feed solution and system maintenance are needed to reduce the energy use and cost of RO operations, and protect the membrane [30]. In addition, the high cost of RO systems is a big impediment to installation for a developing country [31]. While other membrane processes have the

external concentration polarization as a limitation, FO faces with the internal concentration polarization [32]. Reverse salt flux is also one of the demerits of FO [33]. Although FO process is a good alternative to draw water from the solution, it needs other further processes to produce purified water. As a result, using FO alone may be impractical for water purification, but it is suitable for a pre-treatment process [34]. Therefore, other techniques should be studied and developed as alternatives in order to support the demand for desalination and water purification.

Membrane distillation (MD) is an emerging thermal membrane-based desalination technology that employs the difference in the water vapor pressure between feed and permeate side as a driven force. Water vapor is driven by the high partial pressure at the hot feed side passing through the porous membrane, and the water is condensed at the permeate side that has lower water vapor pressure [35]. MD has been successfully tested for desalination [36], purification applications [37], and other wastewater treatments [38, 39]. For these purposes, MD can be used as a stand-alone system and a hybrid process [40, 41]. MD consists of a hot feed side, a membrane and a membrane module, and a permeate condensing side. With simple units, this makes MD easy to operate. Compared to pressure-driven membrane processes, MD has much lower membrane fouling and has high solute or salt rejection [42]. In addition, MD can be performed at low temperatures (30-70 ºC), so low grade energies such as heat waste, solar power, and geothermal energy have been used for MD operation [43-45]. Although MD has many outstanding merits, it still suffers from the low permeate flux, a main drawback. Therefore, in this dissertation, the approaches to overcome this limitation of MD are presented to be as alternatives for desalination and other separations.

1.2 Objectives and Scope of the Study

In this study, the overall objective was to develop the approaches to enhance the MD performance for water desalination and water treatment. The main approach was to use carbon-based nanomaterials such as carbon nanotubes (CNTs) and graphene oxide to modify the commercials membranes for MD. The scope of the study is defined as follows;

1. Modifying the permeate side of commercial membranes by immobilizing GO (graphene oxide), characterizing the modified membrane, and varying the operating conditions (e.g., feed temperature, feed flow rate, and feed concentration) to study the DCMD (direct contact membrane distillation) performance for desalination.

2. Utilizing carbon nanotubes and their derivatives immobilizes on the membranes, characterizing the carbon nanotube immobilized membranes (CNIMs), and studying the DCMD performance with various operating conditions for ammonia removal.

3. Immobilizing carbon nanotubes and their derivatives on the membranes, characterizing the modified membrane, and studying the SGMD performance with various operating conditions for methyl-tert butyl ether (MTBE) separation.

1.3 Dissertation Outline

This dissertation composes of three main parts; Part I- Chapter 1 introduction and Chapter 2 literature review, Part II- Chapter 3, 4, and 5, and Part III- Chapter 6 conclusion and recommendation. In Chapter 3, the performance of membrane modified by graphene oxide on the permeate side of membrane was assessed and compared to the original commercial membrane using DCMD. Chapter 4 presents the approach to enhance the ammonia separation using carbon nanotube and carboxylated carbon nanotube modified membranes via DCMD. Chapter 5 shows the performance of functionalized carbon nanotube and graphene oxide modified membranes in methyl-tert butyl ether (MTBE) separation via sweep gas membrane distillation (SGMD).

CHAPTER 2

LITERATURE REVIEW

In this chapter, the literature on the principle and theory of membrane distillation is reviewed in order to clearly understand how MD works and what factors affect how MD works. The MD applications and the modifications to enhance the MD performance are compiled to review the progress of this technology.

2.1 Principle and Theory of Membrane Distillation

2.1.1 Basic Principle of Membrane Distillation

Membrane distillation is a thermal and membrane-based separation process. The principle of MD is to apply the difference in the vapor pressure of hot feed side and of cold permeate side as a force to transport the vapor molecules through the hydrophobic porous membrane [46, 47]. The feed solution is heated to raise the temperature that results in an increase in vapor pressure at feed side, while the permeate side has lower temperature and lower vapor pressure. This creates the vapor pressure gradient between the two sides of the membrane [48]. The transported molecules through the membrane are condensed on the permeate side in different ways depending on the MD configurations [49] as descripted in the next heading. The hydrophobicity of membrane prevents the penetration of aqueous solution through the membrane due to surface tensions, but let only vapor molecules passing through. The concept of MD is shown as the schematic diagram as Figure 2.1.

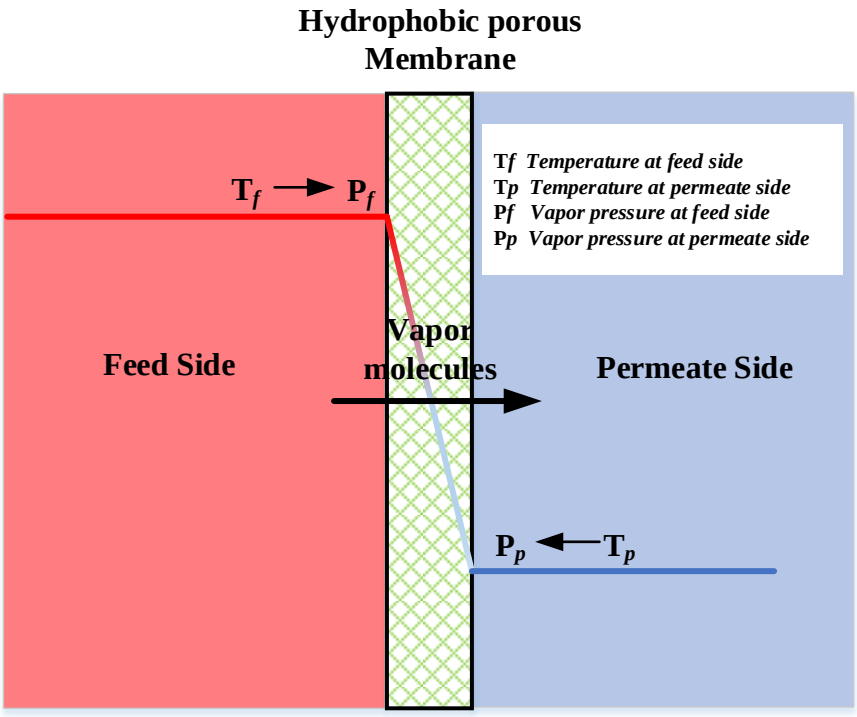

Figure 2.1 Schematic diagram of MD concept.

2.1.2 Membrane Distillation Configurations

In general, MD system can be divided into three parts; feed side, membrane cell/module, and permeate side. Feed side simply consists of feed storage tank, heat source, and a feed circulation system. MD cell or module contains hydrophobic porous membrane, and permeate side composes of a condensing process. There are four standard MD configurations based on the different condensing processes on the permeate side, namely direct contact membrane distillation, air gap membrane distillation, sweep gas membrane distillation, and vacuum membrane distillation [46, 47, 49, 50].

Direct contact membrane distillation (DCMD) is the simplest and the most commonly used MD configuration. While the hot solution is circulated on the feed side of the membrane, the cold aqueous solution is fed to directly contact with the permeate side

of the membrane [49]. In this way, the vapor is condensed inside the MD module [47]. Figure 2.2 shows the schematic diagram of DCMD module. DCMD is suitable for desalination and concentration of fruit juices in the food industry or aqueous acids [47] due to its simple setup as illustrated in Figure 2.3. In addition, DCMD provides reasonable high flux [37]. However, the major disadvantage of DCMD is relatively lower thermal efficiency than other configurations [49].

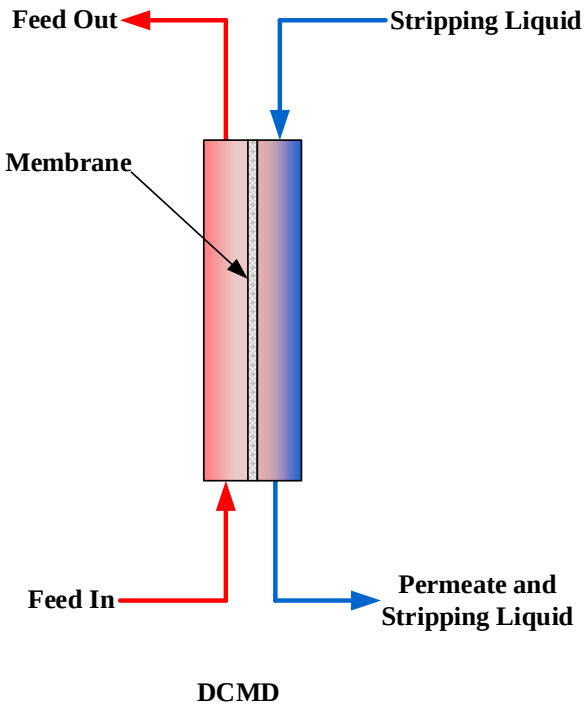

Figure 2.2 Schematic diagram of DCMD module.

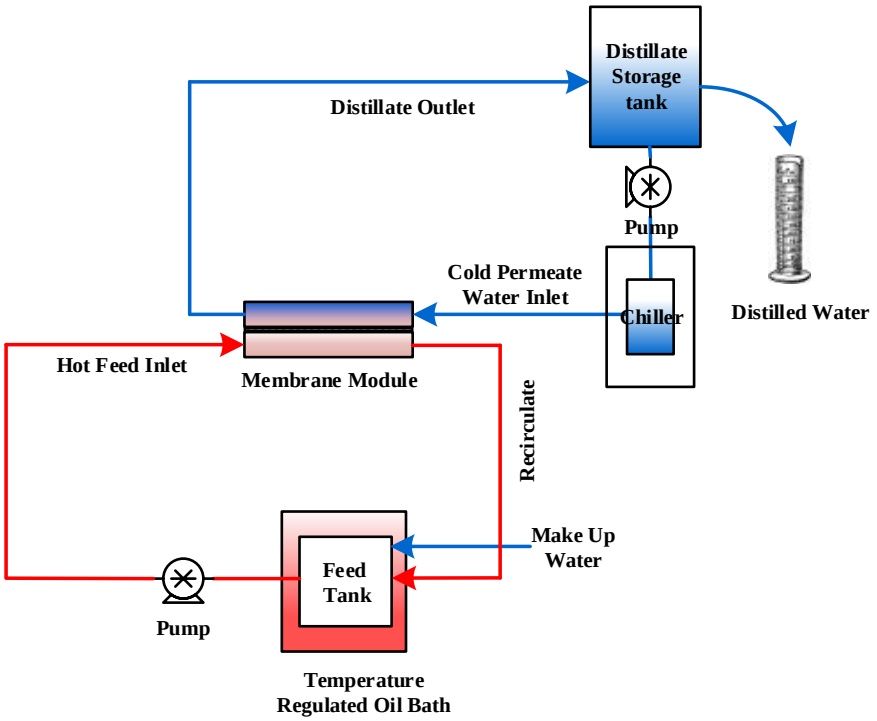

Figure 2.3 Experimental setup of DCMD.

Air gap membrane distillation (AGMD) applies the stagnant air gap inserted between the membrane and cold condensing plate on the permeate side of the MD module [50]. The schematic diagram of AGMD module is depicted in Figure 2.4. In this configuration, the hot solution directly contacts the membrane surface on feed side, the vapor molecules pass through the membrane and the air gap, and then condense on the condensing surface inside the membrane module [47]. The condensing plate is cooled down by a coolant at the opposite side of the air gap. A simple experimental setup of AGMD is shown in Figure 2.5. The air gap in the MD module reduces the heat loss via conduction and makes AGMD as the highest energy efficiency configuration [37]. However, the air gap simultaneously creates the additional vapor transfer resistance

resulting in the lower permeate flux that is considered as a disadvantage of AGMD [37, 51]. AGMD can be used for desalination and separating volatile compounds from aqueous solutions [47].

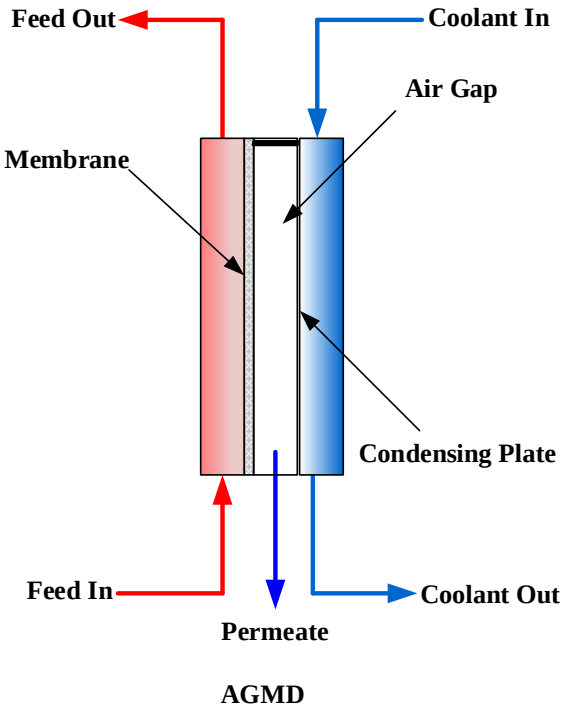

Figure 2.4 Schematic diagram of AGMD module.

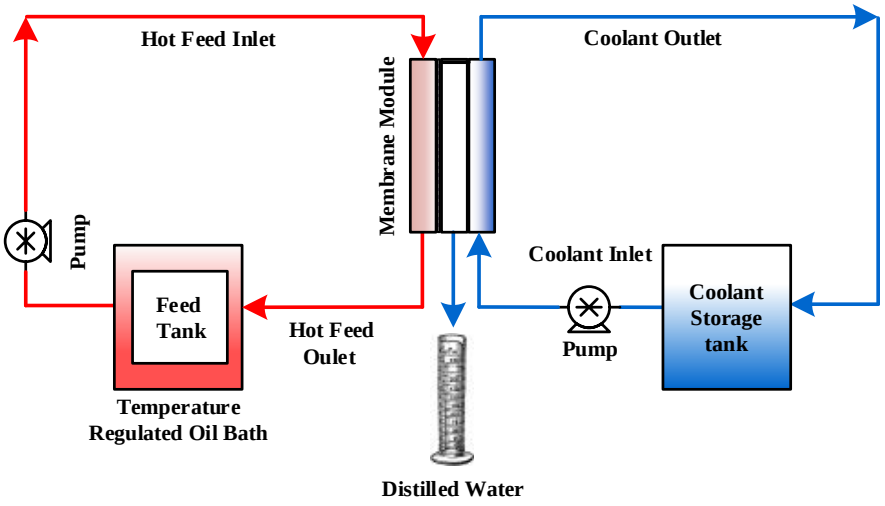

Figure 2.5 Experimental setup of AGMD.

Sweep gas membrane distillation (SGMD) is a MD configuration where, in the permeate side, the inert gas is used to sweep the transferred vapor molecules from the feed side and to carry those molecules to condense outside the MD module [49, 50], while the hot solution is fed and contacts directly on the other side of the membrane as shown in Figure 2.6. The sweeping inert gas not only plays a key role as a gas barrier to reduce the conductive heat loss [47], but also enhances the mass transfer by reducing mass transfer resistance [49]. The main disadvantage of SGMD is the extra costs to operate the external condensation system [49]. Furthermore, due to a small amount of permeate vapor diffusing in a sweep gas volume, a large condenser is required to obtain the high flux [47]. SGMD is proper for removing volatile compounds from aqueous solution [37]. A SGMD experimental setup is represented in Figure 2.7.

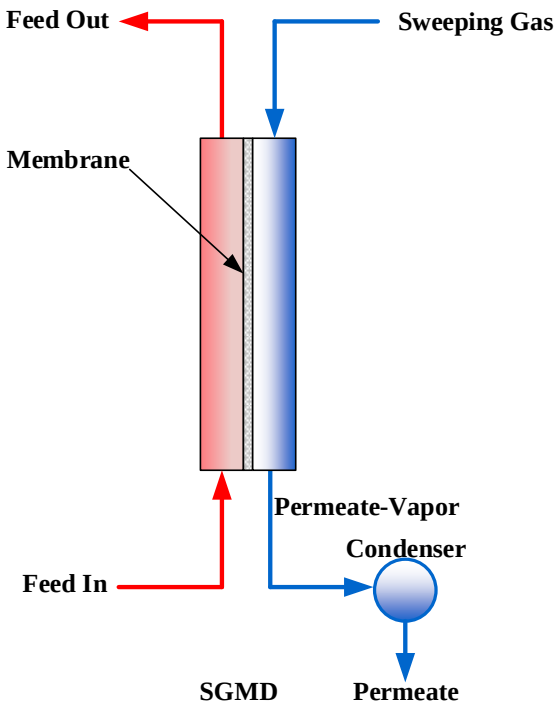

Figure 2.6 Schematic diagram of AGMD module.

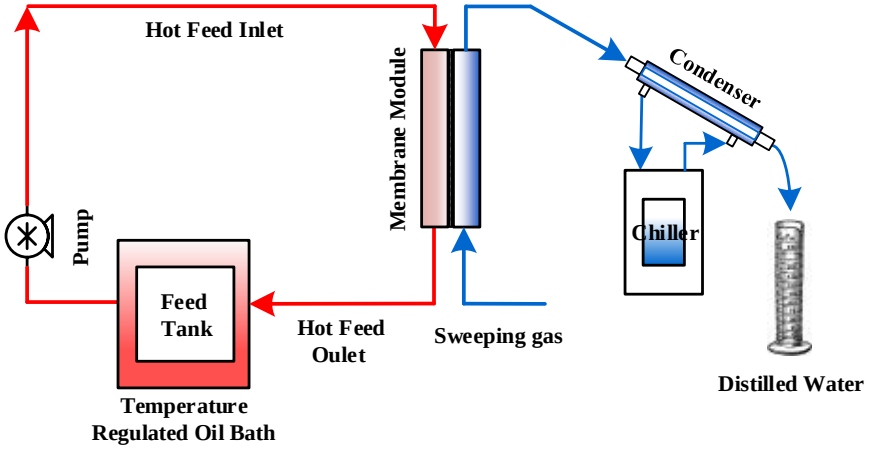

Figure 2.7 Experimental setup of SGMD.

Vacuum membrane distillation (VMD) is the other MD configuration where, in the permeate side, the external condensation system is employed to condense the vapor outside the MD module [47], like SGMD. However, instead of using gas to carry the permeate vapor, the vacuum is applied (as shown in Figure 2.8). The applied vacuum is created by means of a vacuum pump [50] that further connects to the cold vacuum trap. By this means, the conductive heat loss is negligible and the higher flux can be obtained, and both of which are the great advantages of VMD [47]. Nevertheless, applying vacuum can create some disadvantages for VMD, including higher membrane wetting, higher membrane fouling, and lower selectivity [9]. VMD is useful for volatile compound separation from aqueous solutions [37]. An experimental setup of VMD is illustrated in Figure 2.9.

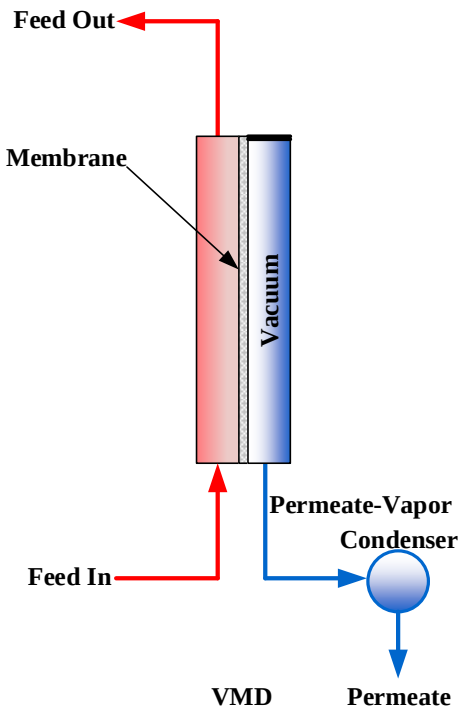

Figure 2.8 Schematic diagram of VMD module.

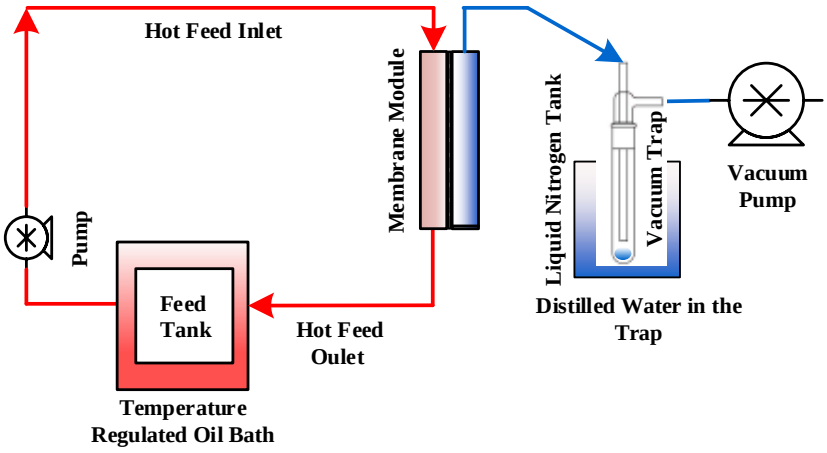

Figure 2.9 Experimental setup of VMD.

The advantages and disadvantages of conventional MD configurations are summarized in Table 2.1.

Table 2.1 Advantages and Disadvantages of Conventional MD Configurations

Configuration	Advantages	Disadvantages
DCMD	The easiest and simplest configuration in design and operation. Minimum requirement of equipment. High and stable permeate flux. Internal heat recovery is feasible.	High temperature and concentration polarization. High heat loss by conduction. Low thermal efficiency.
AGMD	Highest energy efficiency. High permeate flux. Low conductive heat loss. Low fouling tendency. Internal heat recovery is feasible.	Creation of additional mass transfer resistance. Lowest obtained output ratio. Difficulty in module designing and modeling.
SGMD	Low conductive heat loss. Low mass transfer resistance.	Low flux. Difficulty of heat recovery. Required large external condenser.
VMD	Highest permeate flux. Negligible conductive heat loss. Very low thermal polarization.	Higher possibility of membrane pore wetting. High membrane fouling. Low selectivity. Required vacuum pump and external condenser. Difficulty in heat recovery.

Source: [9, 51, 52]

2.1.3 Mass and Heat Transfer

In MD process, there are two phenomena: heat and mass transfer correlatively occurring in the same direction. The temperature gradient from the feed side to the permeate side makes heat transfer, while simultaneously, the difference in vapor pressure results in mass transfer through the membrane [53]. Here, mass transfer will be explained using DCMD

configuration, a typical configuration of MD. There are three consecutive steps of mass transfer in DCMD [49, 54]. First, the vapor molecules are emitted at the liquid/gas boundary layer on the feed side, the second the vapor passes through the membrane pore from the hot feed side to cold permeate side by the vapor pressure gradient, and third the vapor condensed at the gas/liquid boundary layer on the permeate side. In mass transfer, there are two major factors: vapor pressure gradient and the permeability of the membrane that play the role in mass transfer controlling [37]. Mass transfer per a unit of time per a unit of active area of the membrane is termed as the mass flux (*J*), which can be expressed as a linear function of the vapor pressure difference across the membrane [55], as shown in the following equation:

$$J = K(P_f - P_p) \tag{2.1}$$

where *K* is the overall mass transfer coefficient, and *Pf* and *Pp* are partial vapor pressure of average feed and permeate temperatures, respectively. The overall mass transfer coefficient (*K*) is the reciprocal of an overall mass transfer resistance, which is composed of mass transfer resistances of feed layer ($\frac{1}{Kf}$), membrane ($\frac{1}{Km}$), and permeate layer ($\frac{1}{Kp}$). Therefore, *K* can be described in term of mass transfer resistance as:

$$K = \left[\frac{1}{K_f} + \frac{1}{K_m} + \frac{1}{K_p}\right]^{-1} \tag{2.2}$$

In this case, feed and permeate sides of the membrane are in good fluid dynamic conditions, mass transfer resistance of the membrane is dominant, and *Km* varies in line with characteristics of the membrane as seen in the following equation [37]:

$$K_m \propto \frac{d^a \varepsilon}{tb} \tag{2.3}$$

where d^a is pore sizes of the membrane, ε is the membrane porosity, t is the tortuosity of the membrane, and b is the membrane thickness.

Mass transport through the membrane in the MD process have been explained by different types of mechanisms. However, there are three popular models proposed; Knudsen flow, Poiseuille flow (viscous flow), and Molecular diffusion model or transitionary model (a combination between these three models) [9, 37, 47, 50]. Zhongwei et al. [56] proposed that Knudsen flow occurs if the mean free path of water molecules is much larger than the pore size of the membrane and thus there is high possibility that the vapor molecules will collide with the wall of membrane pore. In this case. the Knudsen number (*Kn*) is used to provide the information of which mechanism is dominant inside the membrane pore and the number is defined as:

$$K_n = \frac{l}{d} \tag{2.4}$$

where *l* is the mean free path of the molecules, and *d* is the mean pore size of the membrane. If *Kn* is greater than 1, Knudsen diffusion is the dominant mechanism for the mass transport through the membrane pores; *Kn* is between 0.01 and 1, the combination of Knudsen and Molecular diffusion models is responsible for the mass transport; and if *Kn* is less than 0.01, Molecular diffusion is the dominant mechanism for the mass transport [57].

From the Equation (2.4), it can be seen that Molecular diffusion governs the mass transport when the pore size of membrane is greater than the mean free path of the molecules. Guijt et al. [58] also stated that Molecular diffusion took place only for large pore membrane. In this mechanism, the molecules transfer corresponding to each other under the influence of concentration gradients. In Poiseuille flow, the vapor molecules move as a continuous fluid controlled by the pressure gradient [47], and this mechanism may be considered as one of the mechanisms occurring in the large pore size membrane from the study of Zhongwei [56]. The combination of Knudsen and Molecular diffusion is pointed out that occurs simultaneously for pore size less than 0.5 μm. membrane [59],. while Knudsen diffusion and Poiseuille flow are suggested that can be expressed for de-aerated DCMD [60, 61]. In addition to these three basic mechanisms, Schofield's model and the Dust-Gas model are also popular mass transfer models for membrane distillation [62, 63].

As a non-isothermal process, heat transfer is of critical importance for membrane distillation. Two main heat transfer mechanisms: latent heat and conduction heat transfer work in the MD process [47]. There are three main steps of heat transfer in the MD: heat transfers through the boundary layer of feed side, heat transfers through the membrane, and heat transfers through the boundary layer of permeate side [37, 47, 50].

On the feed side, heat transport from the bulk solution to the membrane surface across the boundary layer and the considerable quantity of heat is used for liquid evaporation. The amount of heat transport across the feed boundary layer (*Qf*) can be expressed as:

$$Q_f = C_f(T_{bf} - T_{mf}) \tag{2.5}$$

where *Cf* is the heat transfer coefficient of the feed side boundary layer, *Tbf* and *Tmf* are the bulk solution temperature and the membrane surface temperature at feed side, respectively.

At the membrane, there are two heat transfer processes occurring: latent heat transferred by the water vapor (*Qv*) and sensible heat conducted across both the membrane matrix and gas contained membrane pores (*Qc*) [47, 49]. These two values can be calculated by following equations:

$$Q_v = J\Delta H_g \tag{2.6}$$

$$Q_c = \frac{\lambda}{b}(T_{mf} - T_{mp}) \tag{2.7}$$

where *J* is the permeate flux, ΔHg is the latent heat of vaporization, λ is the thermal conductivity of the membrane, *Tmf* is the surface temperature at permeate side. Therefore, the total heat flux (*Qtm*) across the membrane can be described as;

$$Q_{tm} = Q_v + Q_c \tag{2.8}$$

or

$$Q_{tm} = \frac{\lambda}{b}(T_{mf} - T_{mp}) + J\Delta H_g \tag{2.9}$$

The thermal conductivity of the membrane (λ) can be expressed as;

$$\lambda = \varepsilon\lambda g + (1 - \varepsilon)\lambda s \tag{2.10}$$

where λg and λs are the thermal conductivity of gas and membrane matrix, respectively.

On the permeate side, the temperature of membrane surface is higher than that of the bulk solution; therefore, heat transports from the membrane surface to the bulk solution across the boundary layer [49]. The amount of heat transport across the permeate boundary layer (*Qp*) can be expressed as;

$$Q_p = C_p(T_{mp} - T_{bp}) \tag{2.11}$$

where *Cp* is the heat transfer coefficient of the permeate side boundary layer, *Tbp* is the bulk solution temperature at permeate side.

2.1.4 Temperature Polarization and Concentration Polarization

During heat and mass transfer in the MD process, two phenomena called temperature polarization and concentration polarization emerge and inevitably result in vapor flux decline[48]. On the feed side of the membrane, the large quantity of heat from feed bulk solution is used to evaporate liquid at the liquid/gas interface and some is conducted

through the membrane to the permeate side [37, 49]. This brings about the drop of bulk feed temperature across the feed boundary layer from T*bf* to T*mf* at the membrane surface. While on the permeate side, the vapor condensation into the cold water and heat transfer from the feed side give rise to increase in the temperature across the permeate boundary layer from T*bp* of the cold permeate stream to T*mp* at the membrane surface (as illustrated in Figure 2.10). This change in temperatures is known as temperature polarization [64].

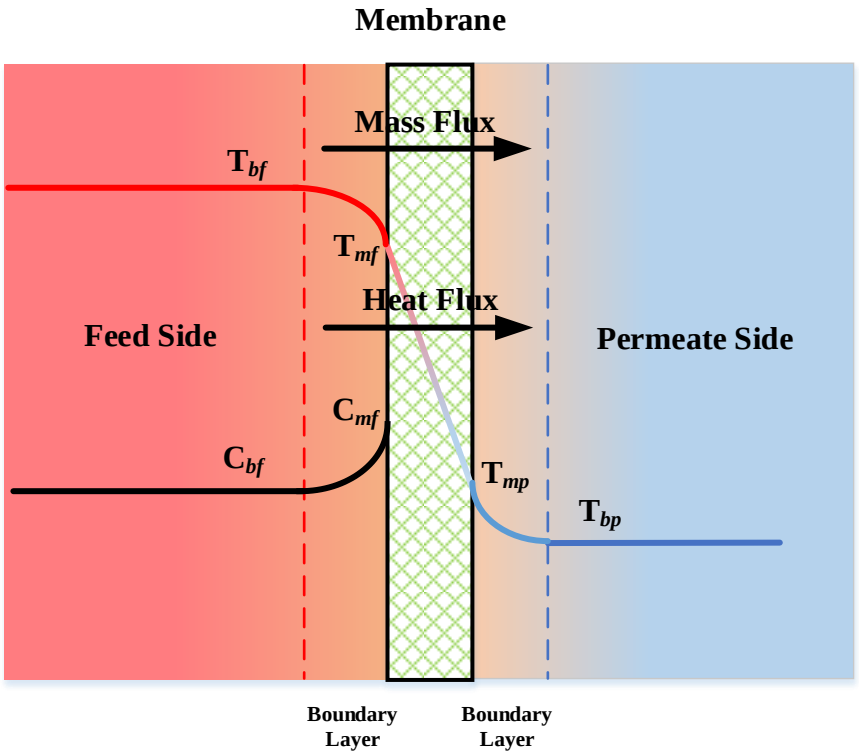

Figure 2.10 Temperature polarization and concentration polarization.

Temperature polarization causes the reduction of vapor pressure, the driving force of MD, and then the decrease in vapor flux. Temperature polarization coefficient (TPC) is basically used to measure the resistance over the overall heat transfer resistance [65]. TPC is defined as the ratio of the transmembrane temperature to the bulk temperature difference;

$$TPC = \frac{(T_{mf} - T_{mp})}{(T_{bf} - T_{bp})} \quad (2.12)$$

The efficiency of the MD process can be designed by using TPC as an indirect index, and usually for good arrangement of fluid dynamic for DCMD, TCP of between 0.4-0.7 is used to the system design [65, 66].

Concentration polarization is a major cause of flux decline in filtration processes, especially pressure-driven membrane processes such as ultrafiltration and reverse osmosis. In these techniques, concentration polarization not only results in flux reduction, but also shortens the lifespan of the membrane [67]. In MD, concentration polarization happens when the water at the liquid/gas interface vaporizes; the concentration of solutes at that point (*Cmf*) become higher than that at the bulk solution (*Cbf*), as illustrated in Figure 2.10. Concentration polarization in MD leads to the reduction of the driving force and the permeate flux [50]. Concentration polarization coefficient (PCP), used to determine the degree of concentration polarization, is defined as the ratio of the solution concentration at the membrane surface to that at the bulk feed[49];

$$CPC = \frac{C_{mf}}{C_{bf}} \quad (2.13)$$

The concentration of solute on the membrane surface (*Cmf*) can be estimated as the following equation [47];

$$C_{mf} = C_{bf}\, exp\left(\frac{J}{\rho\, K}\right) \tag{2.14}$$

Where ρ is the liquid density and K is mass transfer coefficient. However, Khayet [46], Lagana et al. [68], and Martinez [69] pointed out that, compared to temperature polarization, concentration polarization is insignificant in DCMD.

2.1.5 Operating Parameters and their Effects on MD Performance

In MD operation, there are many factors or parameters influencing the performance of the system, e.g., feed and permeate temperature, feed concentration, feed flow rate, permeate liquid and air flow rate, etc. These parameters and their influence on MD performance, especially the permeate flux, will be reviewed in this section.

2.1.5.1 Feed and Permeate Temperature. As a thermally driven process, temperature of feed solution has been proven to directly affects the permeate flux [64, 70, 71]. The increase in temperature rises the vapor pressure of a liquid exponentially according to the Antoine equation. As a result, increasing the operating temperature of MD also builds up the vapor pressure of the system, and then has the exponential effect on the permeate flux. Gunko et al. [70] and Chen et al. [71] described that when the temperature difference between the two sides of membrane surface increases, it results in the positive diffusion coefficient and contributes to the higher vapor flux. This is in line with a study of Srisurichan et al. [72] that pointed out the possibility of the direct relation between diffusivity and temperature. However, Termpiyakul et al. [55] and Zhang et al. [73] believed that increasing feed temperature rises the temperature polarization and leads to the vapor flux depletion. For permeate temperature for DCMD, decreasing the coolant

temperature leads to a significant change in the permeate flux [70, 74]. On the other hand, Banat and Simandl [75] and Matheswaran et al. [76] concluded that there is negligible effect of the cold side temperature on the permeate flux because of insignificant change of vapor pressure at low temperature.

2.1.5.2 Feed Concentration. The concentration of feed solution is a parameter affecting the performance of MD. Unlike the pressure-driven processes, MD can handle the higher concentrations of the feed solution with less membrane fouling and without the significant drop of flux. However, the experimental results showed that the permeate flux decreased with an increase in the feed concentration [48, 77-80]. The reduction of the permeate flux arises from the decrease in the water vapor pressure [77]. Lawson and Lloyd [59] concluded that there are three possible reasons for the reduction of water vapor pressure resulting in flux reduction when the concentration of NaCl solution increases: first, increase in feed concentration decreases the water activity; second, increase in feed concentration creates more concentration polarization and leads to the reduction of mass transfer coefficient of boundary layer at the feed side; last, heat transfer coefficient decreases at boundary layer due to the reduction in the temperature at membrane surface.

2.1.5.3 Feed Flow Rate. Increasing the feed flow rate lessens the thickness of boundary layer, improves the heat transfer coefficient, and consequently, the permeate flux is enhanced [72]. As the thickness of the feed boundary layer becomes thin, the temperature and concentration at liquid-gas interface become closer to those values at the bulk feed solution [81] and results in the reduction of temperature and concentration polarization [48, 71]. This is in line with a study of Izquierdo-Gil et al. [82] that found the temperature and concentration polarization reduce with an increase in feed flow rate.

2.1.5.4 Permeate Liquid Flow Rate. In theory, permeate flux can be enhanced by increasing permeate liquid flow rate. Temperature polarization declines when the permeate flow rate increases, and temperature at the gas/liquid interface gets closer to the temperature of the bulk liquid. This promotes driving force across the membrane and enhances the permeate flux [83, 84]. This is confirmed by Shojikubota et al. [85]. They indicated that the permeate flow rate is important to the permeate flux. On the other hand, Banat and Simandl [75] pointed out that increasing the permeate flow rate has negligible effect on the flux product.

2.1.5.5 Other Parameters. The effects of other operating parameters have also been studied in order to improve the MD performance such as the air flow rate in SGMD, air gap in AGMD, and vacuum pressure in VMD and operation time.

Air flow rate or sweeping gas velocity in the permeate side is the important parameter in SGMD. Permeate flux enhancement with increasing in the air flow rate or gas velocity has been reported [86, 87]. This is due to the enhancement of heat transfer with an increase in the air recirculation rate by reducing the temperature polarization effects at the permeate membrane surface. As a result, the temperature at the boundary layer becomes close to that of the bulk permeate side, and therefore, the driving force is improved [88]. In addition, the sweeping gas also extends the pressure difference between feed and permeate side that also promote the driving force [89]. Xie et al. [90] studied the removal of ammonia by SGMD. They found that increasing an air flow rate of 0.4 to 3.0 L/min enhanced the ammonia removal from 48 to 96% in 2 h.

In AGMD, the size of air gap affecting the MD performance has been studied [82, 91]. Enlarge the air gap causes the reduction of permeate flux due to increasing in the mass

transfer resistance, so reducing the thickness of air gap reduces the resistance and then improves the performance of MD. Alklaibi and Lior [92] indicated that narrowing the width of air gap increased the flux by double, and the gap of less than 1 mm. will give a more dramatic result. Pangarkar and Deshmukh [93] studied the theoretical and experimental analysis of AGMD and they reported that by reducing the air gap thickness from 10 to 5 mm., the permeate flux was theoretically and experimentally enhanced by 35.5 and 41.1%, respectively.

The driving force for MD comes from the difference in the pressure of the feed and permeate side. Increasing the pressure on the feed side or decreasing the pressure on the permeate side can rise this driving force and, consequently, enhance the permeate flux. Vacuum used for reducing the pressure on the permeate side has been studied by Bandini et al. [94, 95], Sivakumar [96], Lovineh [97], and Banat [98]. They found that decreasing in vacuum pressure of permeate side significantly improved the permeate flux. Wu et al. [99] employed VMD to remove 1,1,1-trichloroethane (TCE) from water. They indicated that TCE removal efficiency slightly increased when the vacuum pressure decreased from 100 mmHg to 60 mmHg. However, they pointed out that the removal efficiency of 93.6% could be achieved at the vacuum pressure of 60 mmHg. Similarly, EL-Bourawi et al. [100] studied the ammonia removal from water using VMD and reported that the ammonia flux increased at the lower downstream pressure.

A long period of operating time clearly causes the decline of the permeate flux in MD due to fouling or membrane wetting [59]. Banat and Simandl [101] examined the influence of long operation time (8 weeks) on the flux using trap water as a feed. They discovered that during the first 50 h, the permeate flux increased, and after that the flux

dropped for 160 h., before reaching the steady state. For seawater, the flux declined and arrived the steady state condition earlier about ten days [75]. Drioli and Wu [102] came along with the same result, when 1 M of NaCl had been tested for six days.

2.1.6 Membranes for Membrane Distillation

Membrane is of vital importance for MD. In this section, the membrane types, membrane modules, and characteristics of the membrane including membrane materials and membrane fabrications for MD will be described in some detail.

2.1.6.1 Membrane Types and Membrane Modules. Membranes for MD can be divided into two common types; flat sheet and hollow fiber [37], as illustrated in Figure 2.11.

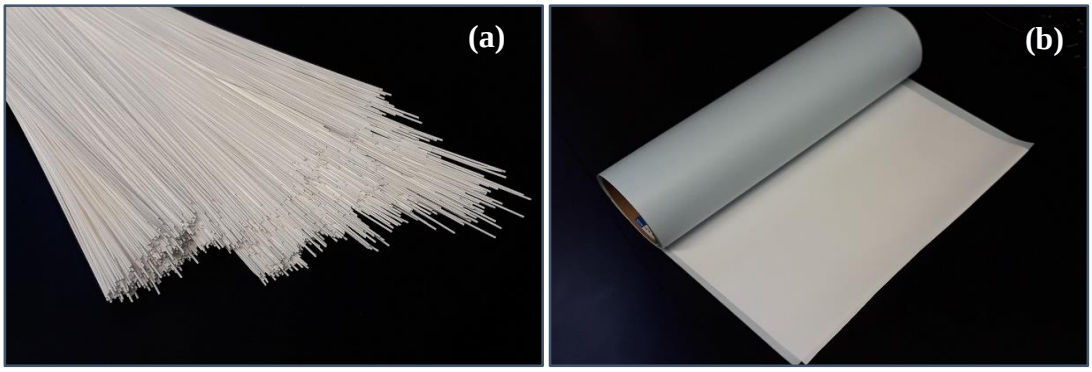

Figure 2.11 Membrane types **a)** hollow fiber, and **b)** flat sheet.

The structures of the two membrane types may be classified into two categories; isotropic and asymmetric membranes. Both of these membranes have the hydrophobic layer in common. Isotropic membrane is the membrane that has the same structure or homogeneous structure throughout the entire membrane or cross-section [42], while

asymmetric membrane may be a membrane with a heterogeneous structure from one single material, or a membrane with two or more layers of the different materials. The former is called the integral asymmetric membrane, while the latter is named the composite membrane. In MD, a composite membrane composes of one active hydrophobic layer and a supporting layer. The supporting layer may be a non-woven or scrim support that provides the mechanical strength for the membrane. Schematics of membrane structures and the examples of the supporting layer are shown in Figure 2.12. The hollow fiber membrane can be both symmetric and asymmetric membranes, while most of the flat sheet membranes are of an asymmetric structure.

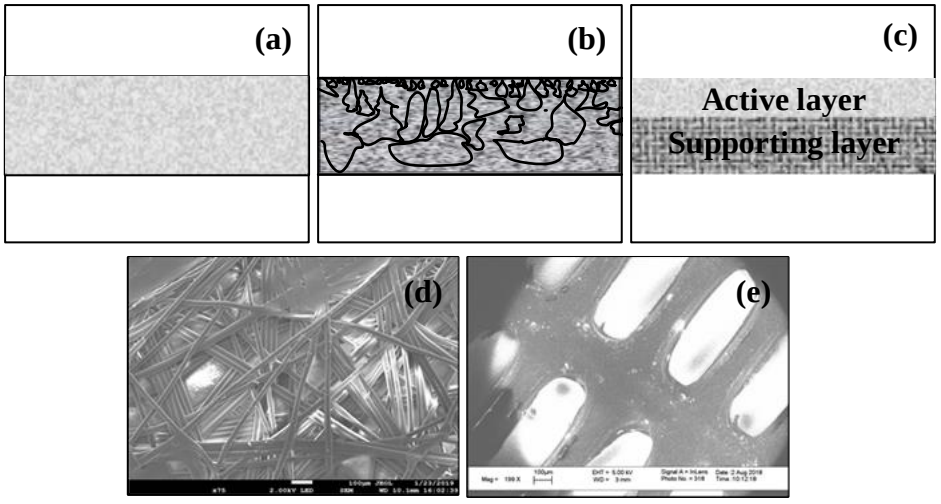

Figure 2.12 Schematics of **a)** isotropic membrane, **b)** integral asymmetric membrane, **c)** composite membrane, and figures of **d)** non-woven, e) scrim support.

The membrane modules may be separated into four types; plate and frame, hollow fiber, tubular membrane, and spiral wound membrane [47]. In a plate and frame module, a flat sheet membrane with/without a spacer is inserted between two circular or rectangular plates. The plates may be metal or polymeric materials such as polytetrafluoroethylene

(PTFE). This kind of module is easy to clean and the membrane is easy to replace, so it is widely used in laboratories. However, packing density, which the ratio of the membrane to the packing volume, of this module may line in the range of 100-400 m^2/m^3 that is quite low. In a hollow fiber module, the hollow fiber membranes with the inner diameters of 50-500 μm are sealed inside a shell tube. The feed solution flows through the hollow fiber and the permeate is received on the outside of the membrane, or vice versa. This module has the highest packing density of all modules with the value of around 3,000 m^2/m^3. The advantages of this module are cost effectiveness and resistance to high pressure operation (over 100 bars) [103]. The advantages of the module are high tendency to fouling and difficulty in cleaning and maintaining. In a tubular membrane module, the module is a tube type module that houses pressure-tight tubes. The diameters of tubular membrane very between 10-25 mm. The advantages of this module are the high effective area, low tendency to fouling, and being easy to clean; but its disadvantages are high operation cost and low packing density with the value of about 300 m^2/m^3. In the spiral wound membrane module, the flat sheet membrane, feed and permeate channel spacers, and the porous membrane support are enveloped and rolled around a perforated central collection tube, and placed into an outer tubular pressure tube. The feed solution axially flows through the feed channel across the membrane surface. The receiving liquid passes through the permeate channel and receives the permeate and is collected in the perforated central collection tube. This module has acceptable energy consumption and good packing density with the value of 300-1,000 m^2/m^3. However, the module is quite sensitive to fouling. Some samples of MD membrane modules are shown in Figure 2.13.

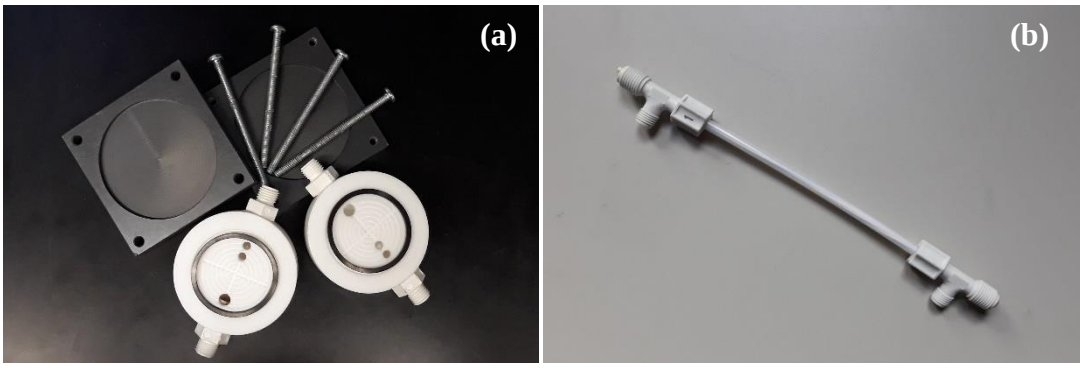

Figure 2.13 Membrane modules **a)** plate and frame, and **b)** hollow fiber.

2.1.6.2 The Characteristics of Membrane for MD. In general, hydrophobic porous membrane is employed for MD to prevent membrane wetting and get as high flux as possible. However, there are other characteristics of the membrane that should be considered to achieve the highest efficiency.

Liquid entry pressure (LEP) is defined as the minimum transmembrane pressure that is required for a pure water or other aqueous solutions to enter into dry membrane pores, by overcoming the force inside the pores, and should be as high as possible [50, 51]. A high LEP can be met by using the materials that have low surface energy, high surface tension, large contact angle, and small maximum pore size. However, the small pore size comes along with the low membrane permeability that results in the low productivity. Therefore, to get the highest permeate flux, an appropriate pore size and pore size distribution must be selected to simultaneously obtain high LEP and high permeability. On the basis of the Laplace equation, Franken et al. [104] proposed the LEP equation as follows;

$$LEP_w = -\frac{2\beta\,\gamma_L \cos\Theta}{r_{max}} \tag{2.15}$$

where β is a geometric pore coefficient determined by the pore structure (equal to 1 for cylindrical pore), γ_L is the liquid surface tension, Θ is the liquid/solid contact angle, and r_{max} is the maximum pore size.

Membrane thickness is an important characteristic that directly influences the permeate flux; as the membrane thickness increases, the mass transfer resistance arises, and the permeate flux declines. Therefore, the thickness of the MD membrane should be as thin as possible. Lagana et al. [68] suggested that the optimum thickness of the membrane should be between 30 – 60 μm. However, thickness of the membrane also affects heat transport through the membrane. The thinner membrane causes a higher heat loss, lower driving force, and consequently the reduction of flux product. Then, a compromise between the heat transfer and mass transfer resistance should be made to maximize the permeate flux by choosing the proper thickness [50].

Thermal conductivity of the MD membrane must be as low as possible to reduce heat loss as much as possible [49]. The thermal conductivity can be reduced by using a membrane with high porosities because the gases entrapped in the pores have the lower conductive heat transfer coefficient by an order of magnitude, compared to that of the used membrane materials [50]. In addition, the reduction of membrane conductivity can be made by increasing the heat transfer resistance using bi-layered or multi-layered composite porous membranes with hydrophobic and hydrophilic materials. A very thin hydrophobic layer at the feed side promotes high vapor permeability, while a thick supporting

hydrophilic layer at the permeate side enhances heat resistance and prevent the rupture of the membrane [50].

Mean pore size and pore size distribution are the characteristics used to calculate vapor flux and vapor transport coefficient. Membranes used in MD process with pore sizes between 100 nm and 1 μm have been reported [59, 103]. In general, a membrane with large pore size is needed for MD to obtain the high permeability and high flux product. On the other hand, the small pore size membrane is necessary to get the high value of LEP to prevent membrane wetting. Therefore, a proper pore size membrane should be chosen to maintain the maximum flux. In fact, the membranes for MD demonstrate a pore size distribution instead of the uniform pore size. However, in general, the mean pore size is used to calculate the mass transfer coefficient rather than the pore size distribution. In this case, Khayet et al. [57] suggested that the calculation must be carefully done, while Martinez et al. [105] obtained a similar result when both values were employed.

Membrane porosity and tortuosity of the membrane are important for mass and heat transfer in MD. Membranes with high porosity provide the large space for vapor evaporation and low conductive heat loss. Therefore, such a membrane gives the high permeate flux [47, 50, 106]. Porosity is defined as the ratio between pore volume and the total volume of the membrane. According to Onsekizoglu [49], the porosity of MD membranes lines in the range of 65-85%. The porosity (ε) can be calculated by using Smolder-Franken's equation [107].

$$\varepsilon = 1 - \frac{\rho_m}{\rho_p} \tag{2.16}$$

where $_m$ and ρ_p are the densities of membrane and polymer material, respectively. Tortuosity (τ) is defined as the deviation of the pore structure from the straight cylindrical pores to the membrane surface [50] or the average length of the pores [49]. High tortuosity refers to the high diffusion path of the vapor molecules, and then low permeability rate and results in low vapor flux. The most successful correlation was given by Srisurichan et al. [72].

$$\tau = \frac{(2-\varepsilon)^2}{\varepsilon} \tag{2.17}$$

High temperature stability and chemical stability are the characteristics that are necessary for MD membranes. In many applications of MD, the membranes have to encounter with high temperature or high concentrated solution conditions. Long-term, the membranes may not be able to resist to these harsh conditions, and consequently fail to degrade or decompose [9]. Therefore, the temperature and chemical stability of the membrane materials for the fabrication of MD membranes should be carefully considered to have the proper membranes for each application of MD.

2.1.6.3 Membrane Materials and Membrane Fabrication. Membranes for MD must be hydrophobic materials by nature. Much more attention has been paid on polymeric materials due to the practical possibility to modify their intrinsic properties. The most common polymeric materials employed to fabricate the MD membrane are

polytetrafluoroethylene (PTFE), polypropylene (PP), and polyvinylidenefluroride (PVDF), due to their low surface energy [49] (as listed in Table 2.2).

Table 2.2 Surface Energy and Thermal Conductivity of the Polymeric Materials

Polymer	Surface energy ($\times 10^3$ N/m)	Thermal conductivity ($Wm^{-1}K^{-1}$)
PTFE	9-20, 19.1	~0.25
PVDF	30.3	~0.19
PP	29, 30.0	~0.17
PE	31, 33.2	-

Source: [37, 49, 51]

As mentioned in the previous section, the membrane should have surface energy and thermal conductivity as low as possible. Among these materials, PTFE exhibits good chemical and thermal stability, the most hydrophobic polymer that is suitable for membrane fabrication, but its disadvantages are high thermal conductivity and difficulty of membrane processing. PP has good chemical, thermal resistance, and the lowest thermal conductivity [65], and PP membrane provides the highest permeate flux [108]. PVDF has good chemical, thermal resistance, mechanical strength, and moderate permeate product. However, it has the highest surface energy that PVDF membrane is prone to have the highest wettability. In addition, other polymers and copolymers such as polystyrene (PS) and polyethersulfone (PES), polyethane-co-chlorotrifluoroethene (ECTFE), polyvinylidene fluoride-co-tetrafluoroethylene (PVDF-co-TFE), polyvinylidene fluoride-co-chlorotrifluoroethene (PVDF-co-CTFE), and polytetrafluoroethylene-co-hexafluoropropylene (FEP) have been used for MD as well [42].

There are several methods for producing membrane from polymeric materials, including sintering, track-etching, template leaching, stretching, phase inversion, and

electrospinning. However, since the first three methods produce relatively low porous membranes, only the last three methods will be explained in this review.

Stretching is a popular technique without any solvent to fabricate microporous membranes used in MF and UF including MD. In this technique, the desired polymer is heated above the melting point and extruded into the thin sheet shape that will be stretched in order to make the pores [109, 110]. Although this technique is suitable for the highly crystalline polymers, semi-crystalline polymers such as PTFE and PP can employ the technique [42]. Normally, there are two steps in stretching; starting with cold stretching followed by hot stretching. Cold stretching in the same direction of the extrusion is used to initiate the micropores in the original film, while hot stretching is perpendicularly applied to the film to increase and control the desired pore structure of the membranes [111]. Stretching technique is widely used to produce the membrane commercially [112].

Unlike stretching technique, phase inversion uses solvents as a main component in the process. The process is based on the transition from a liquid phase to a solid phase [42]. The homogeneous polymer liquid mixture is transformed in a controlled condition to a solid state. The transformation can be achieved in different ways, namely: immersion precipitation, thermally induced phase separation, evaporation-induced phase separation, and vapor-induced phase separation. However, it is worth nothing that, among these methods, only the first two are commonly used to fabricate the polymeric membranes with the different morphologies [113]. The details of these methods can be seen in the literature [111]. The limitation of this technique is that only dissolved polymers are suitable to fabricate the membranes.

Electrospinning is a relatively novel technique to fabricate the porous membranes with polymeric nanofibers [114, 115]. The electrospinning process is composed of a metallic syringe, a high voltage power supply and a ground collector [42]. In the process, the polymer solution in the syringes is pumped through the needle tips and the polymeric droplets are formed. A high voltage is applied between the needle tips and the collector to overcome the surface tension of the droplet. When the surface tension is overcome, a charged fiber jet is formed. After the solvent evaporates, a solid polymeric fiber is formed and randomly deposited on the grounded collector; this results in the creation of the fibrous structure. Electrospinning can produce the porous membranes with high porosity, interconnected open pore structure that provides high permeate flux and high energy efficiency. However, with high porosity and open pores, the salt retention is an issue for this kind of membrane. In addition, to produce the membrane with the maximum pore size, the sufficiently small fiber diameters are required, while this is still a limitation of the technology [42].

2.2 Applications of Membrane Distillation

Membrane distillation was introduced and patented for the first time in 1963 by Bodell and intentionally used to distill saline water [116]. Since the beginning of the 1980s, MD process has been receiving much attention and mainly used for producing pure water from seawater, but it has also been applied for other applications [37, 65, 117] at the laboratory scale. In this section, the applications of MD will be reviewed by dividing into two main applications: water purification and other separations.

2.2.1 Water Purification

In principle, membrane distillation has high rejection for non-volatile dissolved compounds or salts almost 100 % and lower membrane fouling, compared to pressure-driven membrane processes such as RO or other filtration techniques [42]. Shirazi et al. [36] employed DCMD to desalting seawater and achieved the salt rejection of 99.99%.Therefore, MD has been mainly used for desalting seawater or desalination [92, 108].

Investigations were carried out to measure the efficiency of various types of membrane and membrane materials through different MD configurations for desalination, except SGMD. Zu et al. [118] employed PTFE hollow fiber membranes with different degree of stretching for desalting saline water via VMD. The results showed that all membranes achieved 99.9% salt rejection. Alsalhy et al. [119], used PP hollow fiber membrane for highly saline water desalination. They reported that 99.99 % salt rejection and very low conductivity of the permeate were obtained by VMD. PVDF membranes were also applied for desalination. Flat-sheet PVDF membrane used in MD via DCMD and VMD was reported by Fan and Peng [120]. They found that the permeate flux was as high as 18.9 kg/m^2 h with 99.8% NaCl rejection through DCMD, whilst the flux of 22.4 kg/m^2 h and 99.9% salt rejection were achieved via VMD. Mix polymer materials such PVDE-PTFE can be used to fabricate the membrane for MD. Teoh and Chung [121] fabricated hydrophobic polyvinylidene fluoride–polytetrafluoroethylene (PVDF–PTFE) hollow fiber membranes to use for desalination through DCMD. The results showed that the separation performance of 40.4 kg/m^2 h of the permeate flux and the salt rejection of 99.8% were attained at the feed temperature of 80 ºC. A PVDF membrane fabricated via electrospinning

technique was tested, compared to a commercial PTFE membrane through AGMD [122]. They claimed that the performance in terms of flux of the fabricated membrane was higher than that of PTFE membrane and the salt rejection efficiency of 99.8% was obtained by this membrane.

The effects of the operating parameters have often been examined in MD studies. In general, feed temperature, feed flow rate, and feed concentrations are the main parameters in DCMD, AGMD, and VMD configurations [120, 123-125]. However, other operating parameters have also been investigated for each MD configuration. Safavi and Mohammadi applied VMD for desalting salinity water [124]. They found that an increase in vacuum pressure or reduction in pressure at permeate side directly increased VMD performance in all conditions. Pangarkara and Sane [91]used AGMD for desalination of ground water and seawater. They reported that decrease in air gap thickness from 3.2 mm. to 1.2 mm. resulted in flux increment from ~7 to ~13 kg/m^2 h and from ~12 to ~24 kg/m^2 h for seawater and ground water, respectively.

RO works well with moderate saline water as brackish water (10,000 ppm) and operating pressure of 4.5 MPa [126]. Unlike RO, MD can efficiently deal with high salt concentrations. Alkhudhiri et al. employed AGMD to treat high salinity solutions of NaCl, $MgCl_2$, Na2CO_3, and Na_2SO_4. The concentration of 4000 ppm up to 180,000 ppm of NaCl was investigated and the results showed that although, the permeate flux decreased with an increase in salt concentration, the flux quite kept constant over 5 h running at the concentration of 180, 000 ppm [127]. Safavi and Mohammadi used VMD to desalt NaCl solution with highest concentration of 300, 000 ppm. They found that salt concentration had a higher influence on the permeate flux than feed temperature and feed flow rate.

However, the result of the permeate flux versus operating time as the function of feed concentration was not showed in this study [124]. MD was also applied to treat other high salinity wastewaters such as produced water [128] and landfill leachate [129]. What's more, MD is also used to handle the high salt solution from outlets of other systems such as RO, as a complementary process [130-132].

Since MD can be functioned at low temperatures, different low grade energies– such as heat waste, geothermal energy, and solar power—have been utilized as MD heat sources [43-45, 133-137]. Many MD pilot projects have been investigated and evaluated for their potentials in water treatment. Dow et al. used waste heat from a gas fired power station to operate the MD pilot plant. The plant achieved 92.8% water recovery with more than 99.8 % total dissolved solid rejections. This plant was estimated that it can produce about 8,000 kL of clean water per day and this amount of water can practically supply water to numerous industrial, residential or agricultural sites [43]. El Amali et al. employed DCMD and AGMD to desalt geothermal water; the obtained flux from the system was up to 3-5 kg/m^2 h with the salt rejection of 97%. The authors stated that AGMD is more suitable for geothermal desalination due to the lower energy requirement [136]. Guillén-Burrieza et al. applied the AGMD pilot system using solar energy as a heat source. The temperature up to 85 ºC was set to operate the system and the maximum flux of 7 L/m^2 h was obtained from this system. Nevertheless, inefficiencies to scaling-up MD coupling with transient solar thermal energy that found in laboratories reported was still reported in this study [137]. MD may play the important role in arid and semi-arid remote area that lack of drinkable water, but are often abundant with a high solar intensity. A stand-alone

MD system with solar power has the potential for the desalination of brackish water from wells or seawater and provides sufficient clean potable water for the community [138].

MD has also played a part in wastewater treatment. Criscuoli et al. used VMD to treat the dye solution [139]. They claimed that 100% dye rejection was achieved, and pure water was recovered at the permeate side for all operating parameters. Whereas, Mokhtar et al. employ DCMD to treat the effluent from rubber processing [140], with results showing that DCMD can remove at least 96% of organic carbon (TOC), total dissolved solid (TDS), sulphate, color, turbidity and conductivity. However, flux decline still occurred due to temperature polarization, concentration polarization and membrane fouling. Khayet et al. also used DCMD for humic acid treatment [141]. They reached the conclusion that DCMD was more adequate for the treatment of humic acid solutions than the pressure-driven separation processes due to lower membrane fouling. Lui and Wang [142] applied DCMD for treatment of low radioactive wastewater, and reported that DCMD can separate almost all Cs^{+}, Sr^{2+} and Co^{2+} from wastewater and the permeate flux could be maintained about 60% of the initial flux, even though high salt concentration was used as feed solution. Wu et al. tested the performance of DCMD by treating fermentation wastewater with high organic concentrations [143]. The organic rejection was found to be 95%, while the permeate flux decreased with operating time due to membrane fouling. After 12 h of operation, the feed wastewater was concentrated by a factor of 3.7 on a volumetric basis and the protein concentration in the feed was increased by about 3.5 times, which is suitable for reutilization.

2.2.2 Other Applications

MD has not only been used for desalination and wastewater treatment, it has also been applied for other purposes such as solution concentrating, chemical recovery, and mixed solution separation.

Concentration process is a key unit in food processing. MD has been employed to dewatering aqueous solutions, due to the fact that the MD can remove water even if at a low temperature that does not deteriorate and change the color, flavor, and nutritional characteristics of food and consumes less energy at the same time [49]. Gunko et al. employed DCMD for apple juice concentrating [70]. The results showed that DCMD can concentrate the apple juice with 50% of solid content obtained when the permeate flux reached about 9 L/m^2 h. The solid content can get to 60-65% with further operation, yet this resulted in the reduction of permeate flux due to an increase in the feed concentration. Hausmann et al. applied DCMD to concentrate skim milk and whey [144]. The results showed that MD has potential to dewater from the products with more than 99% rejection of all dairy components. The dry matter of these two products was reached 20% with the permeate flux of about 12 and 20 kg/m^2 h for skim milk and whey, respectively. In addition, MD can be used for concentration or recovery of other solutions. El-Abbassi et al. used DCMD to concentrate polyphenols from olive mill wastewater (OMW) [145]. The results showed that PTFE membrane provided a better separation coefficient (99%) than PVDF membrane (89%), while the OMW concentration factor was 1.72 and 1.4 for PTFE and PVDF membrane, respectively.

Chemical recovery or separation from aqueous solution is one of several applications of MD. Madhumala et al. used MD to recover hydrochloric acid (HCl) from

aqueous solutions in chloralkali and chemical process industries [146]. The feed solution was 32.8 wt.% of aqueous HCl with color forming Fe compounds and heavy hydrocarbon (C_9–C_{14}) impurities. The results showed that colorless aqueous permeate with 33 wt.% of HCl and negligible impurity levels was obtained at a high flux. Gupta et al. applied SGMD with carbon nanotube immobilized membrane (CNIM) to remove isopropanol (IPA) in IPA-water mixture [147]. The enhancement in separation factor was 350% at 70 ºC and mass transfer coefficient was increased by 132% for CNIM, compared to the original membrane. Xie et al. also used SGMD, but for ammonia removal [90]. The feed solution contained 100 mg/L of ammonia and the best performance obtained at the highest temperature and the fastest permeate gas flow rate was 97% ammonia removal that made the treated water containing only 3.3 mg/L of ammonia. Banat and Al-Shannag succeeded in recovery of acetone-butanol-ethanol (ABE) from aqueous solution via MD [148]. They also found that butanol could be separated with the highest selectivity and flux, though it has the highest boiling point. With the different volatility of the chemicals, MD can also be applied to separate a chemical from a mixture. Tomaszewska and Mientka employed MD to separate HCl from a mixture of HCl and sulphuric acid (H_2SO_4) [149]. HCl is a volatile compound, while H_2SO_4 remained in the mixture, so HCl can be separated from this mixture by MD. At higher concentration of both acids, HCl was removed from the mixture under the process conditions. From the experiments, the HCl flux significantly increased with an increase in the temperature.

MD can be used not only as a stand-alone system, but it also with other membrane techniques such as FO or RO as a hybrid system. Zhang et al. used a hybrid system of FO and MD to recover water from oily wastewater [41]. They stated that at least 90% water

recovery could be achieved and oil and salt were almost rejected by the hybrid system. Wang et al. employed the same hybrid system to concentrate the protein solution [150]. The results showed that the hybrid system is stable in continuous operation and is promising for the concentration of pharmaceuticals/protein solutions in the future. MD along with crystallizer called membrane distillation crystallization (MDC) can be used to produce salt crystals [151]. In the system, MD is used to dewater in order to generate the supersaturation in crystallizer where the salt crystals are produced by precipitation.

2.3 Approaches to Enhance the Performance of MD

Although the MD system showed several merits in water purification and other separation, the system has some demerits. One of the disadvantages of MD is that there are no the modules and specific membranes for MD available in the market. However, a major disadvantage of MD for competition with other techniques used in industrial sector is the low permeate flux [49]. A variety of methods have been developed to enhance the permeate flux of MD. The approaches may be divided into two main categories: process modification and membrane improvement.

2.3.1 Process Modification

Various methods have been adopted to modify the MD process in order to enhance the performance of the system. Techniques such as microwave irradiation, ultrasonic irradiation, turbulence promoters, and air bubbling have been employed to improve the permeate flux and the different mechanisms were proposed to support the enhancement of flux.

Microwave, the electromagnetic wave, has been widely applied in water treatment and wastewater treatment [152, 153], including MD. Ji et al. investigated the application of microwave to VMD to desalt NaCl solution [154]. The experimental setup was designed by placing the MD module in the microwave cavity. They reported that microwave irradiation could successfully bring uniform heating in the radial direction of the membrane module and significantly enhance the permeate flux in VMD. The maximum mass transfer coefficient increased about 27.7% at the temperature 60 ºC. The proposed mechanism was that, with the high dielectric constant of water, the microwave can be used to break the hydrogen bond of water-water and water-salt clusters which accelerate the escape of molecules from the bulk solution. Roy et al. presented the results of microwave-induced membrane distillation (MIMD) where microwave radiation was used as a heat source for DCMD [155]. The results showed that the flux enhancement for MIMD was 52% higher than that of conventional heating, while the mass transfer coefficient of MIMD was nearly 99% higher than what was observed under conventional heating. They claimed that the enhancement in MIMD was due to non-thermal effects such as the generation of nanobubbles, localized superheating, and breaking down of the hydrogen-bonded salt–water clusters. Microwave was also applied to reduce the scaling in MD and the decrease of flux. Humoud et al. investigated the scaling reduction of high concentration of $CaCO_3$, $CaSO_4$, and $BaSO_4$ solutions in MIMD on carbon nanotube immobilized membrane [156]. Their experimental setup is illustrated in Figure 2.14. The results indicated that the salt deposition on the membrane for MIMD was 50-79% less that of the conventional heating. They concluded that MIMD not only provided a higher flux, but also significantly reduced fouling with the inorganic scalants.

Ultrasonic irradiation has been used to enhance the performance of MD [157, 158]. Two main mechanisms of ultrasonic technique, namely ultrasonic cavitation and acoustic streaming, were proposed for the enhancement of permeate flux [159]. Acoustically excited bubble break-ups was attributed to the ultrasonic cavitation. The bubble break–ups generated the hydraulic pressure impulses that led to increase in the vapor partial pressure in feed side, while the vapor pressure in permeate side kept constant and resulted in the permeate flux enhancement. Acoustic streaming is an averaged jet stream that resulted from acoustical fluctuations nearby the membrane surface. The streaming induced feed flow turbulence near the membrane surface which reduced temperature polarization and concentration polarization and led to flux enhancement. With different mechanical effects generated from ultrasonic, this technique has also been applied to mitigate the membrane fouling in MD [160]. Hou et al. employed ultrasonic irradiation to control the membrane fouling from silica scaling [161]. The results demonstrated that the permeate flux was stable and enhanced by 43% with ultrasonic irradiation. They explained that the continuous liquid-membrane interface stimulation was ascribed to microstreaming, shock wave, and acoustic vortex streaming; this effectively kept the membrane clean and consequently fouling was controlled.

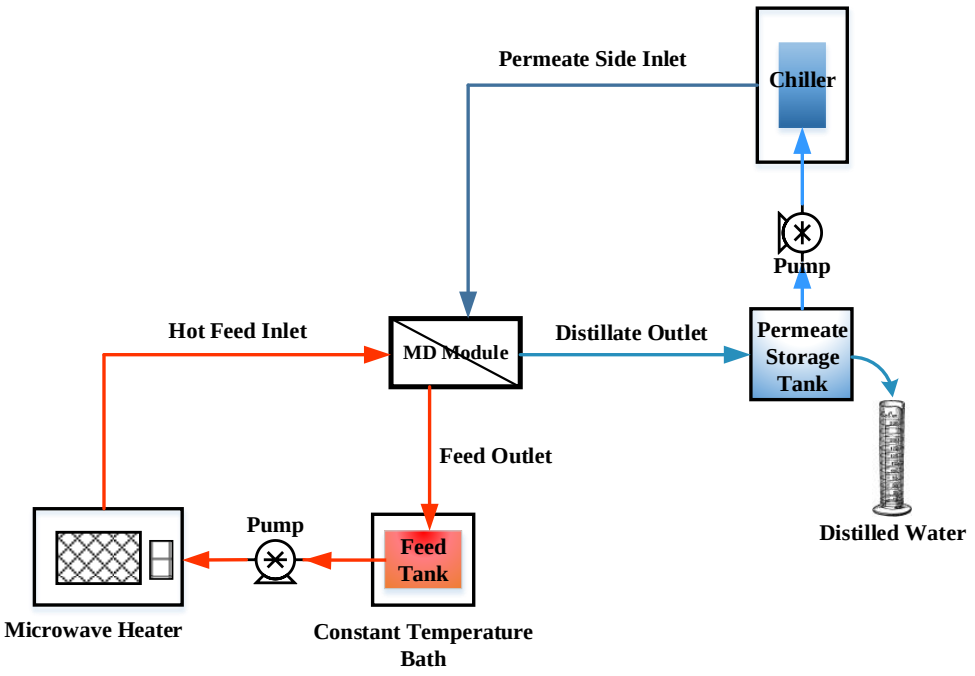

Figure 2.14 Experimental setup of MIMD in the reduction of scaling.
Source: [156]

Several concepts have been introduced to MD module modification in order to obtain the flux enhancement. Channel spacer, a turbulence promoter, is one of the concepts used to improve the performance of MD [162-166]. Martinez-Diez et al. reported that the permeate flux was increased, when spacer or screen separator was placed in a flat membrane module [162]. The heat transfer coefficient for heat and mass transfer equation indicated that there was the appearance of turbulences in liquid/vapor interface when the channel spacer was used. Phattaranawik et al. used the spacer-filled channels in DCMD [163]. They found that, with spacer-filled channels, the permeate flux was enhanced by 31-41% higher than without spacers. The results from calculation indicated that the temperature polarization coefficients were considerably increased when the spacer was filled in the channel. This is in line with the previous study. Shakiab et al. used computational fluid dynamics simulations to investigate the effect of spacer orientation on

the temperature polarization in MD [166]. The results showed that the orientation of spacer affected the temperature polarization and heat transfer rate. For instance, when spacer filaments touched the top or bottom surfaces of a membrane, the temperature polarization is high which results in low heat transfer rates. Whereas these filaments are detached from the membrane, temperature polarization is lower. In addition to the spacer, other turbulence promoters such as baffles and modification of membrane geometries have been tested to improve the permeate flux [167]. Teoh et al. employed different hollow fiber membrane modules with baffles and modified hollow fiber geometries in MD. They found that the permeate flux was significantly enhanced with baffles, which could increase the heat transfer coefficients from 2600 W/(m^2 K) for the unbaffled module to 3150 and 3750 W/(m^2 K) for the window and helical baffles, and suppressed the temperature polarization in the module. Meanwhile, the application of hollow fiber membrane configurations with wavy geometries (namely twisted and braided modules) provided permeate flux as high as 36% without any external turbulent promoter.

Air or gas bubbling is a technique applied in MD [168-173]. Chen et al. incorporated gas bubbling into DCMD to investigate its effect on the MD performance [168]. They reported that the gas bubbling not only enhanced the permeate flux by 26%, but also delayed the formation of salt deposition that resulted in the procrastination of flux decline, compared to the module with spacers. This was due to intensified local mixing and physical flow turbulence in the liquid boundary layer on the feed side. Wu et al. studied the effects of air bubbling on the performance of VMD and the heat and mass transfer [171]. The results showed that the air-bubbling method clearly improved the performance of VMD with an enhanced flux of about double. The study also showed that altered flow

pattern with air-bubbling was the key factor affecting the mass and heat transfer efficiencies. With the modeling study, the result indicated that temperature polarization coefficient (TPC) and concentration polarization coefficient (CPC) in VMD process were greatly affected by flow patterns. Warsinger et al. carried out the experiment by incorporating air recharging and superhydrophobic membrane to study the mechanism for preventing fouling in membrane distillation [172]. The effect of maintaining air layers on the surface of superhydrophobic membrane on membrane fouling was studied. The mechanism of fouling prevention was proposed that the air layers may replace fouling gels, decrease the area of feed in contact with the membrane, lower foulant adhesion, and improve superhydrophobicity of the membrane.

2.3.2 Membrane Improvement

Membrane substantially influences mass and heat transfer phenomena in MD and directly indicated the performance of the system. Therefore, membrane improvement has continuously received attention from researchers in this field. Hydrophobicity of the membranes have been improved by novel hydrophobic materials and surface medication methods. These developments have stimulated the significant growth in MD field.

2.3.2.1 Novel Hydrophobic Materials for Membrane Fabrication. Novel hydrophobic membranes have been synthesized by a copolymer between the soluble PVDF and the highly hydrophobic PTFE. The advantages of this copolymer are well solubility in common solvents and high hydrophobicity and tensile strength. Moreover, the copolymer is also appropriate to make microporous hydrophobic membranes for MD via different processes. Polyethane-co-chlorotrifluoroethene was used to fabricate flat sheet and hollow fiber membranes [174, 175]. The result showed that the ECTFC flat sheet membrane had

excellent hydrophobicity [174], high permeate flux, and high salt rejection including exceptional anti-fouling properties, while the ECTFE hollow fiber membrane had as high as 97% of salt rejection and the lower intensity of pore wetting compared to PVDF membrane [175]. Feng et al. applied polyvinylidene fluoride-co-tetrafluoroethylene to make flat sheet membrane for DCMD [176]. They reported that the PVDF-co-TFE membrane exhibited the high contact angle and high permeate flux over the PVDF membrane. Zheng et al. fabricated the hydrophobic flat sheet membranes using polyvinylidene fluoride-co-chlorotrifluoroethene via the non-solvent induced phase separation (NIPS) process for membrane distillation (MD) and studied the effect of LiCl-based mixed additives on the membrane properties [177]. They found that the mixture of PEG and LiCl with the ratio of 1:1 showed optimal properties and MD performance for combining the structure of higher hydrophobicity and pore interconnectivity, small pore size, and narrow pore size distribution.

Copolymers mixed with other hydrophobic materials such as CNTs have been utilized to prepare the MD membrane. To gain additional mechanical and hydrophobic properties, Tijing et al. employed polyvinylidene fluoride-co-hexafluoropropylene (PcH) mixed with 1-5wt% of CNTs to fabricate the membrane via electrospinning process [178]. The mixed matrix membranes demonstrated highly-porous structure, comparable pore sizes with a commercial flat-sheet PVDF, higher porosity (>85%), higher flux with 33-35% enhancement. They claimed that their nanofiber membranes containing CNTs with one-step electrospinning fabrication had high potential for DCMD desalination application.

Sole CNTs have also been employed to fabricate membranes for MD. Dumee et al. used CNTs to make the self-supporting carbon nanotube (CNT) Bucky-Papers for DCMD [179]. The self-supporting carbon nanotube (CNT) Bucky-Papers membranes exhibited

highly hydrophobic with contact angle of 113°, 90% porosity, and provided a flux rate of ~12 kg/m^2 h at a water vapor partial pressure difference of 22.7 kPa with 99% salt rejection.

2.3.2.2 Surface Modification. Diverse membrane modification techniques with hydrophilic polymers and other materials such as carbon-based materials have been applied to alter the properties of membrane surface for MD. The examples of these methods—namely chemical modification, plasma technology, surface modifying macromolecules, and immobilization of carbon-based materials—will be reviewed in this section.

Chemical membrane modification is the method that chemically coats the hydrophobic materials on the polymer base which is hydrophilic or hydrophobic polymers. A spin coating method was adopted to coat hydrophobic styrene-butadiene rubber on polyamide membranes. The modified membrane provided the flux as high as 5-17 kg/m^2 h with 99.9% salt rejection [180]. Yang et al. employed perfluoropolyether to modify a PVDF hollow fiber membrane for DCMD [181]. The modified membrane displayed higher hydrophobicity and mechanical strength; smaller maximum pore sizes and narrower pore size distributions led to more sustainable fluxes and higher water quality (distillate conductivity < 1 μS cm^{-1}). Razmjou et al. modified the PVDF porous membrane by depositing TiO2 nanoparticles via a low temperature hydrothermal (LTH) process, and then coating by a low surface energy material H, 1H, 2H, 2H-perfluorododecyltrichlorosilane [182]. The liquid entry pressure (LEP) and water contact angle of the modified membrane were increased from 120 kPa and 125° to 190 kPa and 166°, respectively. Although the results showed that the pure water flux of the modified membrane was lower than that of the virgin membrane particularly at higher temperatures;

the ability for salt rejection of the modified membrane was found to be higher over the period of the experiment.

Hydrophobic polymer layers can simply be coated on the polymeric surfaces via the plasma spray process. A hydrophobic polymer material in the form of powder is injected into a plasma flame, where it is rapidly heated and accelerated to a high velocity and spread on the membrane surface. Vinyltrimethylsilicon/tetrafluoro- methane mixture was used to coat a cellulose nitrate (CA) via plasma technique under medium vacuum pressure [183]. The modified hydrophilic membrane exhibited the hydrophobic property with water contact angles of 120º and salt rejection of 96.4%. The flat sheet and the hollow fiber hydrophilic polyethersulfone membranes displayed the higher contact angle of 120º and 144º, after they were coated with tetrafluoromethane via high vacuum plasma modification [184, 185], and there was no leakage during DCMD operation.

Fluorinated surface modifying macromolecule was used to hydrophobize the membrane via the phase inversion process. The molecules can be mixed with hydrophilic polymers such as polyetherimide (PEI) [186] and polysulfone (PSU) [187]. In the fabrication process, the macromolecules move to the membrane surface to minimize the surface tension and form the hydrophobic layer. Essalhi and Khayet tested this composite porous hydrophobic/hydrophilic membrane with DCMD and AGMD [186]. They reported that this membrane was more suitable for DCMD than AGMD for desalination. The results showed that the permeate flux of DCMD was 2.7–3.3 times higher than that of the AGMD, while the permeate flux of AGMD was 14.9 kg/m^2 h with salt rejection of higher than 99.4%.

Carbon-based materials such as CNTs, GO and their derivatives have been employed to modify the MD membranes for desalination and other separations. Carbon nanotubes exhibit hydrophobic property in nature, which is suitable for the hydrophobization of the membrane for MD. In addition, these materials have a high specific surface area (SSA), rich porous structure and high sorption capability [188]. Roy et al. immobilized carbon nanotube immobilized membrane (CNIM) on the porous polypropylene membrane for desalination using DCMD [189]. They reported that the permeate flux for CNIM was as high as 36.8 kg/m^2 h at 70 ºC, which was 51.5% higher than the original PP membrane at salt concentration of 10,000 ppm of feed solution, and the salt rejection was greater than 99.9% at the same salt concentration. For CNIMs, the mechanisms for flux enhancement in desalination were adsorption-desorption of water vapor on CNT surface and water vapor interaction with polar functional groups, resulting in activated diffusion, and membrane hydrophobicity enhancement by the hydrophobic polymer binder (as illustrated in Figure 2.15). Bhadra et al. made the bilayered structure carbon nanotube (CNT) immobilized membrane for DCMD desalination [190]. The PTFE membrane was coated with CNTs functionalized with a hydrophobic octadecyl amine group on the feed side, while carboxylated CNTs was immobilized on the permeate side of the membrane. These immobilization improved the hydrophobicity on the feed side to provide higher water vapor permeation and turned the permeate side to more hydrophilic to facilitate the condensation of water vapor. They reported that the flux from the bilayered structure membrane was as high as 121 kg/m^2 h at 80 °C, which was an enhancement of 70% over the unmodified membrane. Bhadra et al. also developed the immobilized graphene oxide on the PTFE membrane [191]. The water vapor flux was found to be as

high as 97 kg/m^2 h at 80 °C with complete salt rejection. They proposed that the enhancement in flux was attributed to multiple factors, including selective sorption, nanocapillary effect, reduction in temperature polarization as well as the presence of polar functional groups in graphene oxide. In addition to desalination, the carbon-based nanomaterials immobilized membranes have also been applied for solvent separation. Gupta et al. applied the CNIM to remove isopropanol (IPA) from its aqueous solution by SGMD [147]. The modified membrane provided the higher selectivity and mass transfer coefficient than the corresponding unmodified PTFE membrane. The maximum enhancement in a separation factor was 350% at 70 °C and a mass transfer coefficient was 132% at a feed flow rate of 42 mL/min. In addition, Gethard et al. utilized CNIM to simultaneously concentrate pharmaceutical waste and generate pure water [192]. They claimed that the performance of CNIM was highly superior to the pristine membrane with greater enrichment factor of 421% and mass transfer coefficients of 543%.

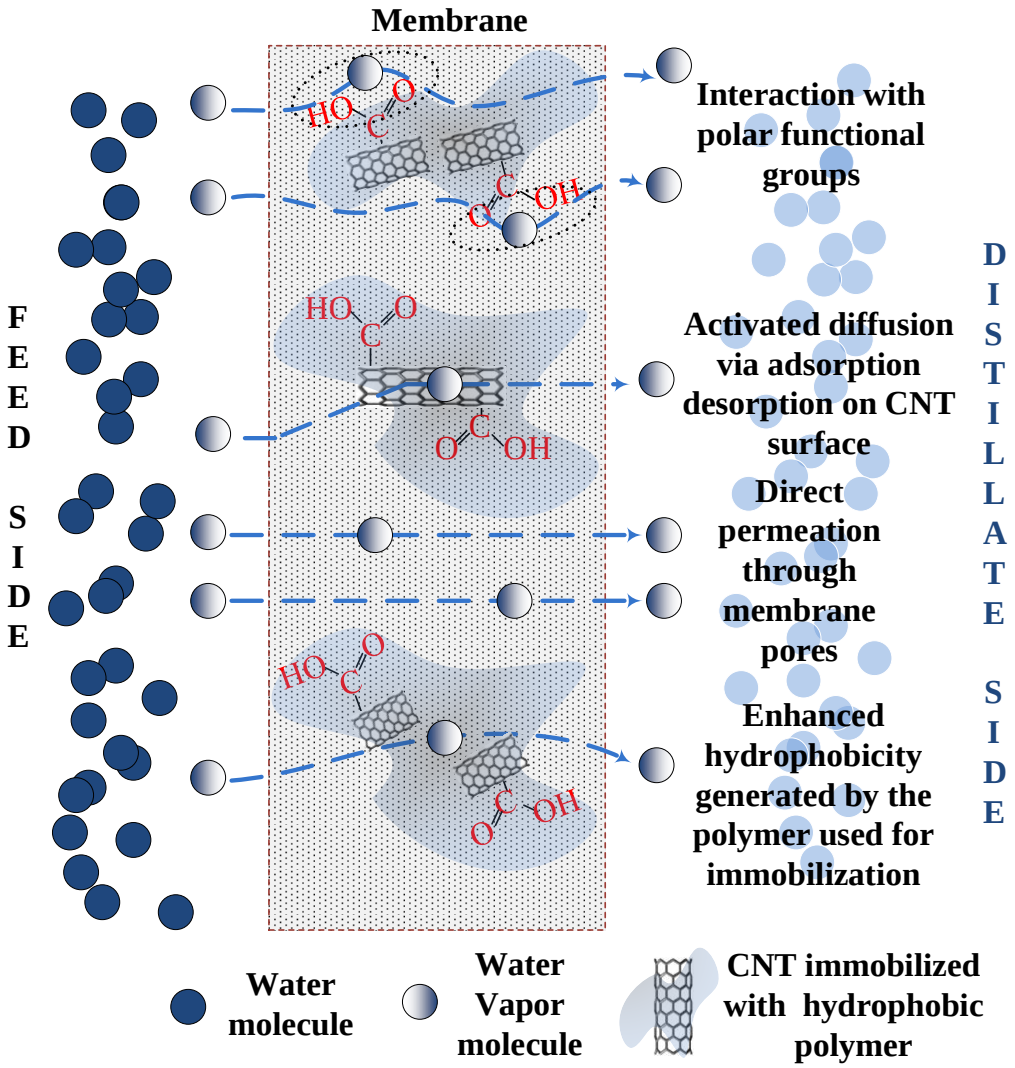

Figure 2.15 Schematic of proposed mechanisms for CNIM.
Source: [189]

CHAPTER 3

IMMOBILIZATION OF GRAPHENE OXIDE ON PERMEATE SIDE OF A MEMBRANE DISTILLATION MEMBRANE TO ENHANCE FLUX

3.1 Introduction

The demand for clean water has considerably increased around the world and is becoming a critical issue due to increasing population and growing industrialization [193]. The consumption in industrial sector alone was up by more than 200% in 2015 compared to 1995 [194]. The amount of freshwater in the world is limited and much of it is polluted, consequently brackish or sea water are attractive sources of pure water [36]. However, energy efficient, cost effective desalination processes are important for that to happen. There are two most popular techniques for desalination namely reverse osmosis (RO) and multi-stage flash (MSF) distillation [16, 195]. While these are well established techniques that have much merit, they face limitations such as high energy consumption, fouling and high capital investment [196]. As a result, alternative desalination technologies including solar evaporation and membrane distillation (MD) are being explored [16, 155].

In MD process, a hot feed is used to generate a vapor pressure gradient across the porous hydrophobic membrane and the vapors are condensed in a cold permeate [189, 197, 198]. The process can be conducted at a relatively low temperature (50-90 ºC), hence waste heat, solar energy or geothermal energy can be utilized as heat sources for heating the brine [43, 134, 199-201]. Other advantages include high rejection of the dissolved non-volatile species, able to handle highly concentrated brine with less fouling, low operating pressure, and less space requirement compared to MSF [9, 197, 202, 203]. However, MD still is faced with some barriers such as relatively low water vapor flux in comparison with other

conventional systems, flux reduction due to temperature and concentration polarization, pore wetting and membrane fouling, and lack of high-efficiency membranes [103, 204].

Several hydrophobic polymers including polytetrafluoroethylene (PTFE), polypropylene (PP), polyvinylidenedifluoride (PVDF) have been utilized as membrane materials [47, 59, 198, 205] and different methods have been employed for the synthesis and modification of these membranes to improve the performances [190, 206-217]. Nanotechnology has enabled the development of advanced membranes based separation techniques [190, 203, 206, 208, 211, 213-216, 218-220]. Nanomaterials (NMs) such as Fe_3O_4, TiO_2, SiO_2, carbon nanotubes (CNTs), nanodiamonds (NDs) and graphene oxide (GO) have been incorporated via blending or coating method to improve the membrane efficiency [189-191, 203, 206, 214-216, 220-222], and different functionalized CNTs were used to fabricate a bilayered structures that have shown significant enhancement in flux [190]. Recently, GO has found a niche in membrane separations [223, 224]. The GO is comprised of highly oxidized graphene sheet having various functional groups including hydroxyl, carbonyl and epoxy groups on its surface. These functional groups minimize the aggregation of GO in dispersion state, provide reaction moieties and make GO hydrophilic [225]. Recent studies have shown that GO could potentially improve the mechanical properties as well as selectivity, antifouling, and the permeate flux [214, 226-228].

In MD, membrane itself plays the crucial role in enhancing the flux and selectivity. While most of the researches have focused on different membrane modifications [206, 209, 210, 212, 214, 228], our previous studies have shown that permeate side hydrophilization of the membrane can improve the water vapor permeation rate significantly [202]. The rapid water vapor removal from the permeate side boundary layer is one of the most

important consideration in increasing the concentration gradient for enhanced mass transfer. However, hydrophilization using strong oxidizing agents are quite hazardous and tend to reduce the mechanical strength of the membrane. An approach that involves NM modification by immobilizing hydrophilic NMs has the advantage of improving membrane characteristics as well as easy adjustment. GO can be significantly hydrophilic with high oxygen content and it is conceivable that the hydrophilicity of the permeate side can be improved by incorporation of GO. In our previous study, the immobilization of the GO in the feed side have shown significant enhancement in flux [191]. There, the GO was instrumental in enhancing the partition coefficient and permeation of water vapor from the feed side. In the present study, we present a complimentary approach where the GO is immobilized on the permeate side. Here, the GO enhances the overall flux by providing sites for condensation of the permeated water vapor, which facilitates the rapid removal of water thus enhancing overall mass transport.

3.2 Materials and Methods

3.2.1 Materials

Sodium chloride (NaCl), acetone, GO sheet (42-52 % carbon), and polyvinylidene difluoride (PVDF) powder (mol. wt.~500 K) were purchased from Sigma–Aldrich. Deionized water was used in all experiments. The membrane used in the MD experiments was flat composite PTFE membrane supported with polypropylene nonwoven fabric (Advantec MFS, 129 μm thick, 0.2 μm pore size and 70% porosity).

3.2.2 Experimental Procedure

MD experiments were conducted in the direct contact MD (DCMD) configuration. Figure 3.1 shows the schematic diagram of the MD system used in the laboratory. The system consists of a DCMD cell and PTFE membrane with an effective contact area of 11.94 cm^2. The feed and permeate flow were regulated by peristaltic pumps (MasterFlex Easy Load, Cole-Parmer, USA). The hot aqueous NaCl solution at different concentrations was passed through the feed side of the membrane in the DCMD cell and the cold distilled water was pumped through the permeate side of the membrane. Additional hot water was supplied to the feed water reservoir throughout the experiment to maintain concentration constant. A counter current flow mode was used for feed and permeate water flow through the module. The constant temperature water bath (Neslab Water Bath Model GP 200, NESLAB Instruments, Inc, Newington, NH, USA) was used to maintain constant feed temperature, and the permeate temperature around 18ºC was controlled by a bench top chiller (Polyscience LS5, Cole-Parmer, USA). Temperatures of feed and permeate side were monitored by temperature sensors (Four-channel Data Logging Thermometer, RS-232, Cole-Parmer, USA). The experiment was repeated for three times and less than 1% relative standard deviation was observed.

3.2.3 Fabrication of GOIM-P

In fabrication of the graphene oxide immobilized membrane on the permeate side (GOIM-P), the uniform dispersion of GO in the organic solvent and immobilization of GO on the membrane surfaces are considered most important steps during membrane fabrication. Ten mg of GO was added to 8 gm of acetone and sonicated for ten hours to ensure uniform dispersal of GO into the organic solvent. 0.2 mg of PVDF was separately dissolved in 2

gm of acetone and the PVDF solution was finally mixed with GO suspension. The mixed PVDF-GO suspension was then cast drop wise slowly and uniformly on the permeate side of the membrane to immobilize the GO on the surface. After that, the immobilized membrane was rinsed with extra acetone to remove excess PVDF from the membrane pores and the surface.

3.2.4 Characterization of GOIM-P

A scanning electron microscopy (SEM, Model LEO 1530, Carl Zeiss SMT AG Company, Oberkochen, Germany) was used to characterize the morphology of the fabricated GOIM-P. The samples for SEM was prepared by cutting the membranes into a square of 0.5 cm x 0.5 cm, placing on a specimen stub followed by carbon coating. The GOIM-P was further illustrated by Raman spectroscopy (Thermo Fisher DXR Raman microscope). The thermal stability of GOIM-P was investigated by thermal gravitational analysis (PerkinElmer, TGA 8000). The contact angles measurements were used to study the hydrophobicity/hydrophilicity of the permeate surface using an Attension apparatus (model Theta). The water drop method on dry membrane was employed and five measurements were taken to obtain the average value.

3.3 Results and Discussion

3.3.1 GOIM-P Characterization

Figure 3.2a, b and c show the SEM images of the unmodified PTFE membrane (feed side and permeate side), and GOIM-P (permeate side), respectively. Figure 3.2a clarifies the presence of active pores on the membrane feed surface. While Figure 3.2c demonstrates

the change in morphology from Figure 3.2b due to the immobilization of the GO on the permeate surface.

Raman spectra of the GOIM-P are shown in Figure 3.3. Prominent Raman peaks of support polypropylene layer on the permeate side of the composite membrane were observed at 800, 1500, 2700 and 3000 cm^{-1} [229]. The presence of GO on the membrane is shown at 1349 cm^{-1} that could be ascribed to the graphite defect in the sp^3 domain via oxidation and an additional peak at 1597 cm^{-1} is due to stretching mode of graphite [230].

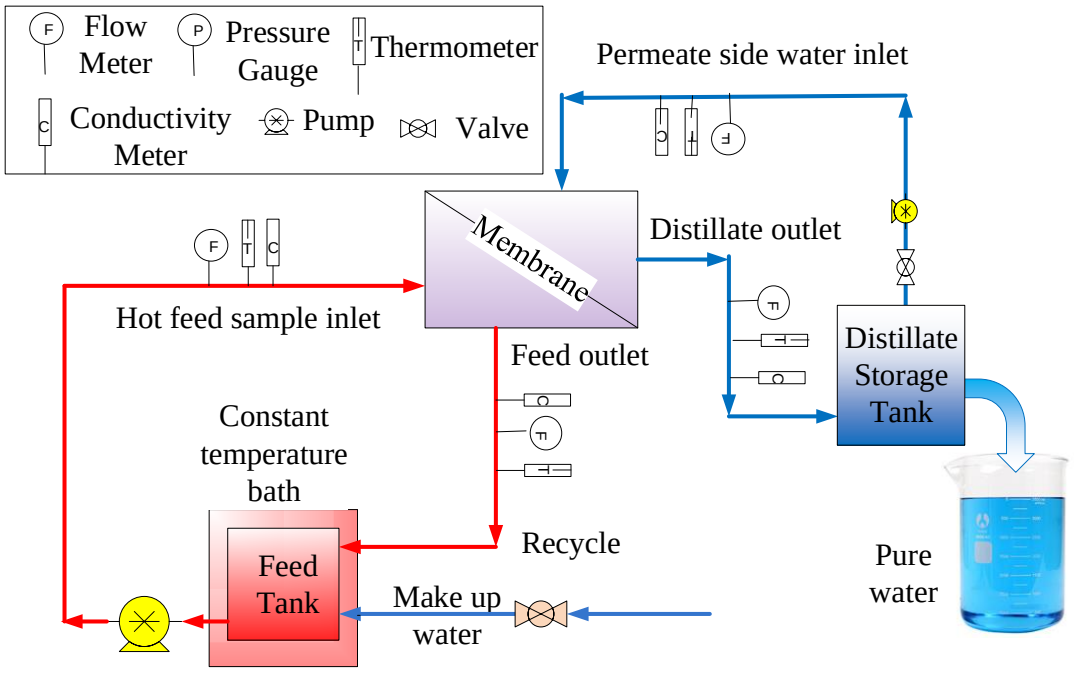

Figure 3.1 Schematic diagram of the experimental set up for DCMD application.

The thermal stability is an important parameter for membranes used in MD as the membranes must resist with high temperature salt solution. In this study, TGA curves were used to evaluate the stability of GOIM-P in comparison with unmodified membrane as shown in Figure 3.4. The weight loss at around 230 ºC to 330 ºC was due to the

decomposition of PP as the supporting layer, while PTFE began to decompose at around 460-470 ºC. It was observed that the presence of GO provided additional thermal stability of the modified membrane. Increasing in the thermal stability of GOIM-P could be due to GO particles and the functional groups on GO that play the role as a reducing and sacrificed agent that lead to slow down or limit the degradation process [231]. The result is in line with what have been reported previously [190, 217].

The hydrophobicity on the permeate surface of GOIM-P was determined by contact angle analysis. After GO immobilization, the contact angle on the permeate side of the modified membrane showed a decrease from 94º ±2 to 75º ± 2. Decreasing of contact angle implied that the hydrophilicity on the permeate side of the GOIM-P increases by increasing the surface energy and this was expected to enhance the membrane performances. The contact angle values and photographs of permeate side of unmodified and GOIM-P are shown in Figure 3.5.

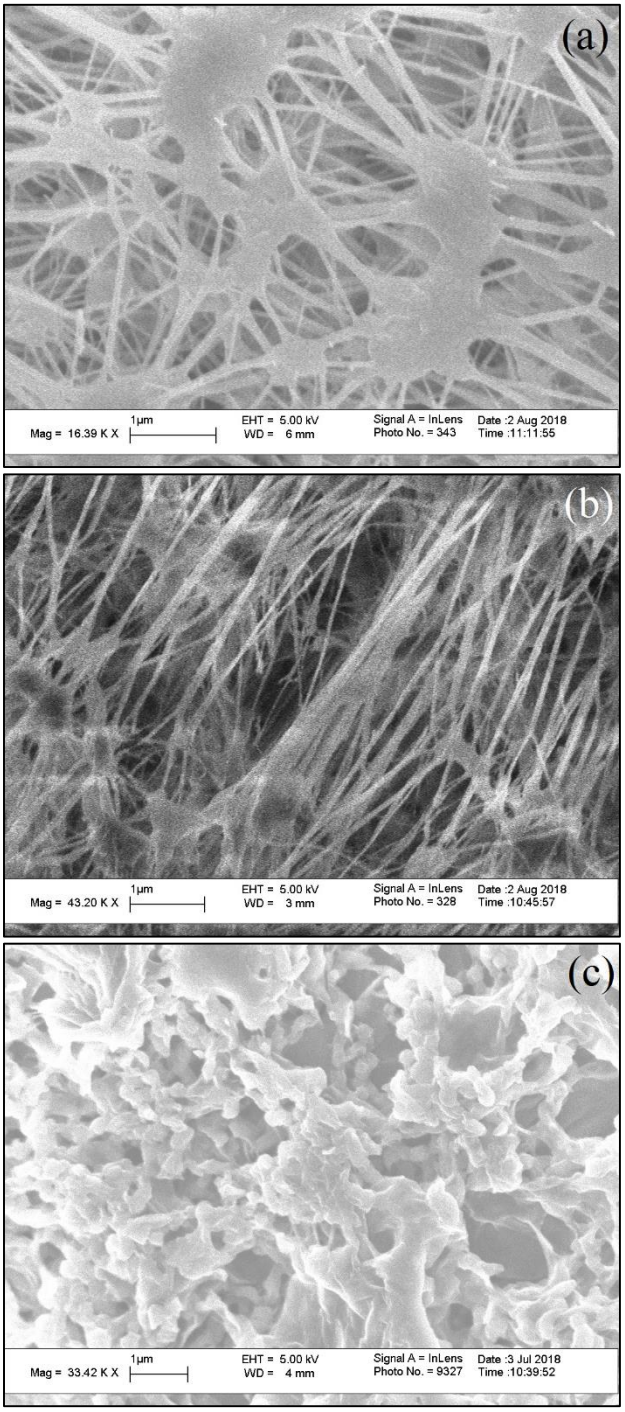

Figure 3.2 Scanning electron micrographs of **a)** feed side, **b)** permeate side of the unmodified PTFE membrane, and **c)** GOIM-P (permeate side).

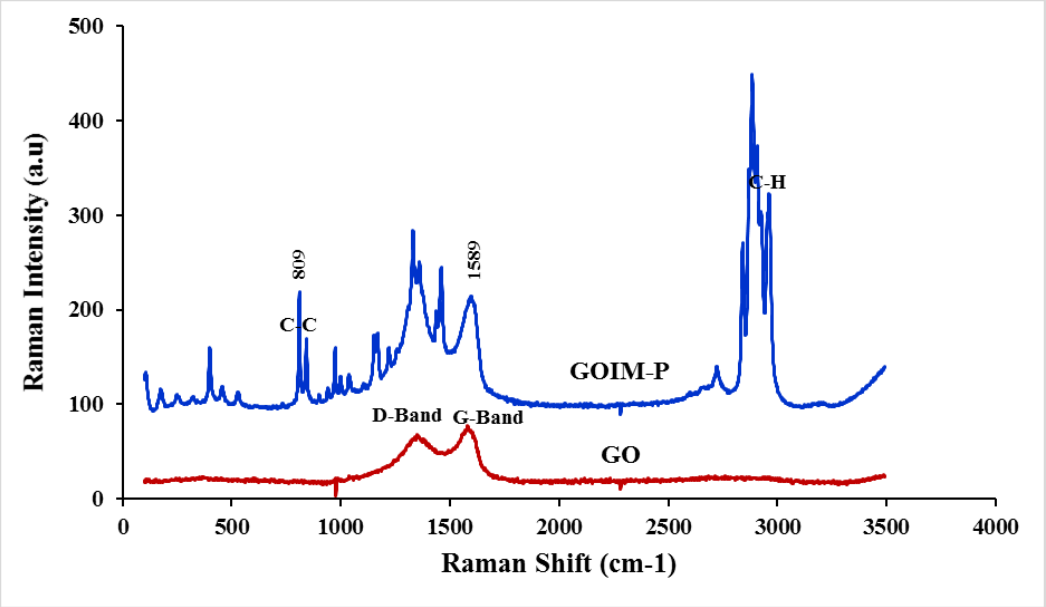

Figure 3.3 Raman spectra of the permeate surface of GOIM-P.

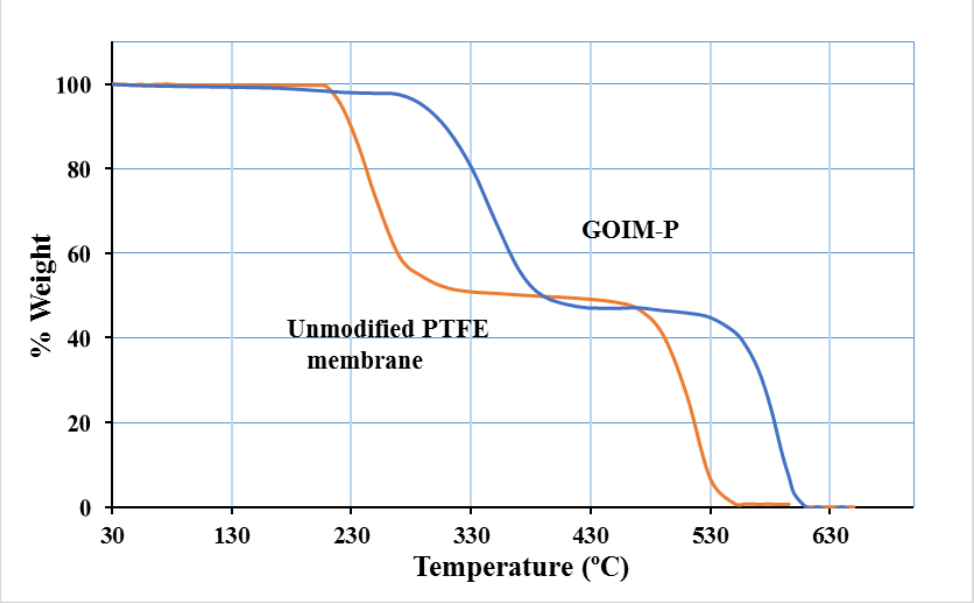

Figure 3.4 TGA curves of unmodified and GOIM-P.

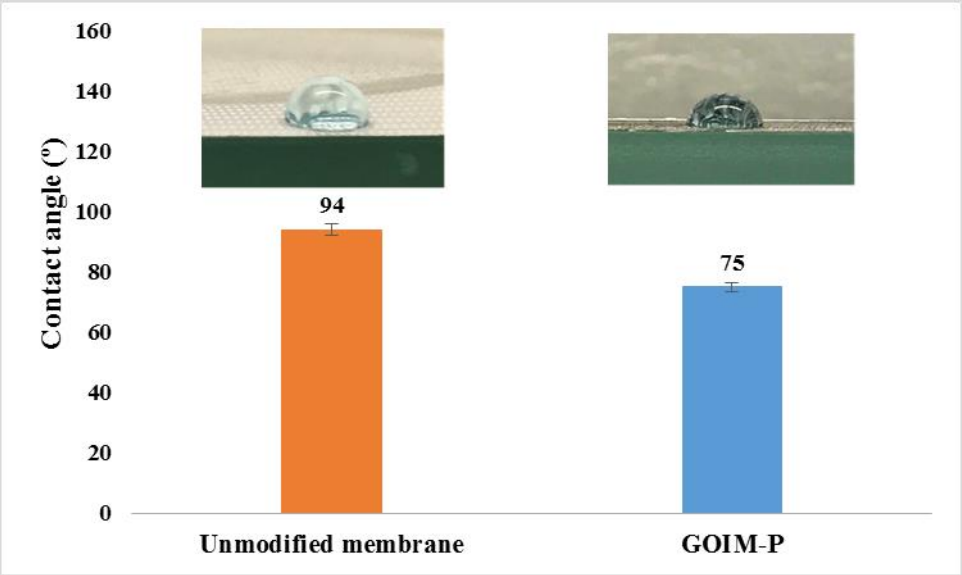

Figure 3.5 Contact angle and photographs of permeate side of unmodified and GOIM-P.

3.3.2 DCMD Performance of GOIM-P

The overall permeate flux, J, is expressed as:

$$J_w = \frac{W_p}{t \cdot \mathrm{A}} \tag{3.1}$$

Where, *Wp* is the total mass collected from the permeate side, t is the run time and A is the effective membrane area. Temperature, feed flow rate and salt concentration were varied in the experiment to evaluate the performance of the GOIM-P, and of the unmodified membrane.

The effect of temperature on permeate flux of the GOIM-P compared to the pristine membrane is illustrated in Figure 3.6 a. It is clear from the figure that the fluxes significantly increased with increase in temperature for both membranes. Increasing in

vapor pressure with temperature plays the major role in flux increment [232]. It is clearly seen that the GOIM-P produced higher amount of permeated water compared to the pristine membrane. Maximum permeate flux was 64.5 kg/m^2.h at feed temperature of 80°C, which is 15% higher compared to the pristine membrane.

The influence of increasing feed flow rate at a constant temperature of 60°C and 200 mL/min permeate flow rate is displayed in Figure 3.6 b. It was observed that the permeate flux increased with increase in feed flow rate in both membranes and the GOIM-P offered higher water vapor flux compared to the unmodified one. The increased feed flow rate enhances the turbulence and reduces the boundary layer effect at the membrane-feed solution interface. These results in the reduction of temperature polarization and improve the permeate flux [37, 233].

Figure 3.6 c shows the effect of varying salt concentrations in feed solution on permeate flux. With increase in concentration, both membranes show a decrease in water vapor flux as expected. The increase in feed salt concentration led to the reduction of the water activity at the membrane-solution interface and the formation of additional boundary layer directly affect the driving force across the membrane and reduces the water vapor flux. Similar results have been reported before [234, 235]. As a result of increasing salt concentration from 3400 to 34000 ppm, the permeate flux reduced from 29.7 to 24.3 kg/m^2.h and 33.9 to 26.8 kg/m^2.h for the unmodified membrane and GOIM-P, respectively. The conductivity of the permeated water did not change with varying salt concentrations indicating complete rejection of the salt.

3.3.3 Mass Transfer Coefficient

The overall, mass transfer coefficient can be described as:

$$J_w = k(P_f - P_p)$$

$$\text{or } k = \frac{J_w}{(P_f - P_p)} \tag{3.1}$$

Where, J_w is the water vapor flux, k is mass transfer coefficient, P_f and P_p are partial vapor pressure of average feed and permeate temperatures. The mass transfer coefficients were found to be higher for GOIM-P as compared to the unmodified membrane.

Table 3.1 summarizes the change in mass transfer coefficients of GOIM-P and the unmodified membrane with varying feed flow rate at 60°C. Both membranes exhibited increased mass transfer coefficient with increase in feed flow rate. The diffusion of the water vapor through the boundary layers mainly controls the overall mass transfer rate of the process. At higher feed flow rate, the turbulence increased that led to the reduction in the boundary layer resistance and significantly increased the mass transfer coefficients. Among these two membranes, GOIM-P exhibited higher mass transfer coefficient in comparison with the pristine membrane.

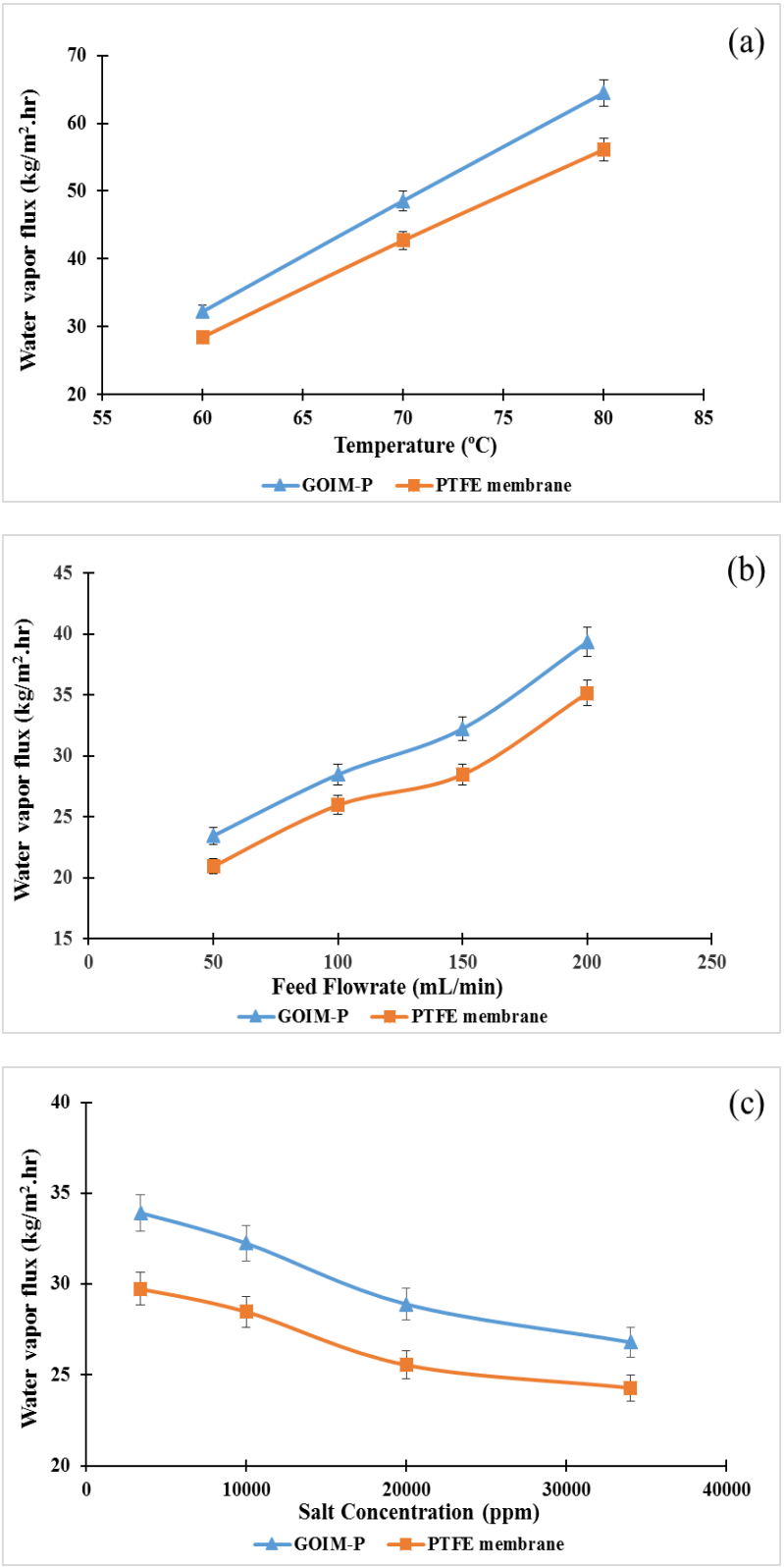

Figure 3.6 Effect of **a)** temperature on water vapor flux, **b)** feed flow rate on water vapor flux, and **c)** feed concentration on water vapor flux.

Table 3.1 Effect of Varying Feed Flow Rate on Mass Transfer Coefficient at 60°C

Feed flow rate (mL/min)	k (kg/m^2.s.Pa) ×10^{-7}	
	Unmodified Membrane	GOIMP
50	3.3	3.7
100	4.1	4.5
150	4.5	5.1
200	5.6	6.2

3.3.4 Stability and Salt Breakthrough

The quality of permeate side water was carefully investigated to monitor the stability of modified membrane and salt breakthrough. The stability of GOIM-P was tested for a long period of operation as shown in Figure 3.7. The permeated water was monitored throughout the experiment to ensure the quality of water by measuring the conductivity of the permeate side water and using Raman spectroscopy [223, 236]. The results did not show any leakage of salt through the membrane and the presence of GO in the permeate water samples.

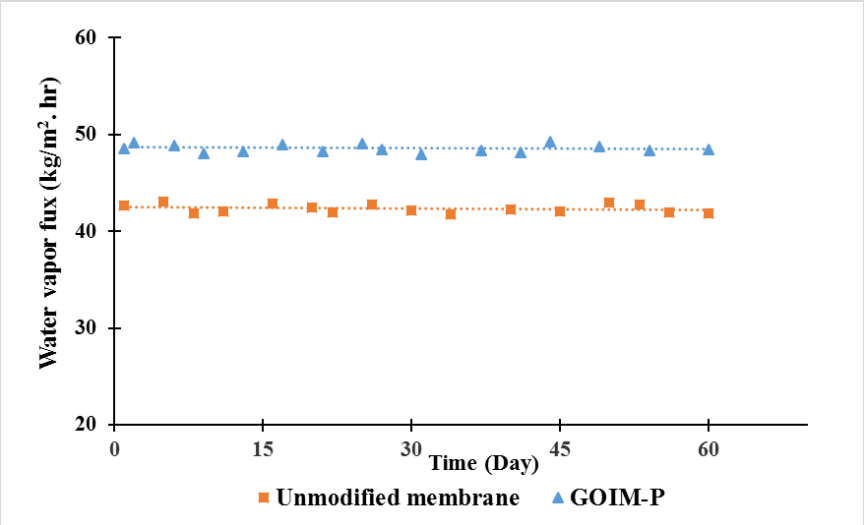

Figure 3.7 Stability of the membranes at a 70 °C feed temperature and 10,000 ppm of NaCl solution.

3.4 Proposed Mechanism

The proposed mechanism in GOIM-P is shown in Figure 3.8. A significant enhancement in water vapor flux was noticed with the inclusion of GO in the permeate side. The hydrophilicity of the membrane permeate side was enhanced due to the presence of polar epoxy, carboxyl and hydroxyl functional groups on GO that allows the water vapor to interact with the modified permeate surface [237, 238]. In MD, the water vapor permeation through the membrane is steered by the vapor pressure gradient present across the membrane. A boundary layer compromising probably of both liquid and vapor phases is formed on both side of the membrane. Although, the feed side layer remains unchanged in GOIM-P, the hydrophilic surface permitted fast water vapor removal, destabilization of vapor-gap and mass transfer resistance reduction between the bulk permeate and membrane surface. These effects are equivalent to the contraction in permeate side boundary layer [202, 239, 240], which led to an enhancement in water vapor permeation through the membrane.

3.5 Conclusion

Graphene oxide was successfully immobilized on the permeate side of the PTFE membrane to increase the pure water flux in direct contact membrane distillation. It was evident that the introduction of hydrophilicity on the permeate side was effective in rapid condensation and removal of the permeate thus enhancing mass transfer coefficient. The DCMD performance of GOIM-P was consistently superior compared to the pristine membrane and attaining a maximum water vapor flux of 64.5 $kg/m^2.h$ at 80°C, which is 15% higher. The membrane was also found quite stable for a longer period of operation.

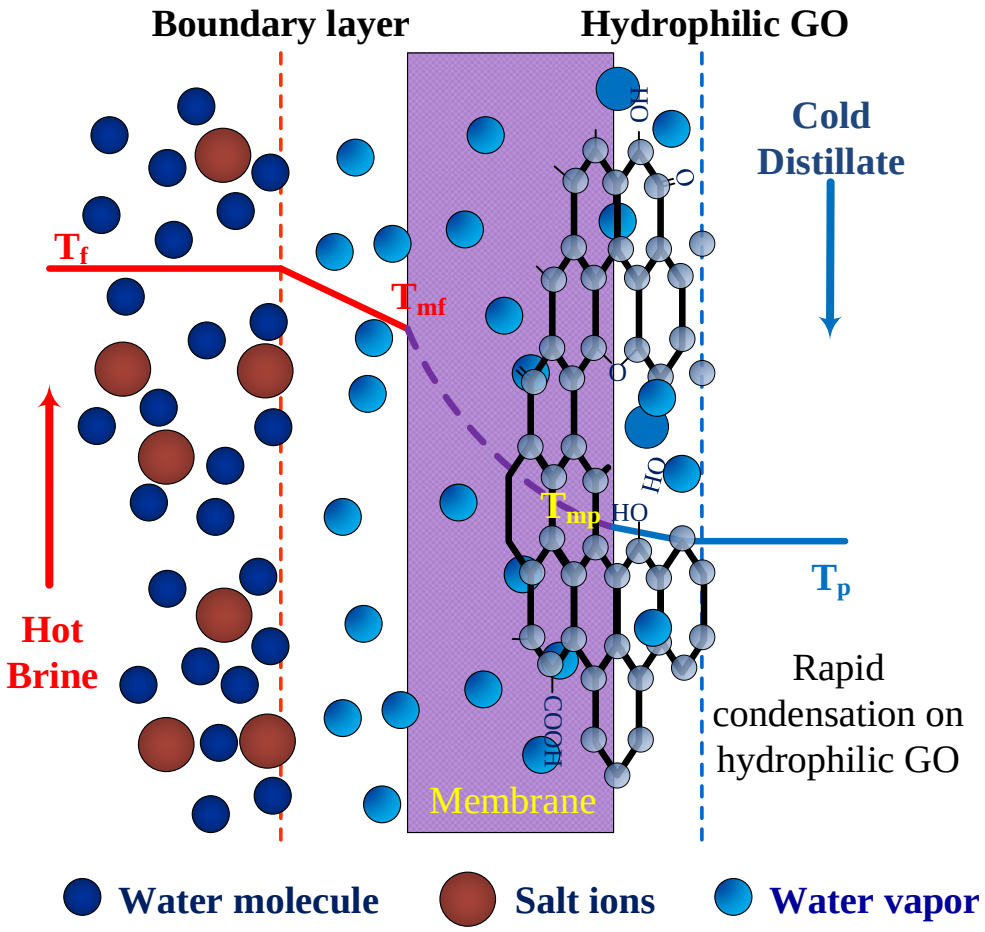

Figure 3.8 Proposed mechanism for GOIM-P.

CHAPTER 4

FUNCTIONALIZED CARBON NANOTUBE IMMOBILIZED MEMBRANE FOR LOW TEMPERATURE AMMONIA REMOVAL VIA MEMBRANE DISTILLATION

4.1 Introduction

Ammonia is a major water pollutant that is directly or indirectly generated from industrial, agricultural and domestic sources. It has high solubility in water, and a small quantity of ammonia can dramatically deteriorate an aquatic environment, and cause considerable harm to water resources [241]. Ammonia can also be converted to a nitrogen source that causes algal bloom, so the accumulation of ammonia in water resources may lead to eutrophication, oxygen depletion and consequently the death of living organisms [242]. Therefore, removing ammonia from water and wastewater is of significant importance.

Ammonia can be removed from water and wastewater via air stripping, adsorption [243, 244], ion exchange [245, 246], and biological treatment [247, 248]. However, these techniques have their limitations including high cost and low efficiency [100]. They also leave large footprints. For examples, biological processes require large space and huge quantities of chemicals, and the effluent air from the stripping process need further purification before emission [100, 249]. As a result, there is a need for alternate separation techniques for ammonia removal.

Membrane distillation (MD) is an emerging separation technique that uses the difference in a vapor pressure between hot feed side and cold permeate side as a driving force [47]. MD has been used as a separation process in a variety of applications such as desalination, waste water treatment, food concentration and volatile organic separations [47, 50, 100, 250-252]. Low temperature operations (40-70^{o}C) is one of the major merits

of MD, so low grade thermal energy, solar or geothermal energy can be used as a heat source for MD [9, 197, 253]. High rejection of non-volatile species, low operating pressure, and relatively low fouling [197] are other advantages of MD that make it attractive over other conventional means. MD has been studied for ammonia separation [87, 90, 100, 241, 250, 251] and the results have shown reasonable removal efficiencies.

Besides module and system configurations [204], the membrane itself is a significant component for enhancing the MD efficiency. Various hydrophobic polymers [42] and modifications via stretching, phase inversion, selective hydrophilization and electrospinning have been used to synthesize and modify MD membranes [42, 180, 185, 186, 202, 211, 212, 217]. However, only the flat-sheet PTFE membrane and the hollow-fiber PP and PVDF membrane have been reported for ammonia separation [87, 90, 100, 241, 250, 251]. More recently, membrane modification by immobilizing nanomaterials such as carbon nanotubes (CNTs) and graphene oxide (GO) have been carried out to enhance membrane properties in MD [189, 191, 198, 222, 254]. The results have shown that flux and stability can be improved by such modifications [191, 203, 255]. CNTs have been used in different membrane applications where they have played the role of sorbents for selective solute transport [147, 256-259]. Simple membrane structures have been made by immobilizing CNTs on conventional membranes (CNIMs) that have led to significantly higher flux and reduced fouling in MD [147, 189, 198, 203, 260-262]. They have been used in desalination, solute concentration as well as for the efficient separation of organic compounds such as, isopropanol (IPA) from aqueous mixtures [147]. A major advantage of CNTs is that surface modification can lead to selective adsorption of solute this increasing the flux and overall selectivity.

In this study, our objective was to investigate the separation of ammonia from water by using CNIMs. Yet another objective was to see if altering the polarity would lead to enhancement in ammonia flux and selectivity.

4.2 Materials and Methods

4.2.1 Chemicals and Materials

Ammonium chloride (NH_4Cl), sulfuric acid (H_2SO_4), sodium hydroxide (NaOH), and sodium carbonate (Na_2CO_3) used in this study were purchased from Sigma Aldrich (St. Louis, MO). Deionized water was used in all experiments. The membrane used in these experiments was flat composite PTFE membrane supported by polypropylene (ANOW, Hangzhou Anow Microfiltration Co., Ltd, Hangzhou, China: 0.45 μm pore size).

4.2.2 CNIM Fabrication and Characterization

Multi-walled carbon nanotubes (MWCNTs) (OD 20–30 nm, length 10–30 μm, purity >95%) were obtained from Cheap Tubes Inc., Brattleboro, VT. While, the functionalized CNTs were synthesized by binding the carboxyl group on the sidewall of MWCNTs via microwave induced reaction in a Microwave Accelerated Reaction System (CEM Mars) according to the detail in our previous paper [263].

In CNIMs fabrication, uniform dispersion of CNTs in the organic solvent and immobilization of CNTs on the membrane surface are the most important steps. CNIM and CNIM-f were prepared with the same procedure as described in our recent paper [147]. 1.5 mg of raw CNTs or f-CNTs was added to 8 gm of acetone and sonicated for 4 h to ensure the uniform dispersal of CNTs. 0.2 mg of PVDF that acts as a binder, was separately dissolved in 2 gm of acetone and the PVDF solution was finally mixed with CNTs

suspension. The PVDF-CNTs mixture was then cast drop wise slowly and uniformly on the membrane surface to immobilize the CNTs on the surface. The wet CNIMs were kept and dried under the hood overnight.

The morphology of the modified membranes and the deposition of CNTs on the membranes were characterized using the scanning electron microscope (SEM, JEOL; model JSM-7900F). Raman spectroscopy (DXR Raman microscope, Thermo scientific) was used to confirm type of CNTs on the surface of membranes and Fourier-transform infrared spectroscopy (FTIR spectrometer, Agilent Cary 600 Series) was used to analyze the carboxyl groups on f-CNTs. The thermal stability of the membranes was tested by thermal gravimetric analysis (TGA, Perkin Elmer TGA 8000). The hydrophobicity/hydrophilicity of the membrane surfaces was determined by contact angle measurement via the drop method. A droplet of water and 300 ppm ammonia solution was deposited on the surfaces of PTFE membrane and CNIMs using a micro syringe (Hamilton, 0–100 μL). The digital video camera was used to record the droplet positions and the contact angle was measured for five times to obtain the average value.

The measurement of liquid entry pressure (LEP) of PTFE and modified membranes was performed via a method published before [264]. A stainless steel chamber (Alloy Products Corp, 185 Psi Mawp) was filled with the aqueous solution of ammonia. The MD module with a membrane was connected to the liquid chamber. A gas cylinder joined with the chamber was used to increase the pressure above the liquid. The increment of pressure resulted in the liquid starting to enter through the membrane pores. The pressure at the onset of the liquid entry into the membrane was the LEP. The measurement was triplicate to ensure reproducibility.

The gas permeation test was used to calculate the effective surface porosity over the effective pore length of the membranes. The measurement was carried out according to the procedure in the literature [265]. The total molar gas permeation flux per unit transmembrane pressure difference across the porous membrane can be expressed as the equation (1) where the first and the second term in this equation refer to the contribution from Knudsen flow and Poiseuille flow, respectively.

$$\frac{J_i}{\Delta P} = \frac{2}{3}\left(\frac{8RT}{\pi M}\right)^{0.5}\frac{1}{RT}\frac{r\varepsilon}{Lp} + \frac{\overline{p}}{8\mu RT}\frac{\varepsilon r^2}{Lp} \quad (4.1)$$

Where ε is surface porosity, r is mean pore radius of the membrane, μ is the gas viscosity, Lp is effective pore length, $\overline{p}$ is the mean pressure (the average of feed and permeate side pressure), M is the molecular weight of gas, R is the gas constant, and T is temperature (K). The gas permeation flux per unit driving force ($J_i/\Delta P$) can be calculated as follows:

$$\frac{J_i}{\Delta P} = \frac{N_{t,i}}{A_t} \quad (4.2)$$

where ΔP is the transmembrane pressure difference across the membrane area A_t. $N_{t,i}$ is total molar gas permeation rate (mol s^{-1}). The total gas permeation rate through the membrane was measured by a bubble flow meter. From equation (1), the mean pore size (r) and the effective surface porosity over pore length, ε /Lp, can be calculated from the slope (S_0) and the intercept (I_0) as follows:

$$r = \frac{16}{3}\left(\frac{S_0}{I_0}\right)\left(\frac{8RT}{\pi M}\right)^{0.5}\mu \tag{4.3}$$

$$\frac{\varepsilon}{L_p} = \frac{8\mu RTS_0}{r^2} \tag{4.4}$$

4.2.3 Experimental Setup

The MD configuration employed for this study was direct contact membrane distillation (DCMD) where the hot ammonia solution was passed through the feed side of the membrane in the MD module without recirculation, while the cold distilled water was recirculated through the permeate side of the membrane with countercurrent flow. However, it is noted that the concept of CNIMs is equally valid for other forms of MD such as sweep gas and vacuum MD. The schematic diagram of the experimental setup for the DCMD is illustrated in Figure 4.1. The flat MD module was made from PTFE with an active contact area of 11.94 cm^2. Peristaltic pumps (Cole-Parmer, Masterflex L/S compact pump model 77240-00 and Masterflex L/S Easy-Load pump head model 7518-60) were used to circulate the feed and permeate flow. The temperature of feed solution was controlled by the constant temperature water bath (NESLAB Instruments, Inc., Water Bath Model GP 200), and the bench top chiller (Cole-Parmer, Polyscience LS5) was used to maintain the permeate temperature. Inlet and outlet temperatures of the feed and permeate sides were monitored continuously using temperature sensors (Cole-Parmer, Four-channel data logger thermometer).

4.2.4 Experimental Procedure

The ammonia feed solutions with different concentrations were prepared through the addition of measured amounts of ammonium chloride to deionized water. The pH of the

solutions was adjusted to 11.5 by adding the NaOH and measured by pH bench top meter (Thermo Scientific Orion Star A111). The performances of PTFE and modified membranes were investigated with different conditions, i.e., concentrations, temperatures, and feed flow rates of the ammonia feed solutions. The titration method following EPA method # 350.2 (see Appendix) was applied to measure the concentrations of ammonia in the receiving water at permeate side. 0.02 N of H_2SO_4 was used as a titrant, 0.02 N of Na_2CO_3 was the primary standard reagent, and the mixture of methyl red and methylene blue was used as an indicator. Each experiment was repeated three times to confirm the reproducibility.

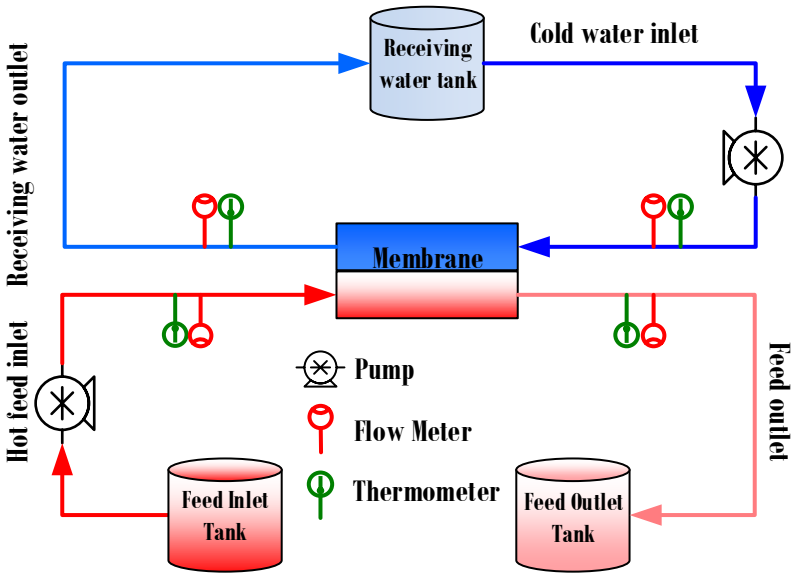

Figure 4.1 Schematic diagram of the experimental setup for the DCMD.

4.3 Results and Discussion

4.3.1 Membrane Characterization

The SEM images of the original PTFE membrane, CNIM, and CNIM-f are shown in Figure 4.2. Figure 4.2a shows the pore structure of the feed side of the PTFE membrane, while Figure 4.2b shows the PP supporting layer on the permeate side. The changes in morphology of the membranes after immobilizing with raw CNTs and f-CNTs at the feed side are shown in Figure 4.2c and d. Both CNTs were uniformly widespread over the entire membrane surface. Raman spectra of PTFE membrane, CNIM, and CNIM-f are presented in Figure 4.3. Prominent Raman peaks of PTFE were at 286, 393, and 730 cm^{-1}, while that of the PP support were between 800 -1200 cm^{-1}. The presence of CNTs on CNIMs showed the signature bands, namely D-band (~1350 cm^{-1}), G-band (~1580 cm^{-1}), and G' band (2683 cm^{-1}). CNIM-f showed the higher intensity of the D-band that was attributed to the high defects on the f-CNTs [266]. FTIR spectra of raw CNTs and f-CNTs are shown in Figure 4.4. The COOH functional groups on the f-CNTs are represented by the peak at 1733 cm^{-1} which can be assigned to the carbonyl (C=O) stretching mode, and the broad peak at 3446 cm^{-1} is attributed to the O-H stretching vibration of carboxyl groups [267, 268].

The photographs of water and aqueous ammonia drops on the surface of the PTFE membrane and CNIMs as well as the associated contact angles are shown in Figure 4.5. The presence of raw CNTs and f-CNTs significantly altered the contact angle of the PTFE membrane. With deionized water, the contact angle for the PTFE membrane was 116 º which clearly showed hydrophobicity, while the contact angles for CNIM and for CNIM-f were 131º and 85º respectively. The increase in contact angle for CNIM was due to the hydrophobicity of the raw CNTs. On the other hand, the polar carboxylic groups of f-CNTs

enhanced the hydrophilicity and significantly reduced the contact angle in CNIM-f. This is in accordance to previous publications [147, 198]. In the ammonia-water mixture, the presence of ammonia reduced surface tension [269] which led to lower contact angles in all membranes as compared to pure water. The average contact angle for PTFE, CNIM, and CNIM-f were 103º, 95º and 80º, respectively. As expected, the contact angles for CNIMs were lower than that for the PTFE membrane, this was due to the higher sorption on the CNTs. Higher ammonia sorption on the surface of CNIM-f can be attributed to the presence of carboxylic groups on CNTs which reduced the contact angle.

The liquid entry pressure (LEP) of PTFE and modified membranes was investigated using DI water and 500 ppm of ammonia solution as feed solutions. The LEP of PTFE and CNIMs tested with DI water and ammonia solution were not significantly different; they were found to be as high as 80 ± 5 Psig. From the gas permeation test, the effective porosity over pore length (ε /Lp) was found to be 1.97×10^{6} m^{-1}. As only a small amount of CNTs was immobilized on the membrane surface, this value did not show any significant change for the CNIMs. This is in line with our previous reports [147, 198].

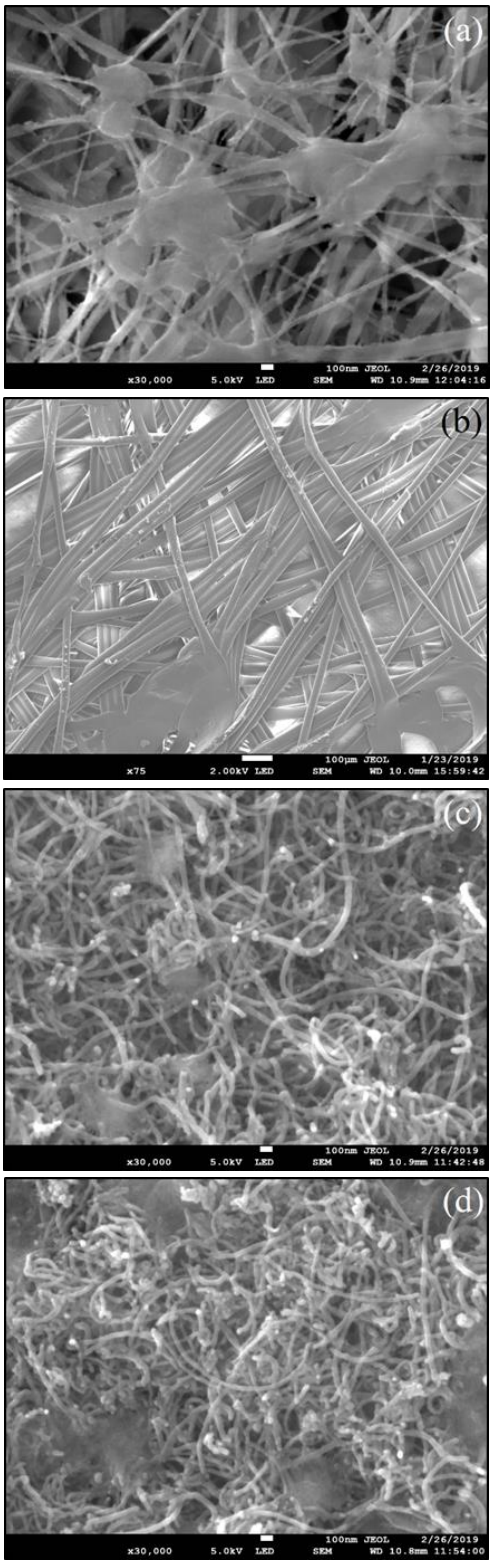

Figure 4.2 SEM images of **a)** the feed side of original PTFE membrane, **b)** the permeate side of original PTFE membrane, **c)** CNIM and **d)** CNIM-f.

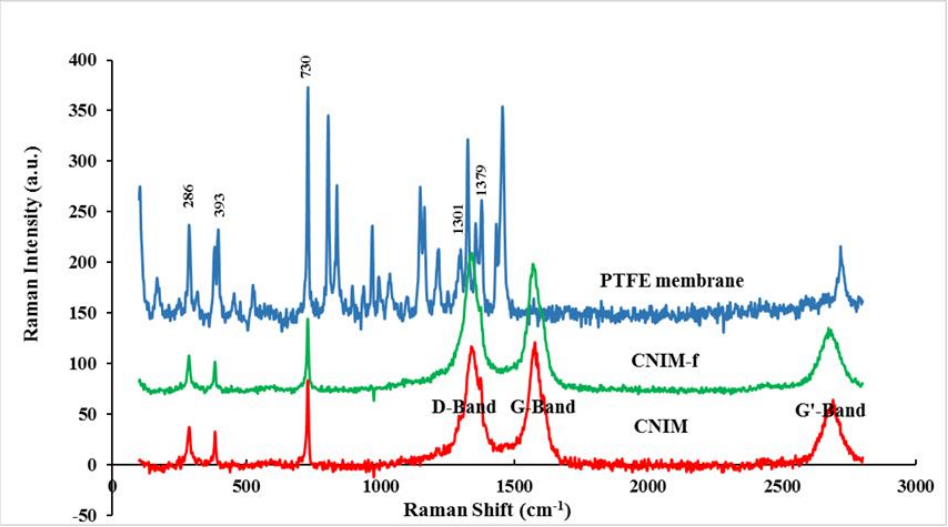

Figure 4.3 Raman spectra of PTFE membrane, CNIM and CNIM-f.

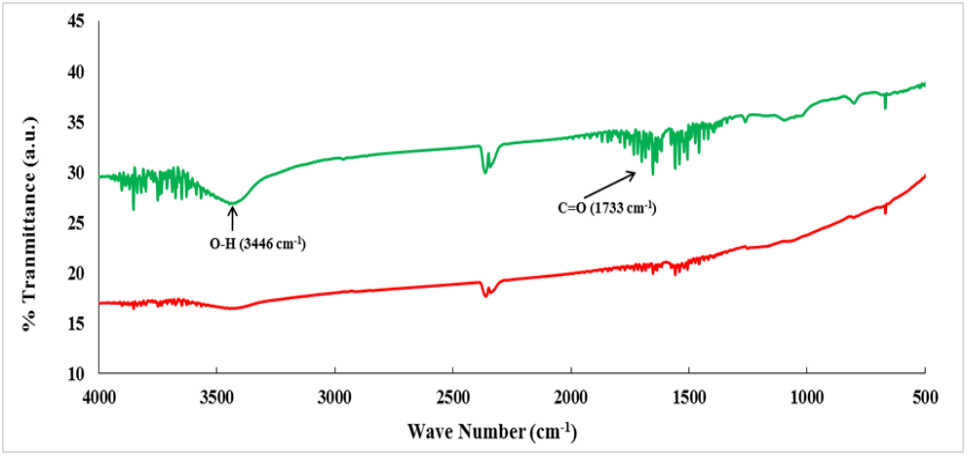

Figure 4.4 FTIR spectra of raw CNTs and f-CNTs.

Figure 4.6 shows the TGA curves of the PTFE membrane and CNIMs. All membranes were quite stable at moderate temperature (T<150 ºC). The initial weight loss of the membrane began at the temperature of ~328 ºC which was due to PP decomposition [270] and further weight loss was observed again at temperature of ~500 ºC, which was

from PTFE [271]. The TGA curves of CNIMs shifted slightly upward, which implied the thermal stability of CNIMs were somewhat higher.

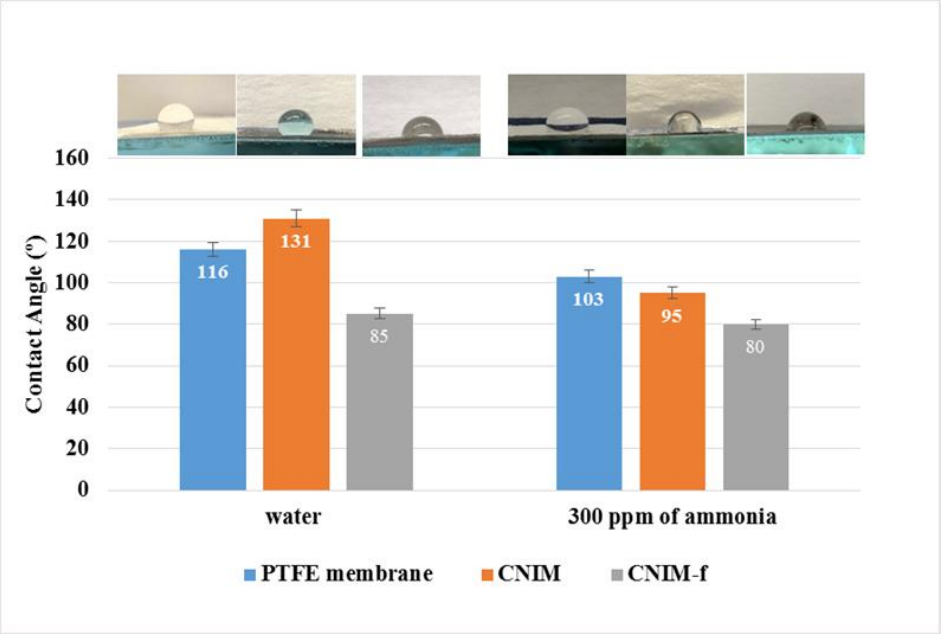

Figure 4.5 Photographs and contact angle of water and aqueous ammonia (300 ppm) drops on PTFE membrane, CNIM and CNIM-f.

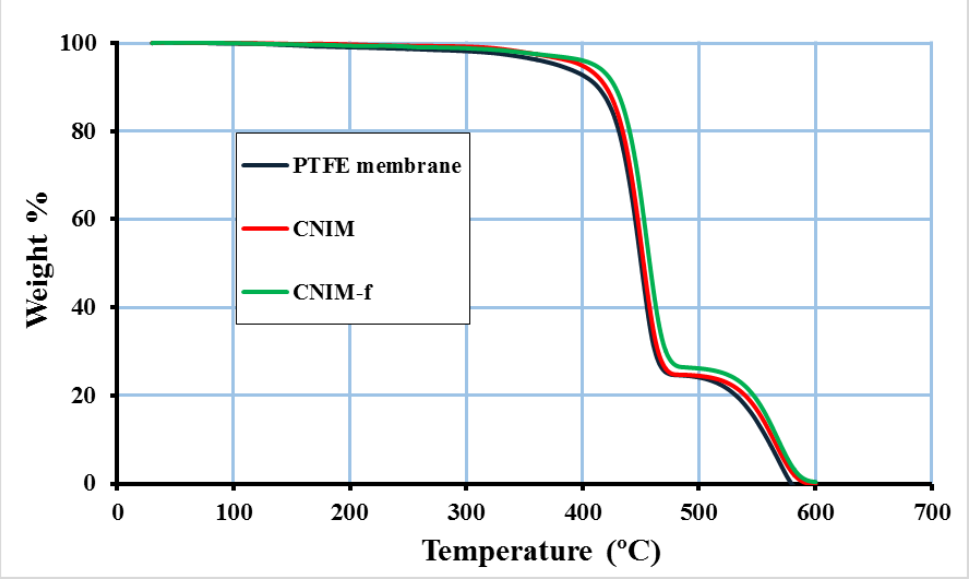

Figure 4.6 Thermogravimetric analysis of PTFE membrane, CNIM, and CNIM-f.

4.3.2 DCMD Performance Using CNIMs and PTFE Membrane

In this study, the performance of modified membranes was assessed in term of permeate flux and the ammonia removal efficiency. The overall permeate flux of species "*i*" (J_i), across the membrane can be described as:

$$J_i = \frac{W_{pi}}{A * t} \tag{4.5}$$

where W_{pi} is the total mass of species "*i*" of the permeate, *t* is the permeate collection time, and *A* is the active membrane surface area. The ammonia removal efficiency can be calculated according to the equation below.

$$\text{Ammonia removal (\%)} = \frac{W_{pi}}{W_{fi}} \times 100 \tag{4.6}$$

where *Wfi* is the total mass of species "*i*" in the feed solution at the beginning.

The effect of varying feed concentration on the ammonia flux and percent removal are shown in Figure 4.7a and b, respectively. Three different ammonia feed concentrations of 100, 300, and 500 ppm at a constant feed flow rate of 15 ml/min and at 40 ºC were investigated. From Figure 4.7a, it is clear that the permeate flux of all membranes significantly increased with an increase in feed concentrations. However, the flux from CNIM and CNIM-f were higher than that of the PTFE membrane. This was due to the fact that the CNTs was an excellent sorbent for ammonia [272]. The presence of CNTs on the

membrane improved the partition coefficient of ammonia. CNIM-f exhibited the higher flux than CNIM where the presence of carboxyl groups played a key role in increasing the ammonia adsorption on the membrane [273]. The highest ammonia flux of 31 g/m^2 h was obtained at the feed concentration of 500 ppm with CNIM-f, and the enhancement was 63 % higher than the PTFE membrane. The percent ammonia removal decreased with an increase in the feed concentration for all membrane as shown in Figure 4.7b. However, both of the CNIMs showed higher percent of ammonia removal and greater stability compared to the PTFE membrane. The highest percent removal was produced by CNIM-f with about 9 % at the concentration of 100 ppm.

The effect of the feed flow rate on permeate flux and ammonia removal efficiency at 40 ºC feed temperature and 300 ppm ammonia concentration was investigated and the results are shown in Figure 4.8a and b, respectively. The feed flow rate was kept low and varied between 5-24 mL/min, while the permeate side flow rate was fixed at 50 mL/min. It can be seen from Figure 4.8a that the permeate flux increased with an increase in the feed flow rate in all membranes. Increase in feed flow rate resulted in the availability of high volume of ammonia solution and consequently vapor pressure into the MD module for separation; and the reduction of temperature and concentration polarization, thus the enhancement in permeate flux. The CNIMs showed higher flux compared to the PTFE membrane for all feed flow rates, and CNIM-f produced the maximum permeate flux of 32 g/m^2 h at 24 mL/min feed flow rate. It was 18 and 52 % higher than the flux of CNIM and PTFE membrane, respectively. Unlike the permeate flux, the percent ammonia removal decreased with an increase in the feed flow rate as illustrated in Figure 4.8b. This was due to the fact that, at low flow rates the residence time was long, and the relatively large

amount of ammonia partitioned on the membranes, especially on CNIM surface. This shorter residence time at high flow rate resulted in a drop in the removal efficiency. The maximum 14% percent removal of ammonia was obtained at 5 mL/min feed flow rate using CNIM-f. It is evident that the CNTs promoted the ammonia permeation.

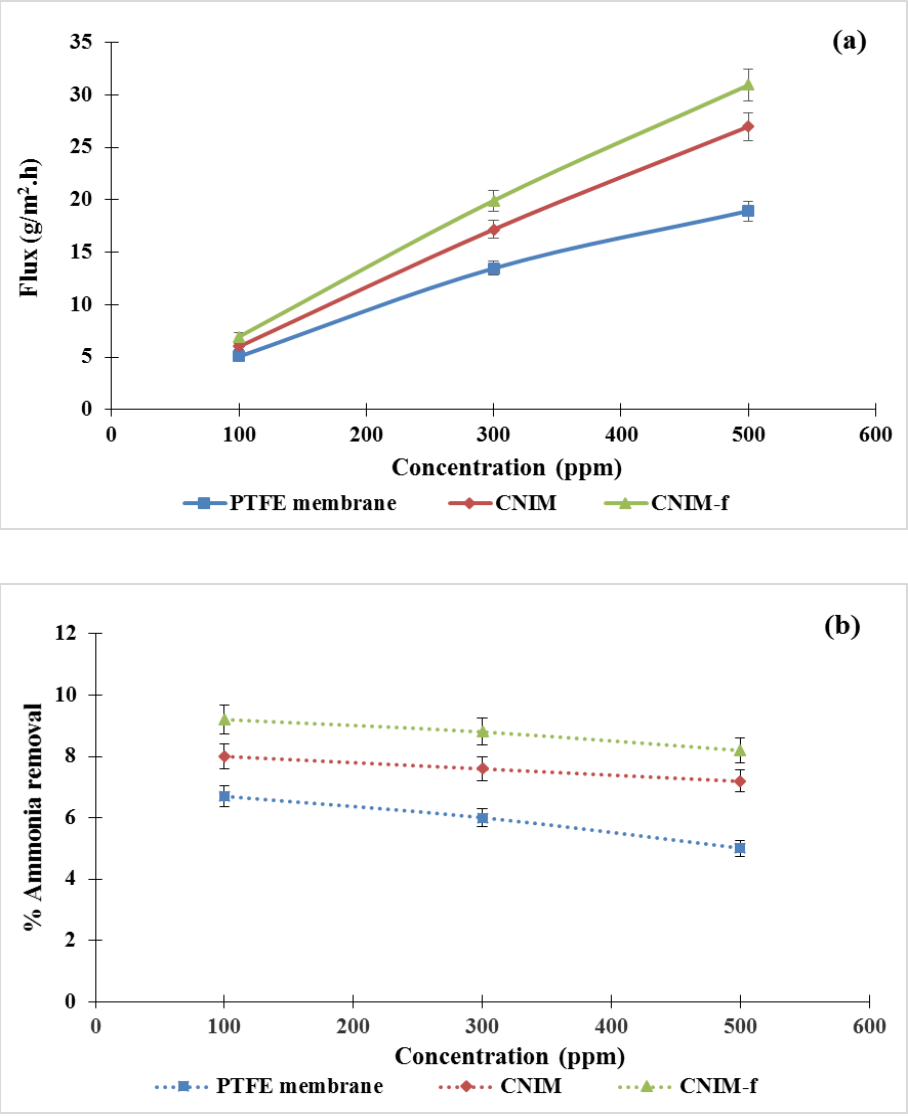

Figure 4.7 a) Effect of feed concentration on ammonia flux, and **b)** % ammonia removal as the function of feed concentration.

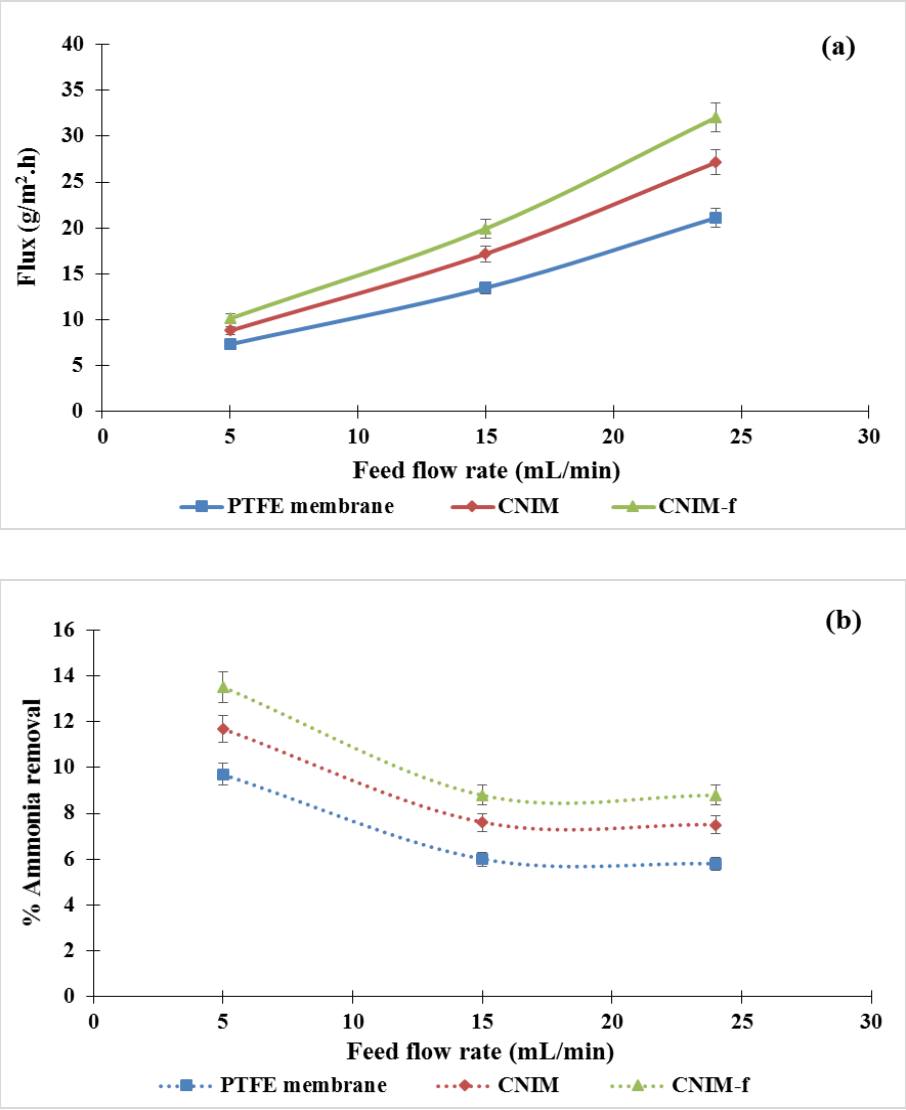

Figure 4.8 a) Effect of feed flow rate on ammonia flux, and **b)** % ammonia removal as the function of feed flow rate.

Figure 4.9a and b show the effect of feed temperature on the ammonia flux and the percent ammonia removal. The feed temperature was varied from 30-50 ºC at a fixed feed flow rate of 15 mL/min and at a feed concentration of 300 ppm. The MD was carried out at low temperatures in order to prevent the evaporation of ammonia from the feed water. From Figure 4.9a, the ammonia flux increased with an increase in temperature for all

membranes due to the increase in vapor pressure with temperature. Overall, the performance of the CNIMs was superior to the pristine membrane at all temperatures. Maximum permeate flux of 25 g/m^2 h was reached by CNIM-f at 50 ºC feed temperature, which was 22 and 45% higher as compared to the CNIM and the PTFE membrane. The amount of ammonia removal also increased with an increase in the temperature for all membranes as illustrated in Figure 4.9b. CNIM-f achieved the highest efficiency with 11% removal at 50 ºC, while the PTFE membrane and CNIM were 8% and 9 % respectively.

The selectivity of ammonia separation was measured as:

$$\text{Selectivity} = \frac{y/(1-y)}{x/(1-x)} \tag{4.7}$$

where *x* and *y* are the mass fractions of ammonia in the feed and the permeate.

Figure 4.10 shows the effect of ammonia selectivity at different temperatures. In general, ammonia selectivity of the membranes tended to decrease with increase in the feed temperatures [90, 251]. Increase in feed temperatures exponentially increased the water vapor pressure that resulted in higher mass of water diffusing through the membrane. At the same time the partition coefficient of ammonia decreased with temperature, and was expected to reduce the overall ammonia selectivity. While the selectivity for the PTFE and the regular CNIM decreased with temperature, the overall selectivity of CNIM-f remained constant and did not decrease with temperature. The carboxylic groups on the f-CNTs facilitated the ammonia transfer across the membrane and maintained the high selectivity.

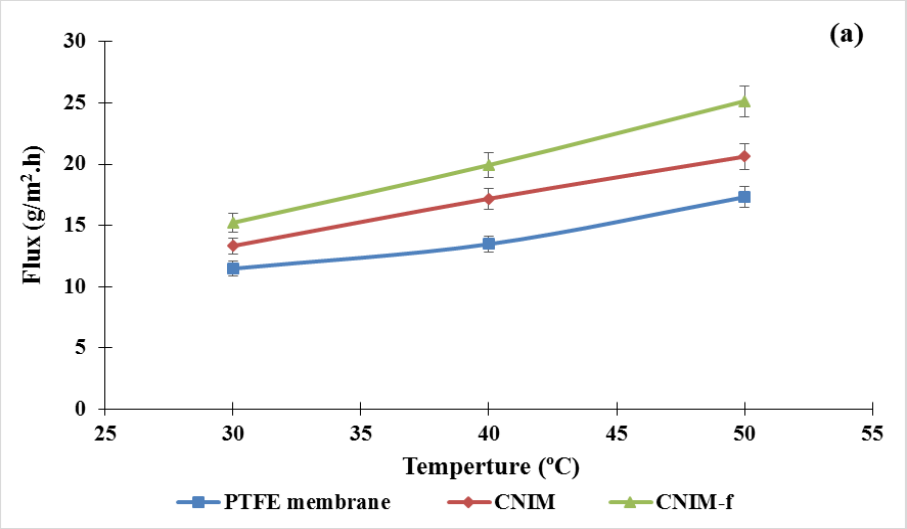

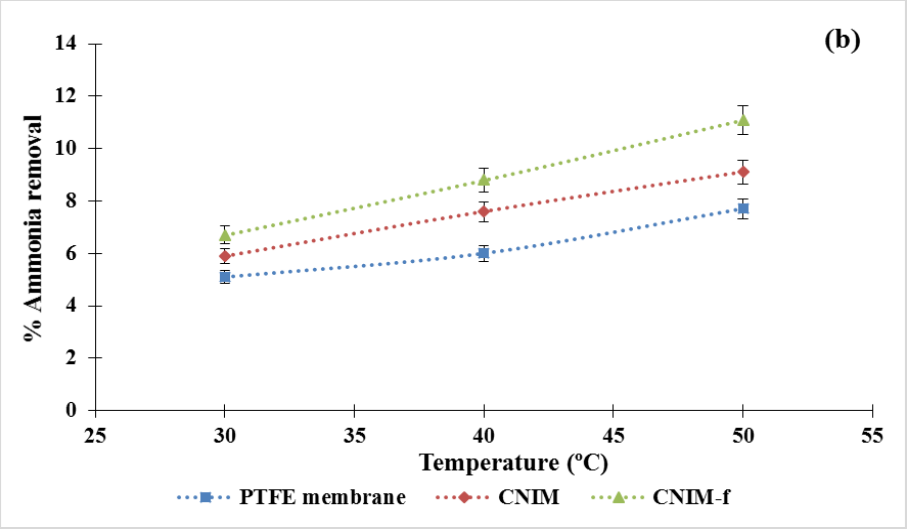

Figure 4.9 a) Effect of feed temperature on ammonia flux, and **b)** % ammonia removal as the function of feed temperature.

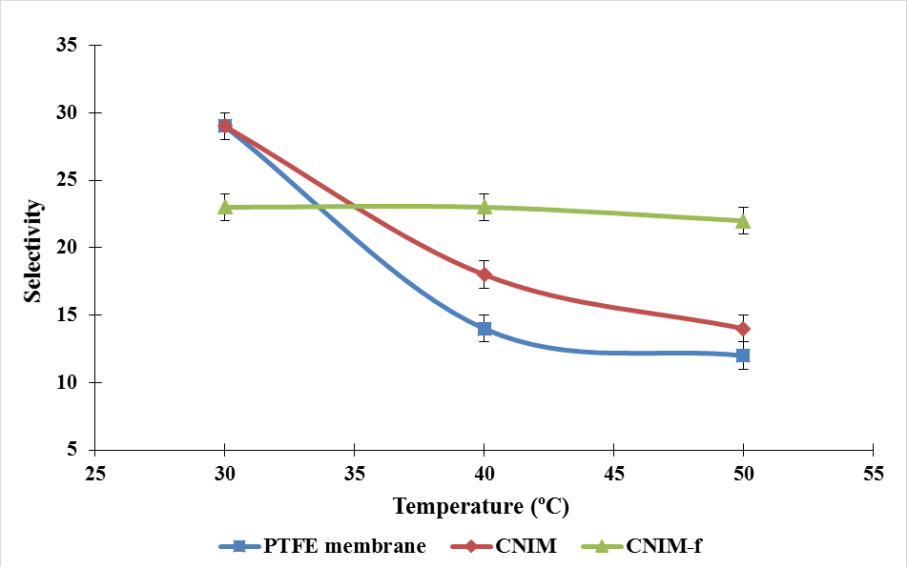

Figure 4.10 Effect of feed temperature on ammonia selectivity of membranes.

4.3.3 Mass Transfer Coefficient

The mass transfer coefficient (k) can be described as:

$$k = \frac{J_i}{(P_f - P_p)} \tag{4.8}$$

Where *Ji* is the flux, P_f and P_p are the partial vapor pressures of the specie *i* in the feed and permeate side, respectively. The partial pressure of ammonia on the feed side was obtained from literature data [274]. Since deionized water was used as the cold receiving water, the partial vapor pressure on the permeate side was considered to be zero.

Table 4.1 shows the effect of various feed temperature on mass transfer coefficients of ammonia for the different membranes at 300 ppm ammonia concentration and 15 mL/min feed flow rate. The mass transfer coefficients of ammonia tended to decrease with

an increase in the feed temperatures. Both CNIMs showed the higher mass transfer coefficients than the PTFE membrane and CNIM-f had the largest mass transfer coefficient at all temperatures. The higher mass transfer coefficients of the CNIMs were attributed to high adsorption and rapid desorption properties of CNTs [147, 198, 203, 275]. The enhancement in mass transfer coefficients of CNIM-f varied from 33 % to 48%, and the maximum effect was observed at 40 ºC.

Table 4.2 shows the mass transfer coefficients of ammonia at flow rates between 5-24 mL/min, feed concentration of 300 ppm at 40 ºC. The mass transfer coefficients increased with the increase in the feed flow rates. High feed flow rates increased the turbulence that led to the reduction in the boundary layer resistance and consequently the mass transfer coefficients were significantly increased at a higher flow rate. The CNIMs showed higher values of mass transfer coefficient as compared to the PTFE due to high adsorption and rapid desorption on CNTs. Once again CNIM-f had the higher mass transfer coefficient than CNIM as the-COOH groups helped in the mass transport. The enhancement in mass transfer coefficients associated to the functionalized CNT was anywhere between 39 % and 52% with the most pronounced effect at 24 mL/min feed flow rate.

Table 4.1. Mass Transfer Coefficient of Ammonia at Various Feed Temperatures 300 ppm of Aqueous Ammonia Feed Solution and 15 mL/min

Temperature (ºC)	Mass transfer coefficient (kg/m^2.s.Pa) ×10^{-7}		
	PTFE Membrane	CNIM	CNIM-f
30	1.79	2.07	2.37
40	1.38	1.76	2.04
50	1.15	1.37	1.67

Table 4.2 Mass Transfer Coefficient of Ammonia at Various Feed Flow Rates and 300 ppm of Aqueous Ammonia Feed Solution at 40 ºC

Flow rate (mL/min)	Mass transfer coefficient (kg/m^2.s.Pa) × 10^{-7}		
	PTFE Membrane	CNIM	CNIM-f
5	0.75	0.90	1.04
15	1.38	1.76	2.04
24	2.16	2.78	3.28

4.3.4 Membrane Stability

The stability of membranes was tested by conducting the experiment for 30 days (8 hrs/day), and it was observed that ammonia flux did not show any significant change over this period of time. The change in pH of permeate was investigated and compared to each other to watch the feed solution breakthrough. During long term experiments, the pH of permeate showed the minor variation within 10.4±0.2 implying that no feed breakthrough occurred.

4.4 Proposed Mechanism

The proposed mechanism for ammonia flux enhancement by CNIMs is shown in Figure 4.11. CNTs have demonstrated several unique sorption properties and have been used in applications such as gas preconcentration and sensors [276-279]. In this study the presence of CNTs significantly improved ammonia flux and mass transfer coefficients when compared to a PTFE membrane that was uncoated. This enhancement was attributed to preferential sorption of NH_3 on CNT as well as f-CNT sites. The higher ammonia flux on CNIM-f compared to the CNIM can be explained by the presence of a large number of carboxylic functional groups on the f-CNT that provided sites for preferential sorption of ammonia [273] thus increasing activated diffusion for ammonia that resulted in flux enhancement and the ammonia flux reported in this study is double of the maximum value reported before [251].

4.5 Conclusions

Ammonia removal by CNIMs made from raw CNTs and f-CNTs were significantly higher than that with the original PTFE membrane. The f-CNTs showed the highest flux, ammonia recovery and mass transfer coefficients under all operational conditions. The maximum flux obtained in CNIM-f was 32 g/m^2 h, which was twice that of what has been reported before. The highest ammonia removal efficiency with CNIM-f was observed to be 14% at the feed flow of 5 mL/min with the constant temperature of 40 ºC and concentration of 300 ppm. Ammonia selectivity on CNIM-f remains constant with increase in temperature while the other membranes showed a decrease. Immobilizing CNTs and f-CNTs on the PTFE surface did not only alter the membrane morphology, but significantly improved partition

coefficients that promoted ammonia transport. This was supported by contact angle measurement data. While the data is presented for DCMD, the concept using functionalized CNTs is valid for all modes of MD.

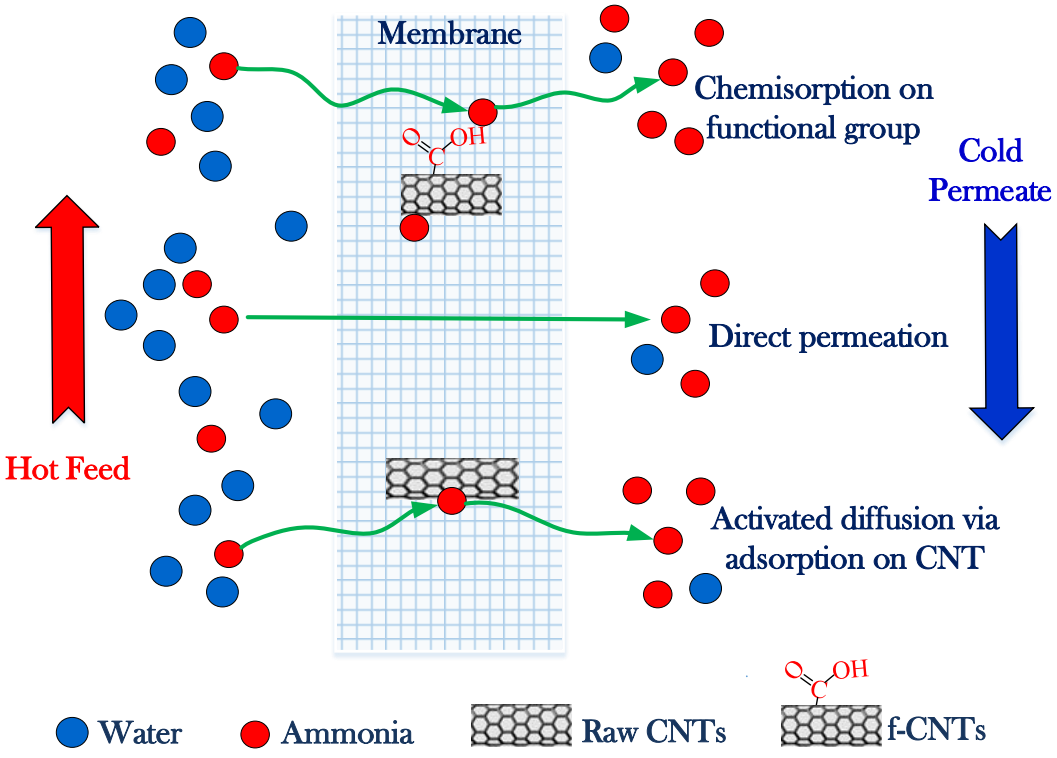

Figure 4.11 Schematic diagram for mechanism proposed on CNIMs.

CHAPTER 5

REMOVAL AND RECOVERY OF METHYL TERTIARY BUTYL ETHER (MTBE) FROM WATER USING CARBON NANOTUBE AND GRAPHENE OXIDE IMMOBILIZED MEMBRANES

5.1 Introduction

Over 20 million tons of methyl tert-butyl ether (MTBE) is produced and used as a fuel additive around the world every year, and it has contaminated ground and surface water all across the globe [280, 281]. Its impact on the environment and human health has been a great concern in the USA and other countries as well [282-288]. MTBE is highly water soluble, has a low Henry's Law constant and low sorption constants [281]. These properties also enhance the mobility of MTBE, and make it difficult to separate from water. Methods such as air stripping, adsorption, oxidation processes and pervaporation have been used for MTBE removal [289-291]. Air stripping is the conventional method for separating MTBE from water. However, this approach works well only at high temperature, which is energy extensive, and lowering the temperature of MTBE-contaminated feed water can reduce the efficiency of this technology significantly. Additionally, the technology is often not practical if the air stream has to be treated [292]. Although the adsorption of low concentration MTBE on activated carbon can be a challenge, this approach also requires a desorption step [293, 294]. Advanced oxidation processes have also been tested, but they can lead to the formation of toxic by-products. Membrane-based processes can overcome some of the shortcomings of the conventional processes mentioned above, and are gaining interest [289]. Membrane-based pervaporation has been applied for MTBE separation from water [295, 296]. The results show a high separation factor for MTBE [296], however, the process has relatively low permeate flux [297].

Membrane distillation (MD) is a thermally-driven, membrane-based process, which has been utilized for desalination and wastewater treatment, including volatile compound separation [47, 147, 197]. The main advantages of MD include high rejection of non-volatile species and relatively low membrane fouling. Furthermore, a low-grade energy, such as solar/geothermal energy, and industrial waste heat have been efficiently used as a heat source, since MD can be operated at low temperature (30-70 ºC) [197, 253, 298]. A key element of the MD system is the membrane, which directly influences the separation performances. This MD process exploits the differential partial vapor pressure between feed and permeate side as the driving force to transport the vapor molecules through the membrane, where the liquid/membrane interface needs to be hydrophobic to prevent membrane pore blocking and wetting. Understanding these interactions at the membrane interface is important for tailoring the membrane properties [299]. A variety of modification methods have been used to promote the hydrophobicity of the membrane surface [42]. For examples, a hydrophobic styrene-butadiene rubber was used to chemically coat on a polyamide membrane [180], while tetrafluoromethane was employed to modify the surface of polyethersulfone membranes by vacuum plasma modification [184]. The hydrophobic materials, such as polypropylene (PP), polyvinylidenefluroride (PVDF), polyethylene (PE), and polytetrafluoroethylene (PTFE) have been used to synthesize MD membranes [52]. However, they tend to be very hydrophobic, and show little affinity for MTBE. We have reported a membrane modification approach using carbon nanotubes (CNTs), f-CNTs and GO [189, 191, 192, 203, 300] to improve the characteristics of the membrane, and have shown an excellent adsorption and transport of solutes, leading enhanced flux and selectivity in desalination, as well as the separation of

organic solvents from aqueous mixtures [147, 191, 298]. Although several techniques have been tested for MTBE removal from aqueous solution, few studies have investigated the removal using vacuum MD [95, 301]. MTBE separation using SGMD with a nanocarbon-modified membrane at low temperature has much potential for performance improvement, and has not been studied. The objective of this project was to study the removal of MTBE from water via SGMD, using carbon nanotube and a graphene oxide-immobilized membrane.

5.2 Materials and Methods

5.2.1 Chemicals and Materials

Methyl tert-butyl ether (MTBE) (99.8%) was purchased from Sigma Aldrich (Sigma-Aldrich Inc, St. Louis, MO, USA). Flat sheet polytetrafluoroethylene (PTFE) membrane with a polypropylene (PP) supporting layer (0.2 μm pore size, 119 μm thickness, and 74% porosity) was obtained from Adventec Toyo Kaisha, Ltd., (Tokyo, Japan). Multi-walled carbon nanotubes (MWCNTs) (OD 20–30 nm, length 10–30 μm, purity > 95%) were purchased from Cheap Tubes Inc., (Brattleboro, VT, USA). Graphene oxide (GO) was obtained from Graphenea Inc., (Cambridge, MA, USA). Deionized water was used in all experiments.

5.2.2 CNIM-f and GOIM Fabrication and Characterization

The functionalized CNTs (f-CNTs) were prepared by bonding the carboxyl functional group on the MWCNT sidewall through microwave-induced reaction in a Microwave Accelerated Reaction System (CEM Mars), as stated in our previous [263].

CNIM-f was fabricated by the procedure, as explained in our recent paper [298]. 1.5 mg of f-CNTs was mixed with 8 gm of acetone and uniformly dispersed by an ultrasonic bath for 4 h. The PVDF solution used as a binder was separately prepared by dissolving 0.2 mg of PVDF in 2 gm of acetone and added to f-CNTs solution. Immobilization of f-CNTs on the membrane was performed by drop casting of the f-CNTs-PVDF mixture on the membrane surface. The modified membrane was dried under the fume hood overnight. GOIM was also fabricated with the same procedure, except sonication for 10 h.

The membrane morphology and the deposition of CNTs and GO on the membranes were characterized using the scanning electron microscope (SEM, model JSM-7900F, JEOL USA Inc, Peabody, MA, USA). The plain membrane, CNIM-f and GOIM were further characterized by Raman spectroscopy (DXR Raman microscope, Thermo Fisher Scientific, Waltham, MA, USA). The instrument was operated by using 532 nm diode-pumped, solid state (DPSS) laser with laser power of 8 mW, and five scans, with each for 2 s, were performed. The thermal stability of the membranes was examined via thermal gravimetric analysis (TGA, model TGA 8000, PerkinElmer Inc, Hopkinton, MA, USA) using N2 in the temperature range of 30-620 ºC, with a heating rate of 10 ºC/min. Contact angle measurement used to illustrate the hydrophobic/hydrophilic property of the membrane surfaces was obtained by the water drop method. Water and 2.5% MTBE solution were used in the contact angle measurement. A micro syringe (Hamilton 0−100 μL) was employed to create 2 μL droplets for the measurement as the method described in our previous paper [298]. Surface free energy of the unmodified and modified membranes

was calculated from contact angle data following the Owens−Wendt (extended Fowkes) model [302] by using water, ethylene glycol, glycerol and propanol as test liquids [303].

The liquid entry pressure (LEP) of PTFE and modified membranes was measured by a procedure mentioned in the article [264]. The membrane module was connected to a stainless steel chamber (Alloy Products Corp, 185 Psi Mawp) filled with the MTBE solution, by the high-pressure tubing (Masterflex Transfer Tubing, PTFE, 1/8" ID x 1/4" OD). Compressed N2 gas was used to build up the pressure in the chamber, and the increased pressure forced the liquid going into the tube. The pressure that drives the liquid, first entering through the membrane pores, is LEP. The triple measurement was carried out to ensure reproducibility.

5.2.3 Experimental Setup

The sweep gas membrane distillation (SGMD) configuration was employed in this study. The MTBE solution was recirculated around the feed side of the membrane, while a dried-inert gas swept the vapor on the permeate side of the membrane. Before being passed through the permeate side, the sweep air was treated according to the procedure in our previous paper [147]. The SGMD setup in this experiment is shown as the schematic diagram in Figure 5.1. The MD module had an active contact area of 11.94 cm^2. An enclosed feed chamber was used to prevent sample loss via evaporation. A peristaltic pump (Cole-Parmer, Masterflex L/S compact pump model 77240-00) was used to recirculate the feed solution. The constant temperature water bath (NESLAB Instruments, Inc., Water Bath Model GP 200) was used to control the temperature of the feed. The temperature sensors (Cole-Parmer, Four-channel data logger thermometer) were employed to continuously monitor the inlet and outlet temperatures of the feed side.

5.2.4 Experimental Procedure

MTBE feed solutions with different concentrations were prepared by adding weighed amounts of MTBE to deionized water. The performances of PTFE and modified membranes were measured under different conditions, i.e., concentrations (0.5, 1.5 and 2.5 wt% MTBE), temperatures (21, 30 and 40ºC), and feed flow rates (20, 30, and 40 mL/min). The air flow rate on the permeate side was kept constant at 2 L/min for all experiments. The change in the feed amount was measured by subtracting the initial and final weight. The concentrations of the MTBE solution were analyzed by a UV Spectrophotometer (UV-1800 UV–Vis Spectrophotometer, Shimadzu Inc, Canby, OR, USA) with λmax at 194 nm. The concentration and weight of the feed solutions before and after the experiments were used to calculate the flux and the selectivity of the membranes. Each experiment was carried out in triplicate to confirm the reproducibility.

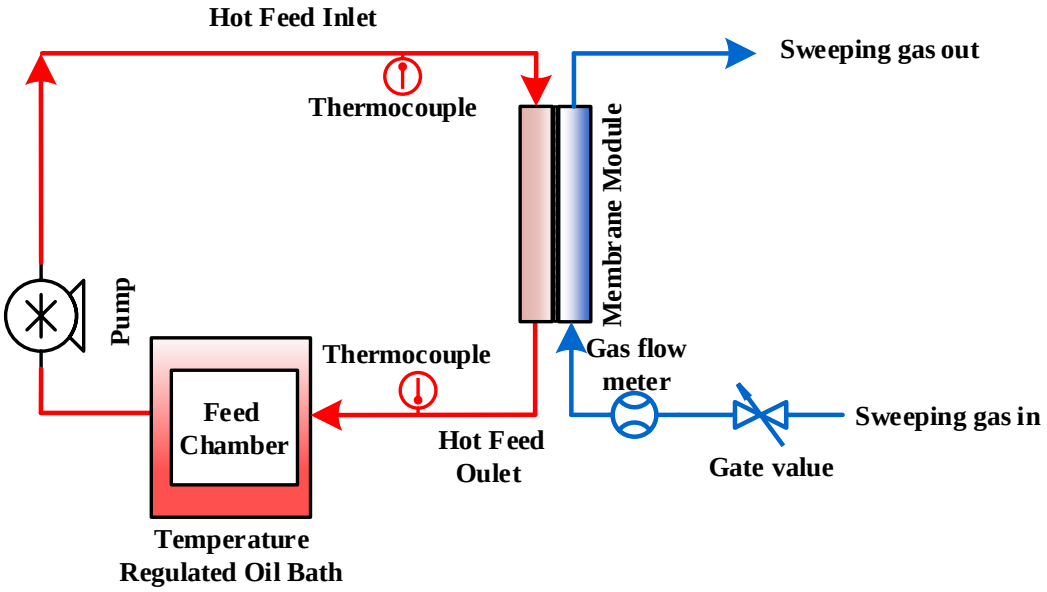

Figure 5.1 Schematic diagram of the experimental setup for the SGMD.

5.3 Results and Discussion

The SEM images of the plain PTFE membrane, GOIM, and CNIM-f are illustrated in Figure 5.2. Figures 5.2a and b show the biaxially stretched microporous structure of the feed and the permeate side of the original PTFE membrane, while Figures 5.2c and d present the morphology of the feed side of the membranes after modification by GO and f-CNTs, respectively. Uniform deposition of GO and f-CNTs was found over the entire membrane surface. Figure 5.3 presents the Raman spectra of the PTFE membrane, GOIM, and CNIM-f. The Raman spectrum of PTFE membrane showed the dominant peaks at 294, 389, 735, and 1383 cm^{-1} [304]. These peaks can also be seen in the spectrum of GOIM and CNIM-f, together with the signature bands of graphitic materials at ~1350 $cm^{-1}$and ~1595 cm^{-1}, called the D and G-band, respectively [305].

The TGA and the derivative thermogravimetry curves of the PTFE membrane, GOIM and CNIM-f are shown in Figures 5.4a and b, respectively. At moderate temperatures (T<150 ºC), all membranes seemed relatively stable. The decomposition of PP resulted in the initial weight loss of the membranes at the temperature of ~350 ºC [270], with significant weight change at the temperature of the 450-500 ºC range. The significant weight loss was noticed again at a temperature of ~500 ºC and the major weight loss was seen at temperatures between 550 and 600 ºC. This was due to the degradation of PTFE [271]. Overall, the TGA of modified membranes clearly shifted upward from the plain membrane, especially the CNIM-f. This implied that the modified membranes have a higher thermal stability than the unmodified ones. Higher thermal stability or the reduction of the thermal degradation of GOIM and CNIM-f could be attributed to the role of GO and CNTs that act as a radical scavenger and sacrificial agent, and their ability in inducing the

barrier effect and high thermal conductivity [231, 306]. However, between GOIM and CNIM-f, the latter had higher thermal stability. This is in accordance with the thermal stability of GO and CNTs as reported in the previous publication [307].

The contact angles of pure water and aqueous MTBE solution on the membrane surface, along with their photos are presented in Figure 5.5. The presence of GO and f-CNTs clearly resulted in the alteration of the contact angle of the drops on the PTFE membrane. Testing with deionized water, the contact angles for the plain membrane was 118º, which decreased to 108 and 112º for GOIM and CNIM-f, respectively. The reduction in the contact angle for GOIM and CNIM-f were attributed to the polar epoxy, carboxyl and hydroxyl functional groups on GO, and the carboxylic groups of f-CNTs. These enhanced the hydrophilicity of the membranes. This is in line with the previous publications [191, 298, 300]. For the MTBE solution, the contact angle for all membranes reduced as expected due to incorporation of the organic moiety in the aqueous solution, which decreased surface tension and eventually led to lower contact angles. For GOIM and CNIM-f, similar contact angle values of 94º and 95º were observed and it was 107º for the plain membrane. Furthermore, the additional reduction of the contact angles for GOIM and CNIM-f compared to that for plain membrane was attributed to the enhanced interaction of the organic moiety with GO and f-CNTs. Surface free energy of the original PTFE membrane and modified membranes was investigated using the contact angles of different liquids, as mentioned before. The surface free energy showed an increase with the membrane modification, using GO and f-CNTs. The surface free energy was 5.54 mJ/m^2 for the plain membrane, and rose to 8.77 and 7.64 mJ/m^2 for GOIM and CNIM-f,

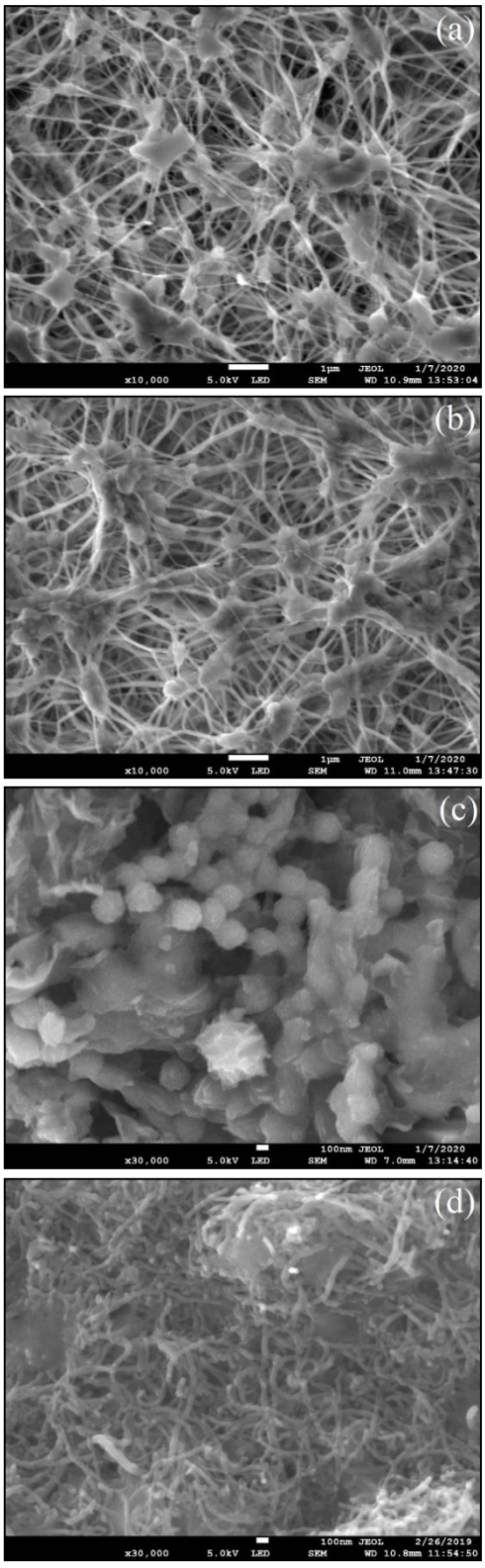

Figure 5.2 Scanning electron microscopy (SEM) images of **a)** the feed side of original PTFE membrane, **b)** the permeate side of original PTFE membrane, **c)** GOIM and **d)** CNIM-f.

respectively. Although, the surface energy of a particular material depends upon various factors, in general, the high surface free energy of modified membranes signify strong molecular attractions, while the low surface free energy of plain membrane indicates weaker attractive forces between the liquid and the membrane surface.

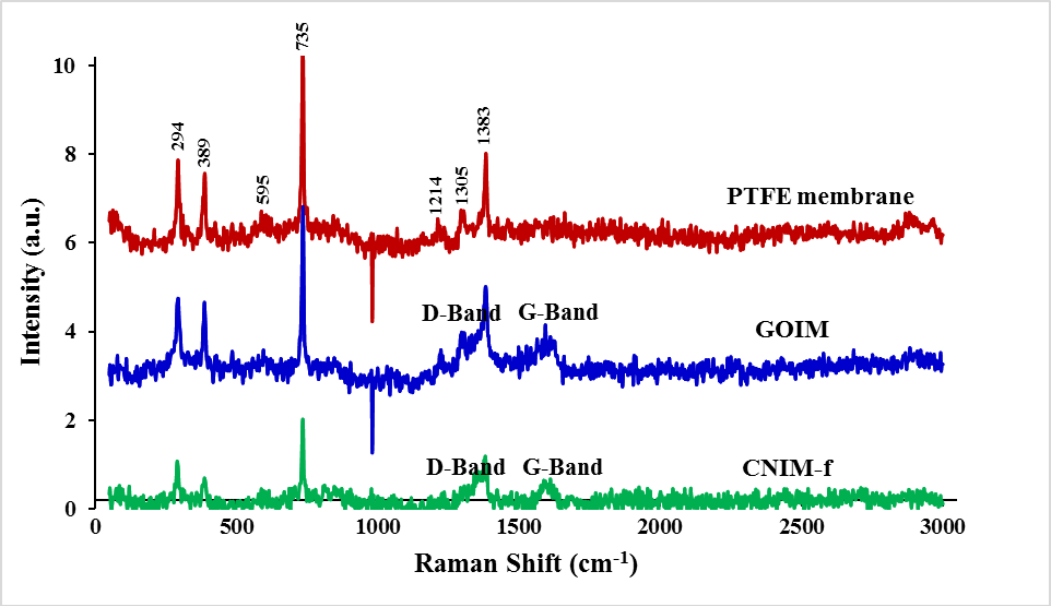

Figure 5.3 Raman spectra of PTFE membrane, GOIM, and CNIM-f.

The measurement of liquid entry pressure (LEP) for plain and modified membranes was made using DI water and 2.5% of the MTBE solution as feed solutions. The LEP of the membranes tested with DI water were 67, 63, and 64 psig, and reduced to 37, 29, and 34 psig when MTBE was used as a feed for the plain membrane, GOIM, and CNIM-f respectively. The reduction of LEP of the membranes when tested with MTBE was attributed to decrease in the surface tension of the liquid and the contact angle. This is due to the fact that LEP is proportional to the surface tension of the liquid and the degree of contact angle, as described in the literature [308]. The LEP of GOIM and CNIM-f were

lower than that of the plain PTFE membrane, due to their lower contact angles due to the reasons given above.

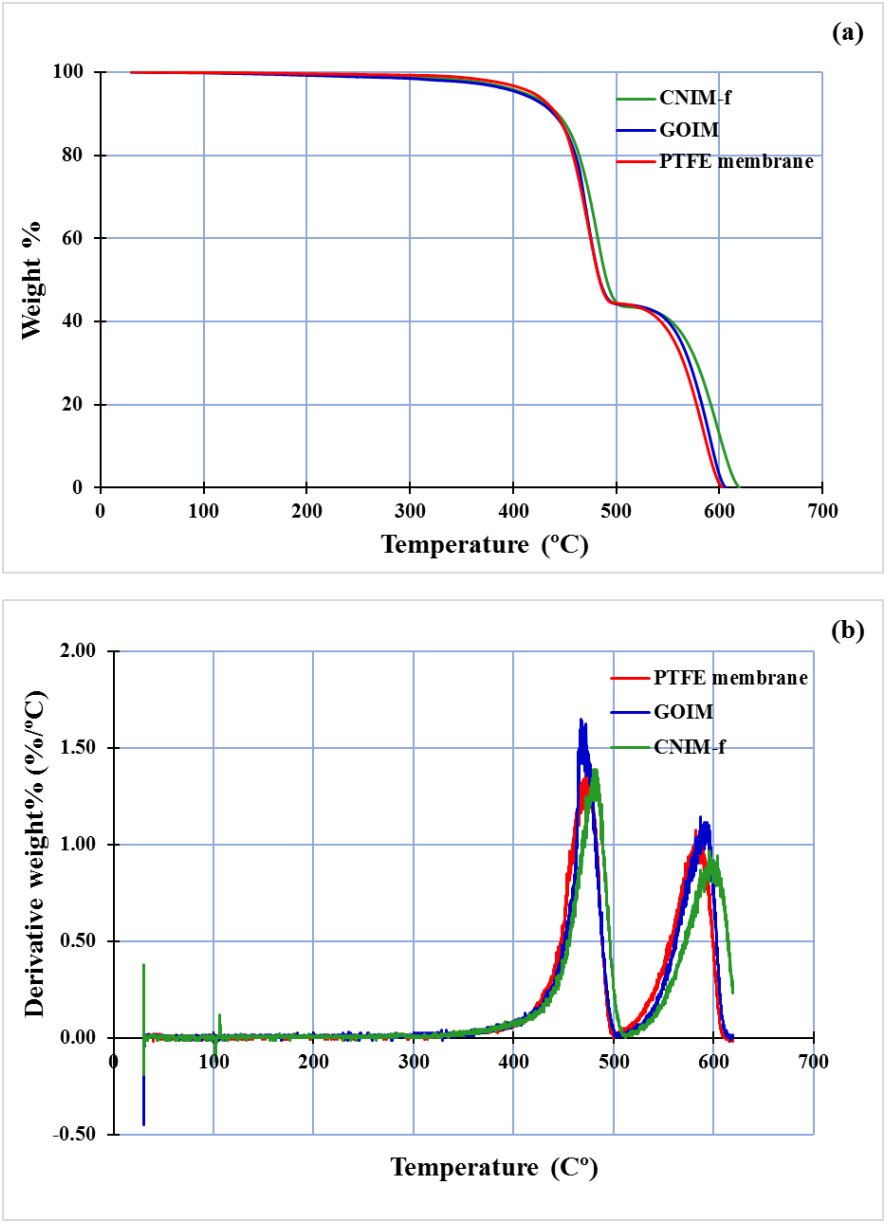

Figure 5.4 Thermogravimetric analysis (TGA) **a)** and the derivative thermogravimetry **b)** of the PTFE membrane, GOIM, and CNIM-f.

5.3.1 SGMD Performance Using GOIM, CNIM-f and PTFE Membrane

In this study, MTBE permeate flux and MTBE removal efficiency were used to evaluate the performance of the modified membranes and compared to a plain PTFE membrane. The overall permeate flux of MTBE (J_{MTBE}), across the membrane can be expressed as:

$$J_{MTBE} = \frac{(W_{0-}W_t)}{A * t} \tag{5.1}$$

Where, W_0 and W_t are the total mass of MTBE of the feed at the beginning of the experiment and after collection time *t*, respectively. *A* is the active membrane surface area. The MTBE removal efficiency can be measured according to the equation below.

$$\%\ \text{MTBE removal} = \frac{(W_{0-}W_t)}{W_0} \times 100 \tag{5.2}$$

The results of varying feed concentration on MTBE flux and percent MTBE removal are shown in Figures 5.6a and b, respectively. The MTBE feed concentrations of 0.5 wt%, 1.5 wt%, and 2.5 wt%, with a constant feed flow rate of 20 mL/min and a temperature of 30 ºC, were examined. From Figure 5.6a, it can be seen that the MTBE flux increased substantially with an increase in feed concentration for all membranes, and the flux of CNIM-f and GOIM were superior to that of the original membrane. The higher flux for CNIM-f and GOIM may be explained by the fact that f-CNTs and GO are the

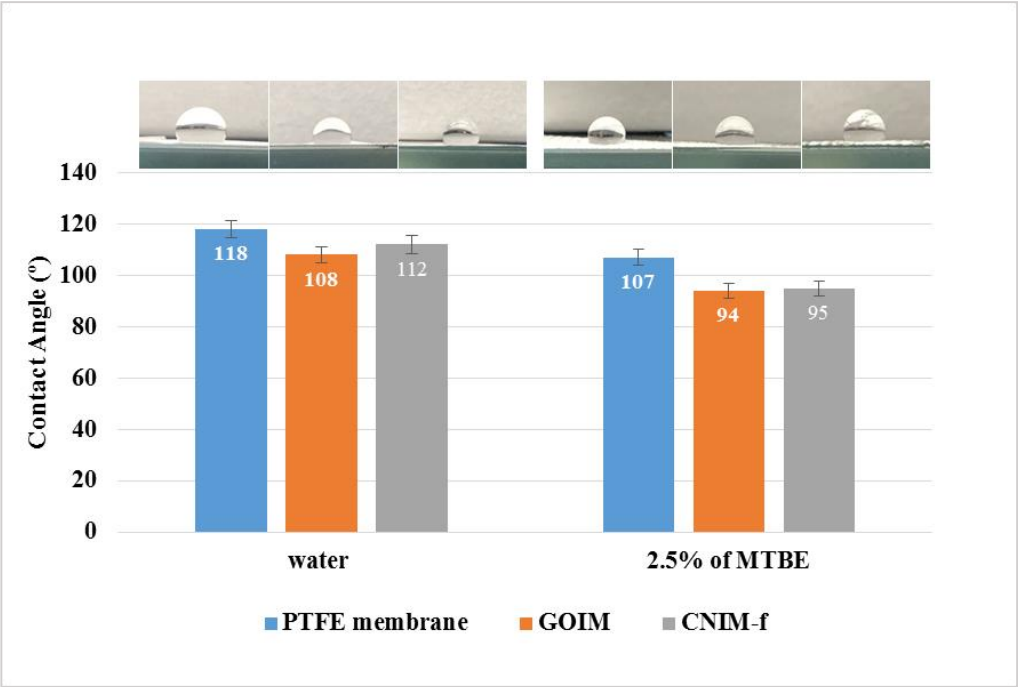

Figure 5.5 Photographs and contact angle of water and aqueous MTBE (2.5 wt%) drops on PTFE membrane, GOIM and CNIM-f.

exceptional sorbents for the organic molecule [188], and lead to the improvement of the partition coefficient of MTBE. However, the high flux of CNIM-f over GOIM may be ascribed to the activated diffusion via adsorption and desorption on the CNT surface that facilitate faster MTBE transfer across the membrane [203, 309]. The highest MTBE flux from CNIM-f was 1.4 kg/m^2 h at the feed concentration of 2.5 wt%, while the maximum enhancement of 21.7% and 11% was obtained at the feed concentration of 0.5 wt%, compared to the PTFE membrane and GOIM, respectively. As shown in Figure 5.6b, the percent MTBE removal declined with the increment of the feed concentrations for all membranes. Both CNIM-f and GOIM still provided the higher percent removal than the plain membranes. The highest removal of 56% was observed for CNIM-f at the feed concentration of 0.5%.

The effects of the feed flow rate on MTBE flux and percent MTBE removal at 30ºC feed temperature and concentration of 1.5 wt% MTBE are shown in Figures 5.7a and b, respectively. The feed flow rate was varied between 20-40 mL/min. As can be seen in Figure 5.7a, it is clear that the MTBE flux steadily rose with an increase in the feed flow rate in all membranes. The increment of the feed flow rate increased the amount of MTBE and the availability of vapor into the MD module per unit time. The increased velocity also led to the reduction of temperature and concentration polarization, and consequently resulted in the permeate flux enhancement [310]. The modified membranes gave higher flux than the original membrane for all flow rates. The CNIM-f yielded the highest permeate flux of 0.98 kg/m^2 h at the 40 mL/min feed flow rate, while the largest enhancements found at the feed flow rate of 20 mL/min, which were 11% and 4%, equated to the PTFE membrane and GOIM, respectively. Like the permeate flux, the percent MTBE removal increased with an increase in the feed flow rate as shown in Figure 5.7b. The CNIM-f presented the most percent removal, it was 39% at the same feed flow rate.

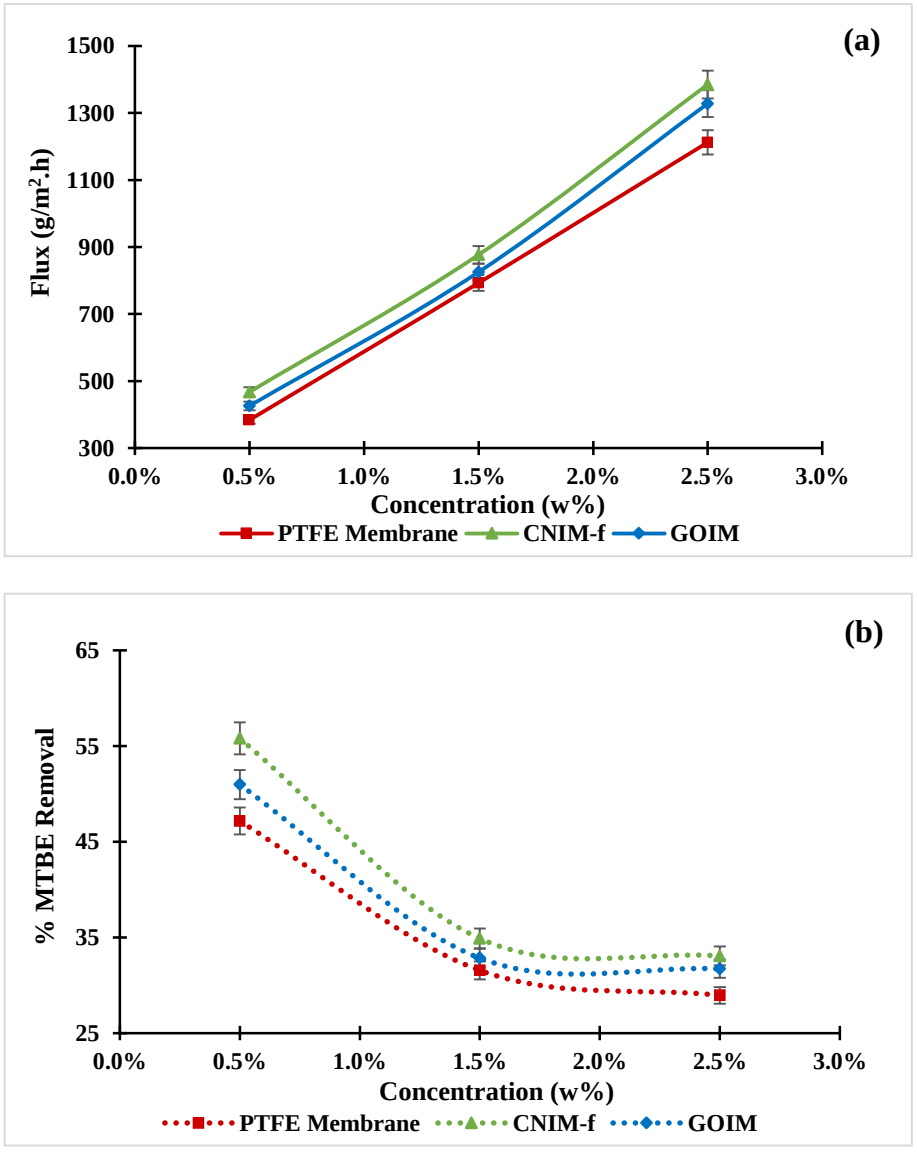

Figure 5.6 a) Effect of feed concentration on MTBE flux, and **b)** % MTBE removal as the function of feed concentration at the feed temperature of 30 ºC and the feed flow rate of 20 mL/min.

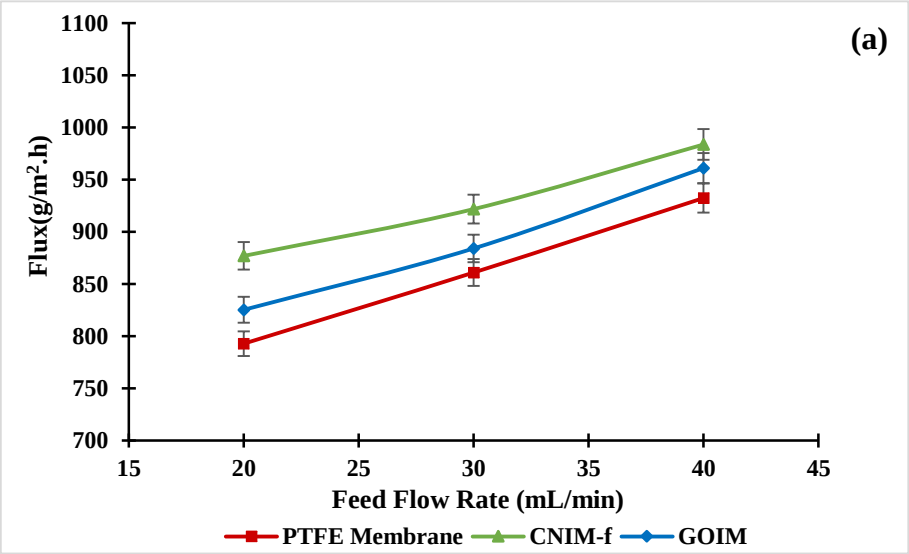

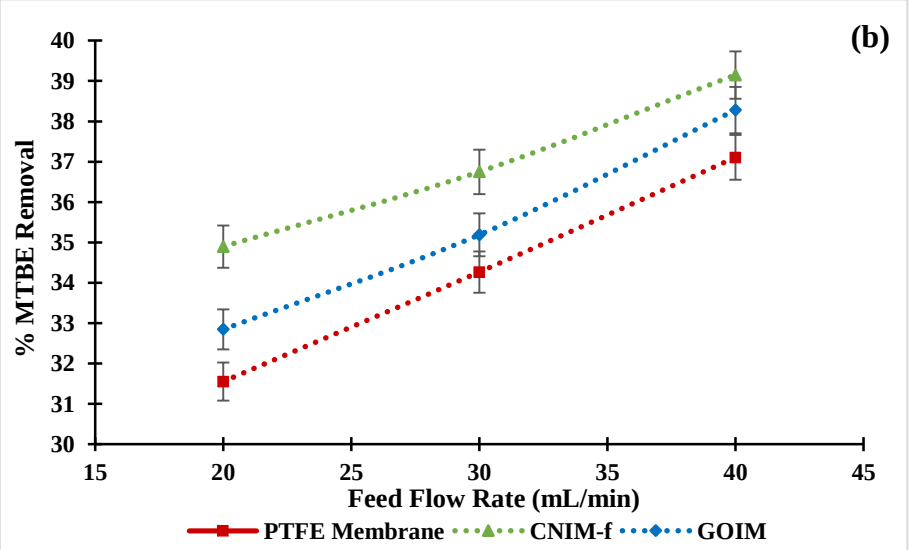

Figure 5.7 a) Effect of feed flow rate on MTBE flux, and **b)** % MTBE removal as the function of feed flow rate at the feed concentration of 1.5 wt% and the feed temperature of 30ºC.

The results of varying feed temperature on MTBE flux and percent MTBE removal are presented in Figures 5.8a and b, respectively. The membrane performances were investigated at three different temperatures: 21, 30, and 40 ºC at a constant feed flow rate of 20 mL/min, and at a feed concentration of 1.5%. As shown in Figure 5.8a, there is a clear trend of increasing the MTBE flux with an increase in temperature for all membranes.

This is due to the fact that the vapor pressure rises with an increase in the temperature, according to Antoine's equation, and then results in the extended vapor pressure difference between feed and permeate side, and consequently the enhancement in permeate flux [311]. Overall, the modified membranes showed better performance than that of the unmodified membrane for all temperatures. The highest flux of 0.97 kg/m^2 h was obtained by CNIM-f at 40 ºC, while the maximum enhancements found at 21ºC were 14% and 10%, over the PTFE membrane and GOIM, respectively. From Figure 5.8b, the percent MTBE removal also raised with the increment of temperature. CNIM-f reached the maximum efficiency with 39% removal at 40 ºC, while GOIM and the pristine membrane were 37% and 34 %, respectively.

The selectivity of MTBE separation can be expressed as:

$$\text{Selectivity} = \frac{y/(1-y)}{x/(1-x)} \tag{5.3}$$

where *x* and *y* are the weight fractions of MTBE in the feed and the permeate, respectively.

The effect of feed concentrations and temperatures on the MTBE selectivity of the membranes are presented in Figures 5.9a and b. In general, the MTBE selectivity of the modified membranes were superior to the original membrane for all operating parameters, and the MTBE selectivity of CNIM-f on average was higher than that of GOIM. The high selectivity of CNIM-f and GOIM over the original membrane is attributed to the facilitated transport of MTBE via f-CNTs and GO across the membrane that promote the membrane selectivity. As shown in Figure 5.9a, the selectivity of all membranes decreased with the

increment of feed concentration. This was ascribed to the negative effect of viscosity [310]. The maximum selectivity of 54 was obtained for CNIM-f at the feed concentration of 0.5 wt%, while the average selectivity of CNIM-f, GOIM, and the plain membrane were 41, 36, and 31, respectively. As can be seen from Figure 5.9b, the selectivity of the membrane, except GOIM, trended to reduce with an increase in the temperature. This may be due to the reduction in sorption capacity with temperature, which affects the overall selectivity. It is also possible that the negative effect of viscosity compensated for the effect of temperature increase, and lead to the selectivity decrease as mentioned in the articles [147, 310]. The highest selectivity of 38 was also achieved by CNIM-f. Although, the selectivity of GOIM had an opposite tendency to the others, its average selectivity did not have a significant difference from that of CNIM-f. The selectivity of GOIM was 33, whereas the selectivity of CNIM-f and the pristine membrane were 34 and 23, respectively.

5.3.2 Mass Transfer Coefficients

The mass transfer coefficient (k) can be expressed as:

$$k = \frac{J_{MTBE}}{(P_f - P_p)} \tag{5.4}$$

where J_{MTBE} is the flux, P_f and P_p are the partial vapor pressures of the MTBE in the feed and permeate side, respectively. The partial pressure of MTBE on the feed side at a particular temperature was obtained from the calculation following Raoult's Law. Since the permeate side of the membrane was dry air, the partial vapor pressure was considered as close to be zero.

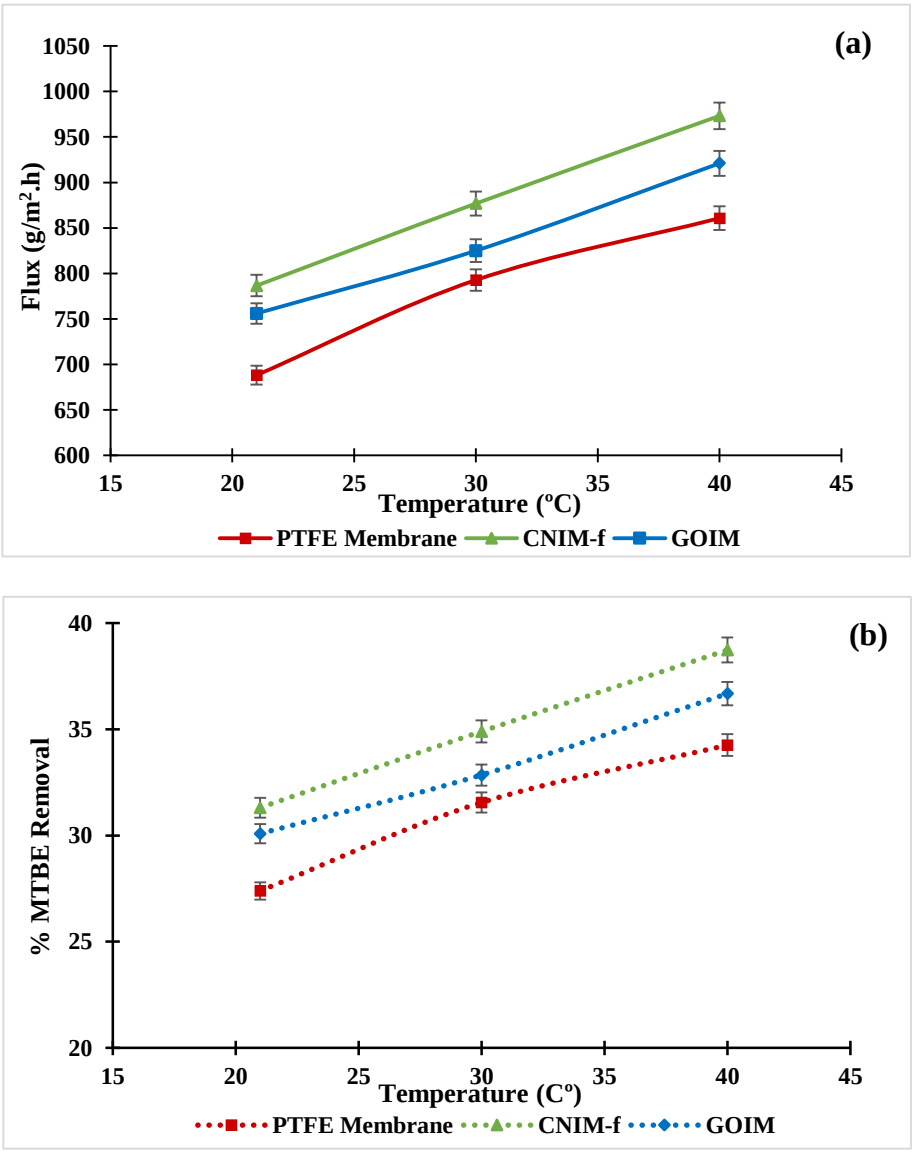

Figure 5.8 a) Effect of feed temperature on MTBE flux, and **b)** % MTBE removal as the function of feed temperature at the feed concentration of 1.5 wt% and the feed flow rate of 20 mL/min.

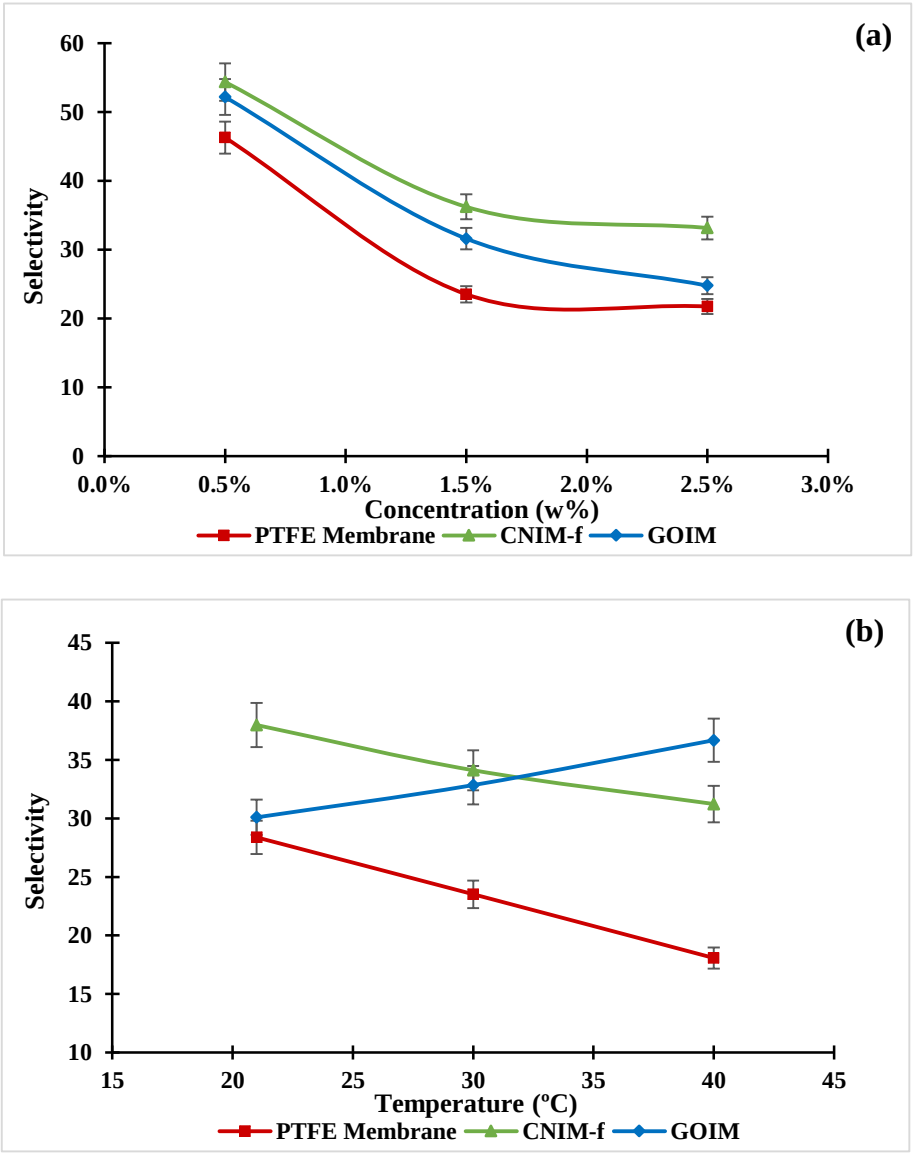

Figure 5.9 Effect of **a)** feed concentration and **b)** feed temperature on MTBE selectivity of membranes.

The permeate flux can be expressed by an Arrhenius-type equation and the activation energy of the transport (*Ea*) can be calculated from this equation [312, 313].

$$J = A\ exp\ [-\frac{Ea}{RT}] \tag{5.4}$$

where J is permeate flux (mol m^{-2} h^{-1}), R is the gas constant (J mol^{-1} K^{-1}), and T is feed temperature (K).

Table 5.1 shows the variation of the mass transfer coefficients (k) of 1.5 wt% MTBE at various feed temperatures, and at a constant feed flow rate of 20 mL/min. With an increase in the feed temperatures, the k values of MTBE tended to decline. The CNIM-f offered the highest mass transfer coefficient, followed by GOIM and the plain PTFE membrane. The larger k values for CNIM-f was ascribed to the activated diffusion of MTBE on the f-CNT surface. The mass transfer coefficient enhancement of CNIM-f varied from 10 % to 14%, compared to the plain membrane. The activation energy (*Ea*) for MTBE was calculated from the equation (5). The activation energies of PTFE membrane, CNIM-f and GOIM were 9, 8.6 and 7.9 kJ/mol, respectively. Although the Ea values for MTBE were lower than that has been reported for chloroform and butanol using MD [314, 315], a direct comparison to those values may not be relevant due to the variations in the nature of chemicals, membranes and process parameters. At the same time, significantly lower values in the range of 1-3 kJ/mol have been reported for THF and methanol for pervaporative separation [316, 317]. However, what is important is that the activation

energy dropped with the CNT and GO modifications indicating facilitated transport with these modifications.

Table 5.1 Mass Transfer Coefficient of 1.5% MTBE Feed Solution at Various Feed Temperatures with a Feed Flow Rate of 20 mL/min

Temperature (°C)	Mass transfer coefficient ($kg/m^2.s.Pa$) × 10^{-6}		
	PTFE Membrane	GOIM	CNIM-f
21	2.19±0.08	2.41±0.08	2.51±0.09
30	1.70±0.02	1.77±0.02	1.88±0.03
40	1.29±0.04	1.38±0.04	1.45±0.07

5.3.3 Membrane Stability

The thermal stability of the membranes was investigated by TGA as mentioned before. The results showed that there is no significant change happening with the membranes at the temperatures below 150 °C, which indicates the safe use of membranes at the operating temperatures of this study. The membrane wetting and change in the MTBE flux were also studied to evaluate the operational stability of the membranes for 30 days (8 hrs/day). No solvent leakage, as well as a change in MTBE flux, were observed over the period of time.

5.4 Proposed Mechanism

The modified membranes, namely CNIM-f and GOIM, showed a significant enhancement in MTBE removal performance over the unmodified one. This could be attributed mainly to the fact that the f-CNTs and GO are excellent adsorbents for volatile organics [188]. The engineered nano-carbon provided high specific surface area and served as sorption sites.

In addition, the surface functional groups, such as the carboxylic group on f-CNTs, and epoxy, carboxyl, carbonyl and hydroxyl groups for GO also play a major role as interaction sites for polar organic compounds like MTBE. Although, it has been reported that, compared to CNTs, GO has a higher specific surface area [318], the CNIM-f provided the larger MTBE flux for this study. The formation of stacked graphene oxide layers on the membrane [319] could reduce the effective sorption sites and hinder the MTBE transport across GOIM, whereas the array of f-CNTs is expected to form as the pathway on CNIM-f, and fast adsorption-desorption on the CNT surface brings about the activated diffusion, and consequently enhances MTBE separation performances [255]. The proposed mechanism for MTBE flux enhancement by CNIM-f and GOIM is shown in Figure 5.10.

5.5 Conclusions

MTBE flux enhancement was achieved by using f-CNTs and GO-modified membranes. CNIM-f performance was superior to both GOIM and the original PTFE membrane in terms of flux, percent recovery, and mass transfer coefficients for all parameter variations. CNIM-f yielded the maximum flux of 1.4 kg/m^2 h at the feed concentration of 2.5 wt%, and the highest percent enhancement and percent MTBE removal were 22% and 56% at the feed concentration of 0.5 wt%, respectively. Incorporation of nanomaterials also improved the membrane selectivity for MTBE, and the overall MTBE selectivity of CNIM-f was highest among the membranes. Immobilization of f-CNTs and GO on the plain membrane significantly enhanced partition coefficients, and that was confirmed by the reduction of the contact angle, which played a part in high MTBE transport. However, the higher MTBE flux for CNIM-f was attributed to the formation of f-CNTs array on the

membrane and fast adsorption-desorption on the frictionless f-CNT surface that led to the activated diffusion.

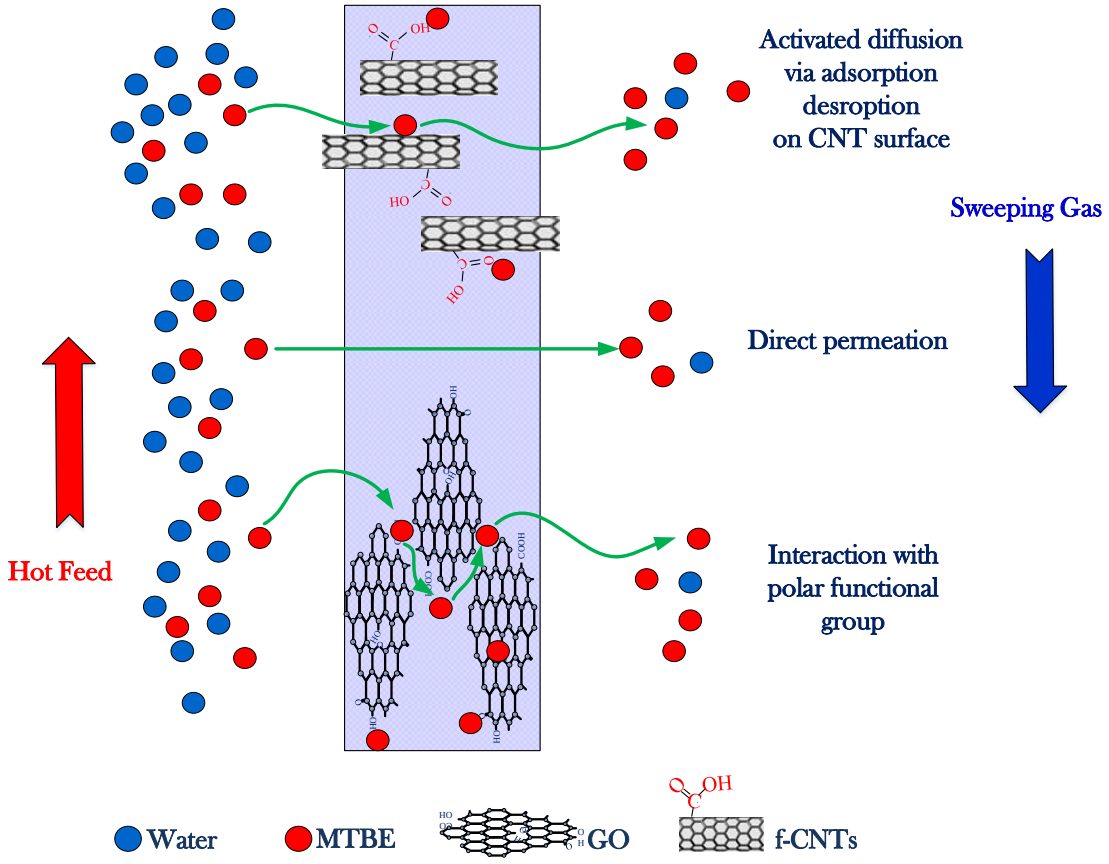

Figure 5.10 Schematic diagram for mechanism proposed on CNIM-f and GOIM.

CHAPTER 6

CONCLUSIONS AND RECOMMENDATIONS

6.1 Conclusions

This dissertation presents the enhancement of MD performance using membrane modification with carbon-based materials, such as CNTs, GO and their derivatives. Three different experiments were conducted to investigate the potentials of the modified membrane for desalination, and solvent separations via DCMD and SGMD. Overall, the membrane modified by CNTs and GO showed the great potentials for water purification, and solvent removal from aqueous solutions.

Graphene oxide was successful in hydrophilizing the permeate side of a commercial PP supported PTFE membrane for DCMD. Immobilization of the GO improved the hydrophilicity of membrane surface at the permeate side. The hydrophilicity of the membrane attracted the surface boundary of the bulk cold water close to the membrane surface, this led to the contraction of the boundary layer on the permeate side and the reduction of mass transfer resistance, and consequently permeate flux enhancement. The polar epoxy, carboxyl, and hydroxyl functional groups on GO also allowed more water vapor and cold water to interact with the modified permeate surface, that facilitate fast condensation and withdrawal of the permeate water vapors. These resulted in water vapor flux enhancement.

Functionalized CNT immobilized membrane (CNIM-f) effectively enhanced the performance of DCMD in ammonia separation. Among the membranes (a original membrane, CNIM and CNIM-f) used in the experiment, CNIM-f showed the highest flux, ammonia recovery, mass transfer coefficients, and overall selectivity. The presence of a

large number of carboxylic functional groups on the f-CNTs provided more sites for preferential sorption of ammonia, and led to increase in activated diffusion for ammonia. Although the result is obtained from DCMD, the concept using functionalized CNTs is valid for all configurations of MD.

Functionalized CNT immobilized membrane (CNIM-f) is also the excellent membrane for MTBE separation via SGMD. Compared to the plain membrane and GOIM, CNIM-f offered the greatest performance in terms of flux, removal efficiency, mass transfer coefficients and overall selectivity. Although the f-CNTs and GO are excellent adsorbents for VOCs, the formation of f-CNT array on CNIM-f was expected to be the pathway of MTBE, and fast adsorption-desorption on the CNT surface resulted in activated diffusion, and consequently enhanced MTBE separation.

6.2 Recommendations

Immobilization CNTs and GO on the commercial membranes using drop casting method can enhance the performance of the modified membrane, and is proper for laboratory scale. However, the thickness and the homogeneity of the coated layer still need to be improved in order to obtain the optimum membrane, and maximum permeate flux. The new coating techniques should be researched, and developed for use in the laboratory in the larger scale.

Nanocarbon material immobilized membranes for MD showed the excellent performance in desalination, and other separations in bench-scale testing. The further pilot scale of MD, using these modified membranes should be performed to assess the feasibility of a full-scale operation.

Computer simulation for MD using the nanocarbon material immobilized membranes should be performed, along with the laboratory experiment to study the mechanisms facilitating the flux enhancement for the modified membrane. Consequently, the obtained data should be used to fabricate the optimum membranes and adjust the operating conditions to enhance the maximum flux.

Synthetic feed solutions are usually used for laboratory to get rid of the interferences during the experiments. However, real water samples, such as seawater and other contaminated waters should be studied to obtain accurate results and understand the issues that may happen in the real world.

The relationship between the contact angle and permeate flux was found. The permeate flux of MTBE is an example. The flux of MTBE increased with a decrease in contact angle. The reduction of contact angles for CNIM-f and GOIM was attributed to the interaction of the MTBE and the polar functional groups on GO and f-CNTs. This enhanced partition coefficient of MTBE on modified membrane and consequently led to higher MTBE transfer. Therefore, the functionalization of nanocarbon with different functional groups should be researched for a future MD study

APPENDIX

METHOD #:350.2
APPROVED FOR NPDES (EDITORIAL REVISION 1974)

TITLE:	Nitrogen, Ammonia (Colorimetric, Titrimetric, Potentiometric Distillation Procedure
ANALYTE:	CAS # Nitrogen 7727-37-9, N CAS # Ammonium 7664-41-7, NH
INSTRUMENTATION:	Titration, Spectrophotometer
STORET No.	Total 00610 Dissolved 0060

1.0 Scope and Application

1.1 This distillation method covers the determination of ammonia-nitrogen exclusive of total Kjeldahl nitrogen, in drinking, surface and saline waters, domestic and industrial wastes. It is the method of choice where economics and sample load do not warrant the use of automated equipment.

1.2 The method covers the range from about 0.05 to 1.0 mg NH_3-N/L for the colorimetric procedure, from 1.0 to 25 mg/L for the titrimetric procedure, and from 0.05 to 1400 mg/L for the electrode method.

1.3 This method is described for macro glassware; however, microdistillation equipment may also be used.

2.0 Summary of Method

2.1 The sample is buffered at a pH of 9.5 with a borate buffer in order to decrease hydrolysis of cyanates and organic nitrogen compounds, and is then distilled into a solution of boric acid. The ammonia in the distillate can be determined colorimetrically by nesslerization, titrimetrically with standard sulfuric acid with the use of a mixed indicator, or

potentiometrically by the ammonia electrode. The choice between the first two procedures depends on the concentration of the ammonia

3.0 Sample Handling and Preservation

3.1 Samples may be preserved with 2 mL of conc. H_2SO_4 per liter and stored at 4°C.

4.0 Interferences

4.1 A number of aromatic and aliphatic amines, as well as other compounds, both organic and inorganic, will cause turbidity upon the addition of Nessler reagent, so direct nesslerization (i.e., without distillation), has been discarded as an official method.

4.2 Cyanate, which may be encountered in certain industrial emuents, will hydrolyze to some extent even at the pH of 9.5 at which distillation is carried out. Volatile alkaline compounds, such as certain ketones, aldehydes, and alcohols, may cause an off-color upon nesslerization in the distillation method. Some of these, such as formaldehyde, may be eliminated by boiling off at a low pH (approximately 2 to 3) prior to distillation and nesslerization.

4.3 Residual chlorine must also be removed by pretreatment of the sample with sodium thiosulfate before distillation.

5.0 Apparatus

5.1 An all-glass distilling apparatus with an 800-1000 mL flask.

5.2 Spectrophotometer or filter photometer for use at 425 nm and providing a light path of 1 cm or more.

5.3 Nessler tubes: Matched Nessler tubes (APHA Standard) about 300 mm long, 17 mm inside diameter, and marked at 225 mm ±1.5 mm inside measurement from bottom.

5.4 Erlenmeyer flasks: The distillate is collected in 500 mL glass-stoppered flasks. These flasks should be marked at the 350 and the 500 mL volumes. With such marking, it is not necessary to transfer the distillate to volumetric flasks.

6.0 Reagents

6.1 Distilled water should be free of ammonia. Such water is best prepared by passage through an ion exchange column containing a strongly acidic cation exchange resin mixed with a strongly basic anion exchange resin. Regeneration of the column should be carried out according to the manufacturer's instructions.

NOTE 1: All solutions must be made with ammonia-free water.

6.2 Ammonium chloride, stock solution: 1.0 mL = 1.0 mg NH_3-N. Dissolve 3.819 g NH_4Cl in distilled water and bring to volume in a 1 liter volumetric flask.

6.3 Ammonium chloride, standard solution: 1.0 mL = 0.01 mg. Dilute 10.0 mL of stock solution (6.2) to 1 liter in a volumetric flask.

6.4 Boric acid solution (20 g/L): Dissolve 20 g H_3BO_3 in distilled water and dilute to 1 liter.

6.5 Mixed indicator: Mix 2 volumes of 0.2% methyl red in 95% ethyl alcohol with 1 volume of 0.2% methylene blue in 95% ethyl alcohol. This solution should be prepared fresh every 30 days.

NOTE 2: Specially denatured ethyl alcohol conforming to Formula 3A or 30 of the U.S. Bureau of Internal Revenue may be substituted for 95% ethanol.

6.6 Nessler reagent: Dissolve 100 g of mercuric iodide and 70 g of potassium iodide in a small amount of water. Add this mixture slowly, with stirring, to a cooled solution of 160 g of NaOH in 500 mL of water. Dilute the mixture to 1 liter. If this reagent is stored in a Pyrex bottle out of direct sunlight, it will remain stable for a period of up to 1 year.

NOTE 3: This reagent should give the characteristic color with ammonia within 10 minutes after addition, and should not produce a precipitate with small amounts of ammonia (0.04 mg in a 50 mL volume).

6.7 Borate buffer: Add 88 mL of 0.1 N NaOH solution to 500 mL of 0.025 M sodium tetraborate solution (5.0 g anhydrous $Na_2B_4O_7$, or 9.5 g $Na_2B_4O_7$ $10H^2O$ per liter) and dilute to 1 liter.

6.8 Sulfuric acid, standard solution: (0.02 N, 1 mL = 0.28 mg NH_3-N). Prepare a stock solution of approximately 0.1 N acid by diluting 3 mL of conc. H_2SO_4 (sp. gr. 1.84) to 1 liter with CO_2-free distilled water. Dilute 200 mL of this solution to 1 liter with CO_2-free distilled water.

NOTE 4: An alternate and perhaps preferable method is to standardize the approximately 0.1 N H2SO4 solution against a 0.100 N Na_2CO_3 solution. By proper dilution the 0.02 N acid can then be prepared.

6.8.1 Standardize the approximately 0.02 N acid against 0.0200 N Na_2CO_3 solution. This last solution is prepared by dissolving 1.060 g anhydrous Na_2CO_3, oven-dried at 140°C, and diluting to 1000 mL with CO_2-free distilled water.

6.9 Sodium hydroxide 1 N: Dissolve 40 g NaOH in ammonia-free water and dilute to 1 liter.

6.10 Dechlorinating reagents: A number of dechlorinating reagents may be used to remove residual chlorine prior to distillation. These include:

a. Sodium thiosulfate (1/70 N): Dissolve 3.5 g $Na_2S_2O_3$ $5H_2O$ in distilled water and dilute to 1 liter. One mL of this solution will remove 1 mg/L of residual chlorine in 500 mL of sample.

b. Sodium arsenite (1/70 N): Dissolve 1.0 g $NaAsO_2$ in distilled water and dilute to 1 liter.

7.0 Procedure

7.1 Preparation of equipment: Add 500 mL of distilled water to an 800 mL Kjeldahl flask. The addition of boiling chips which have been previously

treated with dilute NaOH will prevent bumping. Steam out the distillation apparatus until the distillate shows no trace of ammonia with Nessler reagent.

7.2 Sample preparation: Remove the residual chlorine in the sample by adding dechlorinating agent equivalent to the chlorine residual. To 400 mL of sample add 1 N NaOH (6.9), until the pH is 9.5, checking the pH during addition with a pH meter or by use of a short range pH paper.

7.3 Distillation: Transfer the sample, the pH of which has been adjusted to 9.5, to an 800 mL Kjeldahl flask and add 25 mL of the borate buffer (6.7). Distill 300 mL at the rate of 6-10 mL/min. into 50 mL of 2% boric acid (6.4) contained in a 500 mL Erlenmeyer flask.

NOTE 5: The condenser tip or an extension of the condenser tip must extend below the level of the boric acid solution. Dilute the distillate to 500 mL with distilled water and nesslerize an aliquot to obtain an approximate value of the ammonia-nitrogen concentration. For concentrations above 1 mg/L the ammonia should be determined titrimetrically. For concentrations below this value it is determined colorimetrically. The electrode method may also be used.

7.4 Determination of ammonia in distillate: Determine the ammonia content of the distillate titrimetrically, colorimetrically or potentiometrically as described below.

7.4.1 Titrimetric determination: Add 3 drops of the mixed indicator to the distillate and titrate the ammonia with the 0.02 N H_2SO_4, matching the end point against a blank containing the same volume of distilled water and H_3BO_3 solution.

7.4.2 Colorimetric determination: Prepare a series of Nessler tube standards as follows:

mL of Standard 1.0 mL = mg NH_3-N	mg NH_3-N/50.0 mL
0.0	0.0
0.5	0.005
1.0	0.01
2.0	0.02
3.0	0.03
4.0	0.04
5.0	0.05
8.0	0.08
10.0	0.10

Dilute each tube to 50 mL with distilled water, add 2.0 mL of Nessler reagent (6.6) and mix. After 20 minutes read the absorbance at 425 nm against the blank. From the values obtained plot absorbance vs. mg NH_3-N for the standard curve. Determine the ammonia in the distillate by nesslerizing 50 mL or an aliquot diluted to 50 mL and reading the absorbance at 425 nm as described above for the standards. Ammonia-nitrogen content is read from the standard curve.

7.4.3 Potentiometric determination: Consult the method entitled Nitrogen, Ammonia: Selective Ion Electrode Method (Method 350.3) in this manual.

7.5 It is not imperative that all standards be distilled in the same manner as the samples. It is recommended that at least two standards (a high and low) be distilled and compared to similar values on the curve to insure that the distillation technique is reliable. If distilled standards do not agree with undistilled standards the operator should find the cause of the apparent error before proceeding.

8.0 Calculations

8.1 Titrimetric

$$\frac{\text{mg}}{\text{L}} NH_3 - N = \frac{A\ x\ 0.28\ x\ 1000}{S}$$

where:

A = mL 0.02 N H_2SO_4 used.

S = mL sample.

8.2 Spectrophotometric

$$\frac{\text{mg}}{\text{L}} NH_3 - N = \frac{A\ x\ 1000}{D} x\ \frac{B}{C}$$

where:

A = mg NH_3-N read from standard curve.

B = mL total distillate collected, including boric acid and dilution.

C = mL distillate taken for nesslerization.

D = mL of original sample taken

8.3 Potentiometric

$$\frac{\text{mg}}{\text{L}} NH_3 - N = \frac{500}{D} x\ A$$

where:

A = mg NH_3-N/L from electrode method standard curve.

D = mL of original sample taken.

9. Precision and Accuracy

9.1 Twenty-four analysts in sixteen laboratories analyzed natural water samples containing exact increments of an ammonium salt, with the following results:

Increment as Nitrogen, Ammonia mg N/liter	Precision as Standard Deviation mg N/liter	Accuracy as Bias %	Accuracy as Bias mg N/liter
0.21	0.122	-5.54	-0.01
0.26	0.070	-18.12	-0.05
1.71	0.244	+0.46	+0.01
1.92	0.279	-2.01	-0.04

(FWPCA Method Study 2, Nutrient Analyses)

[320, 321]

REFERENCES

[1] Department of Economics and Social Affairs, U.N. (2017). *World population projected to reach 9.8 billion in 2050, and 11.2 billion in 2100*. Retrieved 15 November, 2019, from https://www.un.org/development/desa/en/news/population/world-population-prospects-2017.html

[2] Hu, Y., Liu, X., Bai, J., Shih, K., Zeng, E.Y., Cheng, H. *Assessing heavy metal pollution in the surface soils of a region that had undergone three decades of intense industrialization and urbanization*. Environmental Science and Pollution Research. 2013; 20(9): 6150-6159.

[3] Ebenstein, A. *The consequences of industrialization: evidence from water pollution and digestive cancers in China*. The Review of Economics and Statistics. 2012; 94(1): 186-201.

[4] Shankar, B., Balasubramanya, N., Reddy, M.M. *Impact of industrialization on groundwater quality–a case study of Peenya industrial area, Bangalore, India*. Environmental Monitoring and Assessment. 2008; 142(1-3): 263-268.

[5] Adegbola, O. *The impact of urbanization and industrialization on health conditions: the case of Nigeria*. World Health Statistics Quarterly. 1987; 40(1): 74-83.

[6] Kurucu, Y., Chiristina, N.K. *Monitoring the impacts of urbanization and industrialization on the agricultural land and environment of the Torbali, Izmir region, Turkey*. Environmental Monitoring and Assessment. 2008; 136(1-3): 289-297.

[7] Schwarzenbach, R.P., Egli, T., Hofstetter, T.B., Von Gunten, U., Wehrli, B. *Global water pollution and human health*. Annual Review of Environment and Resources. 2010; 35: 109-136.

[8] Hunter, P.R., MacDonald, A.M., Carter, R.C. *Water supply and health*. PLoS Medicine. 2010; 7(11): e1000361.

[9] Drioli, E., Ali, A., Macedonio, F. *Membrane distillation: Recent developments and perspectives*. Desalination. 2015; 356: 56-84.

[10] Oki, T., Kanae, S. *Global hydrological cycles and world water resources*. Science. 2006; 313(5790): 1068-1072.

[11] Kolpin, D.W., Furlong, E.T., Meyer, M.T., Thurman, E.M., Zaugg, S.D., Barber, L.B., Buxton, H.T. *Pharmaceuticals, hormones, and other organic wastewater contaminants in US streams, 1999− 2000: A national reconnaissance*. Environmental Science & Technology. 2002; 36(6): 1202-1211.

[12] Pionke, H.B., Gburek, W.J., Sharpley, A.N. *Critical source area controls on water quality in an agricultural watershed located in the Chesapeake Basin*. Ecological Engineering. 2000; 14(4): 325-335.

[13] Bañuelos, G., Pasakdee, S., Finley, J. *Growth response and selenium and boron distribution in broccoli varieties irrigated with poor quality water*. Journal of Plant Nutrition. 2003; 26(12): 2537-2549.

[14] Mekonnen, M.M., Hoekstra, A.Y. *Four billion people facing severe water scarcity*. Science Advances. 2016; 2(2): e1500323.

[15] Iglesias, A., Garrote, L., Flores, F., Moneo, M. *Challenges to manage the risk of water scarcity and climate change in the Mediterranean*. Water Resources Management. 2007; 21(5): 775-788.

[16] Khawaji, A.D., Kutubkhanah, I.K., Wie, J.-M. *Advances in seawater desalination technologies*. Desalination. 2008; 221(1-3): 47-69.

[17] Cheremisinoff, P.N., *Handbook of water and wastewater treatment technology*:Routledge, 2019.

[18] Ciardelli, G., Corsi, L., Marcucci, M. *Membrane separation for wastewater reuse in the textile industry*. Resources, Conservation and Recycling. 2001; 31(2): 189-197.

[19] Snyder, S.A., Westerhoff, P., Yoon, Y., Sedlak, D.L. *Pharmaceuticals, personal care products, and endocrine disruptors in water: implications for the water industry*. Environmental Engineering Science. 2003; 20(5): 449-469.

[20] Field, R.W., Pearce, G.K. *Critical, sustainable and threshold fluxes for membrane filtration with water industry applications*. Advances in Colloid and Interface Science. 2011; 164(1-2): 38-44.

[21] Mavrov, V., Bélières, E. *Reduction of water consumption and wastewater quantities in the food industry by water recycling using membrane processes*. Desalination. 2000; 131(1-3): 75-86.

[22] Scott, K., Hughes, R., *Industrial membrane separation technology*, Netherlands:Springer Science & Business Media, 2012.

[23] Hilal, N., Khayet, M., Wright, C.J., *Membrane modification: Technology and applications*, Boca Raton, Florida:CRC press, 2016.

[24] Geise, G.M., Park, H.B., Sagle, A.C., Freeman, B.D., McGrath, J.E. *Water permeability and water/salt selectivity tradeoff in polymers for desalination*. Journal of Membrane Science. 2011; 369(1-2): 130-138.

[25] Zhang, T.C., Surampalli, R.Y., Vigneswaran, S., Tyagi, R., Leong Ong, S., Kao, C., *Membrane technology and environmental applications*, American Society of Civil Engineers, 2012.

[26] Hillis, P., *Membrane technology in water and wastewater treatment*:Royal Society of Chemistry, 2007.

[27] Hilal, N., Ogunbiyi, O.O., Miles, N.J., Nigmatullin, R. *Methods employed for control of fouling in MF and UF membranes: a comprehensive review*. Separation Science and Technology. 2005; 40(10): 1957-2005.

[28] Schäfer, A., Andritsos, N., Karabelas, A.J., Hoek, E., Schneider, R., Nyström, M., *Fouling in Nanofiltration*, Oxford, UK: Elsevier, 2004.

[29] Nicolaisen, B. *Developments in membrane technology for water treatment*. Desalination. 2003; 153(1-3): 355-360.

[30] Younos, T., Tulou, K.E. *Overview of desalination techniques*. Journal of Contemporary Water Research and Education. 2005; 132(1): 3-10.

[31] Atikol, U., Aybar, H.S. *Estimation of water production cost in the feasibility analysis of RO systems*. Desalination. 2005; 184(1-3): 253-258.

[32] Ma, N., Wei, J., Qi, S., Zhao, Y., Gao, Y., Tang, C.Y. *Nanocomposite substrates for controlling internal concentration polarization in forward osmosis membranes*. Journal of Membrane Science. 2013; 441: 54-62.

[33] Nguyen, H.T., Nguyen, N.C., Chen, S.-S., Ngo, H.H., Guo, W., Li, C.-W. *A new class of draw solutions for minimizing reverse salt flux to improve forward osmosis desalination*. Science of the Total Environment. 2015; 538: 129-136.

[34] Lutchmiah, K., Verliefde, A., Roest, K., Rietveld, L.C., Cornelissen, E. *Forward osmosis for application in wastewater treatment: a review*. Water Research. 2014; 58: 179-197.

[35] Subramani, A., Jacangelo, J.G. *Emerging desalination technologies for water treatment: a critical review*. Water Research. 2015; 75: 164-187.

[36] Shirazi, M.M.A., Kargari, A., Shirazi, M.J.A. *Direct contact membrane distillation for seawater desalination*. Desalination and Water Treatment. 2012; 49(1-3): 368-375.

[37] Camacho, L.M., Dumée, L., Zhang, J., Li, J.-d., Duke, M., Gomez, J., Gray, S. *Advances in membrane distillation for water desalination and purification applications*. Water. 2013; 5(1): 94-196.

[38] Calabro, V., Drioli, E., Matera, F. *Membrane distillation in the textile wastewater treatment*. Desalination. 1991; 83(1-3): 209-224.

[39] Alkhudhiri, A., Darwish, N., Hilal, N. *Produced water treatment: application of air gap membrane distillation*. Desalination. 2013; 309: 46-51.

[40] Ge, Q., Wang, P., Wan, C., Chung, T.-S. *Polyelectrolyte-promoted forward osmosis–membrane distillation (FO–MD) hybrid process for dye wastewater treatment*. Environmental Science & Technology. 2012; 46(11): 6236-6243.

[41] Zhang, S., Wang, P., Fu, X., Chung, T.-S. *Sustainable water recovery from oily wastewater via forward osmosis-membrane distillation (FO-MD)*. Water Research. 2014; 52: 112-121.

[42] Eykens, L., De Sitter, K., Dotremont, C., Pinoy, L., Van der Bruggen, B. *Membrane synthesis for membrane distillation: A review*. Separation and Purification Technology. 2017; 182: 36-51.

[43] Dow, N., Gray, S., Zhang, J., Ostarcevic, E., Liubinas, A., Atherton, P., Roeszler, G., Gibbs, A., Duke, M. *Pilot trial of membrane distillation driven by low grade waste heat: Membrane fouling and energy assessment*. Desalination. 2016; 391: 30-42.

[44] Qtaishat, M.R., Banat, F. *Desalination by solar powered membrane distillation systems*. Desalination. 2013; 308: 186-197.

[45] Sarbatly, R., Chiam, C.-K. *Evaluation of geothermal energy in desalination by vacuum membrane distillation*. Applied Energy. 2013; 112: 737-746.

[46] Khayet, M., Matsuura, T., *Membrane distillation: principles and applications*:Elsevier, 2011.

[47] Alkhudhiri, A., Darwish, N., Hilal, N. *Membrane distillation: A comprehensive review*. Desalination. 2012; 287: 2-18.

[48] Martínez-Díez, L., Vazquez-Gonzalez, M.I. *Temperature and concentration polarization in membrane distillation of aqueous salt solutions*. Journal of Membrane Science. 1999; 156(2): 265-273.

[49] Onsekizoglu, P. *Membrane distillation: principle, advances, limitations and future prospects in food industry*. Distillation-Advances from Modeling to Applications. 2012: 282.

[50] Khayet, M. *Membranes and theoretical modeling of membrane distillation: a review*. Advances in Colloid and Interface Science. 2011; 164(1-2): 56-88.

[51] Abu-Zeid, M.A.E.-R., Zhang, Y., Dong, H., Zhang, L., Chen, H.-L., Hou, L. *A comprehensive review of vacuum membrane distillation technique*. Desalination. 2015; 356: 1-14.

[52] Biniaz, P., Torabi Ardekani, N., Makarem, M.A., Rahimpour, M.R. *Water and wastewater treatment systems by novel integrated membrane distillation (MD)*. ChemEngineering. 2019; 3(1): 8.

[53] Schofield, R., Fane, A., Fell, C. *Heat and mass transfer in membrane distillation*. Journal of Membrane Science. 1987; 33(3): 299-313.

[54] Zhang, J., Dow, N., Duke, M., Ostarcevic, E., Gray, S. *Identification of material and physical features of membrane distillation membranes for high performance desalination*. Journal of Membrane Science. 2010; 349(1-2): 295-303.

[55] Termpiyakul, P., Jiraratananon, R., Srisurichan, S. *Heat and mass transfer characteristics of a direct contact membrane distillation process for desalination*. Desalination. 2005; 177(1-3): 133-141.

[56] Ding, Z., Ma, R., Fane, A. *A new model for mass transfer in direct contact membrane distillation*. Desalination. 2003; 151(3): 217-227.

[57] Khayet, M., Velázquez, A., Mengual, J.I. *Modelling mass transport through a porous partition: effect of pore size distribution*. Journal of Non-Equilibrium Thermodynamics. 2004; 29(3): 279-299.

[58] Guijt, C.M., Racz, I.G., van Heuven, J.W., Reith, T., de Haan, A. *Modelling of a transmembrane evaporation module for desalination of seawater*. Desalination. 1999; 126(1-3): 119-125.

[59] Lawson, K.W., Lloyd, D.R. *Membrane distillation*. Journal of Membrane Science. 1997; 124(1): 1-25.

[60] Schofield, R., Fane, A., Fell, C. *Gas and vapour transport through microporous membranes. I. Knudsen-Poiseuille transition*. Journal of Membrane Science. 1990; 53(1-2): 159-171.

[61] Fane, A.G., Schofield, R., Fell, C.J.D. *The efficient use of energy in membrane distillation*. Desalination. 1987; 64: 231-243.

[62] Schofield, R., Fane, A., Fell, C. *Gas and vapour transport through microporous membranes. II. Membrane distillation*. Journal of Membrane Science. 1990; 53(1-2): 173-185.

[63] Fernández-Pineda, C., Izquierdo-Gil, M., Garcıa-Payo, M. *Gas permeation and direct contact membrane distillation experiments and their analysis using different models*. Journal of Membrane Science. 2002; 198(1): 33-49.

[64] Qtaishat, M., Matsuura, T., Kruczek, B., Khayet, M. *Heat and mass transfer analysis in direct contact membrane distillation*. Desalination. 2008; 219(1-3): 272-292.

[65] Curcio, E., Drioli, E. *Membrane distillation and related operations—a review*. Separation and Purification Reviews. 2005; 34(1): 35-86.

[66] Phattaranawik, J., Jiraratananon, R. *Direct contact membrane distillation: effect of mass transfer on heat transfer*. Journal of Membrane Science. 2001; 188(1): 137-143.

[67] Sablani, S., Goosen, M., Al-Belushi, R., Wilf, M. *Concentration polarization in ultrafiltration and reverse osmosis: a critical review*. Desalination. 2001; 141(3): 269-289.

[68] Laganà, F., Barbieri, G., Drioli, E. *Direct contact membrane distillation: modelling and concentration experiments*. Journal of Membrane Science. 2000; 166(1): 1-11.

[69] Martínez, L., Rodríguez-Maroto, J.M. *On transport resistances in direct contact membrane distillation*. Journal of Membrane Science. 2007; 295(1-2): 28-39.

[70] Gunko, S., Verbych, S., Bryk, M., Hilal, N. *Concentration of apple juice using direct contact membrane distillation*. Desalination. 2006; 190(1-3): 117-124.

[71] Chen, T.-C., Ho, C.-D., Yeh, H.-M. *Theoretical modeling and experimental analysis of direct contact membrane distillation*. Journal of Membrane Science. 2009; 330(1-2): 279-287.

[72] Srisurichan, S., Jiraratananon, R., Fane, A. *Mass transfer mechanisms and transport resistances in direct contact membrane distillation process*. Journal of Membrane Science. 2006; 277(1-2): 186-194.

[73] Zhang, J., Gray, S. *Modelling heat and mass transfers in DCMD using compressible membranes*. Journal of Membrane Science. 2012; 387: 7-16.

[74] Calabro, V., Jiao, B.L., Drioli, E. *Theoretical and experimental study on membrane distillation in the concentration of orange juice*. Industrial and Engineering Chemistry Research. 1994; 33(7): 1803-1808.

[75] Banat, F.A., Simandl, J. *Desalination by membrane distillation: a parametric study*. 1998.

[76] Matheswaran, M., Kwon, T.O., Kim, J.W., Moon, I.S. *Factors affecting flux and water separation performance in air gap membrane distillation*. Journal of Industrial and Engineering Chemistry. 2007; 13(6): 965-970.

[77] Martínez, L. *Comparison of membrane distillation performance using different feeds*. Desalination. 2004; 168: 359-365.

[78] Tomaszewska, M., Gryta, M., Morawski, A. *Study on the concentration of acids by membrane distillation*. Journal of Membrane Science. 1995; 102: 113-122.

[79] Sakai, K., Koyano, T., Muroi, T., Tamura, M. *Effects of temperature and concentration polarization on water vapour permeability for blood in membrane distillation*. The Chemical Engineering Journal. 1988; 38(3): B33-B39.

[80] Alklaibi, A.M., Lior, N. *Transport analysis of air-gap membrane distillation*. Journal of Membrane Science. 2005; 255(1-2): 239-253.

[81] Winter, D., Koschikowski, J., Wieghaus, M. *Desalination using membrane distillation: Experimental studies on full scale spiral wound modules*. Journal of Membrane Science. 2011; 375(1-2): 104-112.

[82] Izquierdo-Gil, M., Garcıa-Payo, M., Fernández-Pineda, C. *Air gap membrane distillation of sucrose aqueous solutions*. Journal of Membrane Science. 1999; 155(2): 291-307.

[83] Courel, M., Dornier, M., Herry, J.-M., Rios, G.M., Reynes, M. *Effect of operating conditions on water transport during the concentration of sucrose solutions by osmotic distillation*. Journal of Membrane Science. 2000; 170(2): 281-289.

[84] Hongvaleerat, C., Cabral, L.M., Dornier, M., Reynes, M., Ningsanond, S. *Concentration of pineapple juice by osmotic evaporation*. Journal of Food Engineering. 2008; 88(4): 548-552.

[85] Kubota, S., Ohta, K., Hayano, I., Hirai, M., Kikuchi, K., Murayama, Y. *Experiments on seawater desalination by membrane distillation*. Desalination. 1988; 69(1): 19-26.

[86] Khayet, M., Cojocaru, C., Baroudi, A. *Modeling and optimization of sweeping gas membrane distillation*. Desalination. 2012; 287: 159-166.

[87] Ding, Z., Liu, L., Li, Z., Ma, R., Yang, Z. *Experimental study of ammonia removal from water by membrane distillation (MD): The comparison of three configurations*. Journal of Membrane Science. 2006; 286(1-2): 93-103.

[88] Khayet, M., Godino, M., Mengual, J. *Theoretical and experimental studies on desalination using the sweeping gas membrane distillation method*. Desalination. 2003; 157(1-3): 297-305.

[89] Khayet, M., Godino, P., Mengual, J.I. *Theory and experiments on sweeping gas membrane distillation*. Journal of Membrane Science. 2000; 165(2): 261-272.

[90] Xie, Z., Duong, T., Hoang, M., Nguyen, C., Bolto, B. *Ammonia removal by sweep gas membrane distillation*. Water Research. 2009; 43(6): 1693-1699.

[91] Pangarkar, B.L., Sane, M. *Performance of air gap membrane distillation for desalination of ground water and seawater*. World Academy of Science, Engineering, and Technology. 2011; 75: 177-181.

[92] Alklaibi, A.M., Lior, N. *Membrane-distillation desalination: status and potential*. Desalination. 2005; 171(2): 111-131.

[93] Pangarkar, B.L., Deshmukh, S.K. *Theoretical and experimental analysis of multi-effect air gap membrane distillation process (ME-AGMD)*. Journal of Environmental Chemical Engineering. 2015; 3(3): 2127-2135.

[94] Bandini, S., Sarti, G.C. *Heat and mass transport resistances in vacuum membrane distillation per drop*. AIChE Journal. 1999; 45(7): 1422-1433.

[95] Bandini, S., Saavedra, A., Sarti, G.C. *Vacuum membrane distillation: experiments and modeling*. AIChE Journal. 1997; 43(2): 398-408.

[96] Sivakumar, M., Ramezanianpour, M., O'Halloran, G. *Mine water treatment using a vacuum membrane distillation system*. APCBEE Procedia. 2013; 5: 157-162.

[97] Lovineh, S.G., Asghari, M., Rajaei, B. *Numerical simulation and theoretical study on simultaneous effects of operating parameters in vacuum membrane distillation*. Desalination. 2013; 314: 59-66.

[98] Banat, F., Al-Rub, F.A., Bani-Melhem, K. *Desalination by vacuum membrane distillation: sensitivity analysis*. Separation and Purification Technology. 2003; 33(1): 75-87.

[99] Wu, B., Tan, X., Li, K., Teo, W. *Removal of 1, 1, 1-trichloroethane from water using a polyvinylidene fluoride hollow fiber membrane module: Vacuum membrane distillation operation*. Separation and Purification Technology. 2006; 52(2): 301-309.

[100] El-Bourawi, M., Khayet, M., Ma, R., Ding, Z., Li, Z., Zhang, X. *Application of vacuum membrane distillation for ammonia removal*. Journal of Membrane Science. 2007; 301(1-2): 200-209.

[101] Banat, F.A., Simandl, J. *Theoretical and experimental study in membrane distillation*. Desalination. 1994; 95(1): 39-52.

[102] Drioli, E., Wu, Y. *Membrane distillation: an experimental study*. Desalination. 1985; 53(1-3): 339-346.

[103] El-Bourawi, M., Ding, Z., Ma, R., Khayet, M. *A framework for better understanding membrane distillation separation process*. Journal of Membrane Science. 2006; 285(1-2): 4-29.

[104] Franken, A., Nolten, J., Mulder, M., Bargeman, D., Smolders, C. *Wetting criteria for the applicability of membrane distillation*. Journal of Membrane Science. 1987; 33(3): 315-328.

[105] Martínez, L., Florido-Díaz, F., Hernandez, A., Prádanos, P. *Estimation of vapor transfer coefficient of hydrophobic porous membranes for applications in membrane distillation*. Separation and Purification Technology. 2003; 33(1): 45-55.

[106] Susanto, H. *Towards practical implementations of membrane distillation*. Chemical Engineering and Processing: Process Intensification. 2011; 50(2): 139-150.

[107] Khayet, M., Matsuura, T. *Preparation and characterization of polyvinylidene fluoride membranes for membrane distillation*. Industrial & Engineering Chemistry Research. 2001; 40(24): 5710-5718.

[108] Al-Obaidani, S., Curcio, E., Macedonio, F., Di Profio, G., Al-Hinai, H., Drioli, E. *Potential of membrane distillation in seawater desalination: thermal efficiency, sensitivity study and cost estimation*. Journal of Membrane Science. 2008; 323(1): 85-98.

[109] Zhu, W., Zhang, X., Zhao, C., Wu, W., Hou, J., Xu, M. *A novel polypropylene microporous film*. Polymers for Advanced Technologies. 1996; 7(9): 743-748.

[110] Trommer, K., Morgenstern, B. *Nonrigid microporous PVC sheets: Preparation and properties*. Journal of Applied Polymer Science. 2010; 115(4): 2119-2126.

[111] Lalia, B.S., Kochkodan, V., Hashaikeh, R., Hilal, N. *A review on membrane fabrication: Structure, properties and performance relationship*. Desalination. 2013; 326: 77-95.

[112] Adnan, S., Hoang, M., Wang, H., Xie, Z. *Commercial PTFE membranes for membrane distillation application: effect of microstructure and support material*. Desalination. 2012; 284: 297-308.

[113] Pinnau, I., Freeman, B.D., *Formation and modification of polymeric membranes: overview*: ACS Publications, 2000.

[114] Gopal, R., Kaur, S., Ma, Z., Chan, C., Ramakrishna, S., Matsuura, T. *Electrospun nanofibrous filtration membrane*. Journal of Membrane Science. 2006; 281 (1-2): 581-586.

[115] Ahmed, F.E., Lalia, B.S., Hashaikeh, R. *A review on electrospinning for membrane fabrication: challenges and applications*. Desalination. 2015; 356: 15-30.

[116] Bodell, B.R.; US Patent. Distillation of saline water using silicone rubber membrane, No.285. 1963.

[117] Tomaszewska, M. *Membrane distillation-examples of applications in technology and environmental protection*. Polish Journal of Environmental Studies. 2000; 9(1): 27-36.

[118] Zhu, H., Wang, H., Wang, F., Guo, Y., Zhang, H., Chen, J. *Preparation and properties of PTFE hollow fiber membranes for desalination through vacuum membrane distillation*. Journal of Membrane Science. 2013; 446: 145-153.

[119] Alsalhy, Q.F., Ibrahim, S.S., Khaleel, S.R. *Performance of vacuum poly (propylene) membrane distillation (VMD) for saline water desalination*. Chemical Engineering and Processing-Process Intensification. 2017; 120: 68-80.

[120] Fan, H., Peng, Y. *Application of PVDF membranes in desalination and comparison of the VMD and DCMD processes*. Chemical Engineering Science. 2012; 79: 94-102.

[121] Teoh, M.M., Chung, T.-S. *Membrane distillation with hydrophobic macrovoid-free PVDF–PTFE hollow fiber membranes*. Separation and Purification Technology. 2009; 66(2): 229-236.

[122] Moradi, R., Karimi-Sabet, J., Shariaty-niassar, M., Amini, Y. *Experimental investigation of nanofibrous poly (vinylidene fluoride) membranes for desalination through air gap membrane distillation process*. Korean Journal of Chemical Engineering. 2016; 33(10): 2953-2960.

[123] Shirazi, M.M.A., Kargari, A., Bastani, D., Fatehi, L. *Production of drinking water from seawater using membrane distillation (MD) alternative: direct contact MD and sweeping gas MD approaches*. Desalination and Water Treatment. 2014; 52(13-15): 2372-2381.

[124] Safavi, M., Mohammadi, T. *High-salinity water desalination using VMD*. Chemical Engineering Journal. 2009; 149(1-3): 191-195.

[125] Geng, H., Wu, H., Li, P., He, Q. *Study on a new air-gap membrane distillation module for desalination*. Desalination. 2014; 334(1): 29-38.

[126] Abbas, A. *On the performance limitation of reverse osmosis water desalination systems*. International Journal of Nuclear Desalination. 2007; 2(3): 205-218.

[127] Alkhudhiri, A., Darwish, N., Hilal, N. *Treatment of high salinity solutions: Application of air gap membrane distillation*. Desalination. 2012; 287: 55-60.

[128] Sardari, K., Fyfe, P., Lincicome, D., Wickramasinghe, S.R. *Combined electrocoagulation and membrane distillation for treating high salinity produced waters*. Journal of Membrane Science. 2018; 564: 82-96.

[129] Zhou, Y., Huang, M., Deng, Q., Cai, T. *Combination and performance of forward osmosis and membrane distillation (FO-MD) for treatment of high salinity landfill leachate*. Desalination. 2017; 420: 99-105.

[130] Duong, H.C., Chivas, A.R., Nelemans, B., Duke, M., Gray, S., Cath, T.Y., Nghiem, L.D. *Treatment of RO brine from CSG produced water by spiral-wound air gap membrane distillation—A pilot study*. Desalination. 2015; 366: 121-129.

[131] Pangarkar, B.L., Sane, M.G., Guddad, M. *Reverse osmosis and membrane distillation for desalination of groundwater: a review*. ISRN Materials Science. 2011; 2011.

[132] Mericq, J.-P., Laborie, S., Cabassud, C. *Vacuum membrane distillation of seawater reverse osmosis brines*. Water Research. 2010; 44(18): 5260-5273.

[133] Jansen, A., Assink, J., Hanemaaijer, J., Van Medevoort, J., Van Sonsbeek, E. *Development and pilot testing of full-scale membrane distillation modules for deployment of waste heat*. Desalination. 2013; 323: 55-65.

[134] Lokare, O.R., Tavakkoli, S., Rodriguez, G., Khanna, V., Vidic, R.D. *Integrating membrane distillation with waste heat from natural gas compressor stations for produced water treatment in Pennsylvania*. Desalination. 2017; 413: 144-153.

[135] Gálvez, J.B., García-Rodríguez, L., Martín-Mateos, I. *Seawater desalination by an innovative solar-powered membrane distillation system: the MEDESOL project*. Desalination. 2009; 246(1-3): 567-576.

[136] El Amali, A., Bouguecha, S., Maalej, M. *Experimental study of air gap and direct contact membrane distillation configurations: application to geothermal and seawater desalination*. Desalination. 2004; 168: 357.

[137] Guillén-Burrieza, E., Blanco, J., Zaragoza, G., Alarcón, D.-C., Palenzuela, P., Ibarra, M., Gernjak, W. *Experimental analysis of an air gap membrane distillation solar desalination pilot system*. Journal of Membrane Science. 2011; 379(1-2): 386-396.

[138] Koschikowski, J., Wieghaus, M., Rommel, M. *Solar thermal driven desalination plants based on membrane distillation*. Water Science and Technology: Water Supply. 2003; 3(5-6): 49-55.

[139] Criscuoli, A., Zhong, J., Figoli, A., Carnevale, M., Huang, R., Drioli, E. *Treatment of dye solutions by vacuum membrane distillation*. Water Research. 2008; 42(20): 5031-5037.

[140] Mokhtar, N., Lau, W., Ismail, A., Veerasamy, D. *Membrane distillation technology for treatment of wastewater from rubber industry in Malaysia*. Procedia CIRP. 2015; 26: 792-796.

[141] Khayet, M., Velázquez, A., Mengual, J. *Direct contact membrane distillation of humic acid solutions*. Journal of Membrane Science. 2004; 240(1-2): 123-128.

[142] Liu, H., Wang, J. *Treatment of radioactive wastewater using direct contact membrane distillation*. Journal of Hazardous Materials. 2013; 261: 307-315.

[143] Wu, Y., Kang, Y., Zhang, L., Qu, D., Cheng, X., Feng, L. *Performance and fouling mechanism of direct contact membrane distillation (DCMD) treating fermentation wastewater with high organic concentrations*. Journal of Environmental Sciences. 2018; 65: 253-261.

[144] Hausmann, A., Sanciolo, P., Vasiljevic, T., Kulozik, U., Duke, M. *Performance assessment of membrane distillation for skim milk and whey processing*. Journal of Dairy Science. 2014; 97(1): 56-71.

[145] El-Abbassi, A., Hafidi, A., García-Payo, M.d.C., Khayet, M. *Concentration of olive mill wastewater by membrane distillation for polyphenols recovery*. Desalination. 2009; 245(1-3): 670-674.

[146] Madhumala, M., Madhavi, D., Sankarshana, T., Sridhar, S. *Recovery of hydrochloric acid and glycerol from aqueous solutions in chloralkali and chemical process industries by membrane distillation technique*. Journal of the Taiwan Institute of Chemical Engineers. 2014; 45(4): 1249-1259.

[147] Gupta, O., Roy, S., Mitra, S. *Enhanced membrane distillation of organic solvents from their aqueous mixtures using a carbon nanotube immobilized membrane*. Journal of Membrane Science. 2018; 568: 134-140.

[148] Banat, F., Al-Shannag, M. *Recovery of dilute acetone–butanol–ethanol (ABE) solvents from aqueous solutions via membrane distillation*. Bioprocess Engineering. 2000; 23(6): 643-649.

[149] Tomaszewska, M., Mientka, A. *Separation of HCl from HCl–H2SO4 solutions by membrane distillation*. Desalination. 2009; 240(1-3): 244-250.

[150] Wang, K.Y., Teoh, M.M., Nugroho, A., Chung, T.-S. *Integrated forward osmosis–membrane distillation (FO–MD) hybrid system for the concentration of protein solutions*. Chemical Engineering Science. 2011; 66(11): 2421-2430.

[151] Tun, C.M., Fane, A.G., Matheickal, J.T., Sheikholeslami, R. *Membrane distillation crystallization of concentrated salts—flux and crystal formation*. Journal of Membrane Science. 2005; 257(1-2): 144-155.

[152] Ma, H., Wang, H., Na, C. *Microwave-assisted optimization of platinum-nickel nanoalloys for catalytic water treatment*. Applied Catalysis B: Environmental. 2015; 163: 198-204.

[153] Remya, N., Lin, J.-G. *Current status of microwave application in wastewater treatment—a review*. Chemical Engineering Journal. 2011; 166(3): 797-813.

[154] Ji, Z., Wang, J., Hou, D., Yin, Z., Luan, Z. *Effect of microwave irradiation on vacuum membrane distillation*. Journal of Membrane Science. 2013; 429: 473-479.

[155] Roy, S., Humoud, M.S., Intrchom, W., Mitra, S. *Microwave-induced desalination via direct contact membrane distillation*. ACS Sustainable Chemistry & Engineering. 2018; 6(1): 626-632.

[156] Humoud, M.S., Intrchom, W., Roy, S., Mitra, S. *Reduction of scaling in microwave induced membrane distillation on a carbon nanotube immobilized membrane*. Environmental Science: Water Research & Technology. 2019; 5(5): 1012-1021.

[157] Hou, D., Zhang, L., Wang, Z., Fan, H., Wang, J., Huang, H. *Humic acid fouling mitigation by ultrasonic irradiation in membrane distillation process*. Separation and Purification Technology. 2015; 154: 328-337.

[158] Zhu, C., Liu, G., Cheung, C., Leung, C., Zhu, Z. *Ultrasonic stimulation on enhancement of air gap membrane distillation*. Journal of Membrane Science. 1999; 161(1-2): 85-93.

[159] Zhu, C., Liu, G. *Modeling of ultrasonic enhancement on membrane distillation*. Journal of Membrane Science. 2000; 176(1): 31-41.

[160] Hou, D., Wang, Z., Li, G., Fan, H., Wang, J., Huang, H. *Ultrasonic assisted direct contact membrane distillation hybrid process for membrane scaling mitigation*. Desalination. 2015; 375: 33-39.

[161] Hou, D., Zhang, L., Fan, H., Wang, J., Huang, H. *Ultrasonic irradiation control of silica fouling during membrane distillation process*. Desalination. 2016; 386: 48-57.

[162] Martınez-Dıez, L., Vázquez-González, M., Florido-Dıaz, F. *Study of membrane distillation using channel spacers*. Journal of Membrane Science. 1998; 144 (1-2): 45-56.

[163] Phattaranawik, J., Jiraratananon, R., Fane, A., Halim, C. *Mass flux enhancement using spacer filled channels in direct contact membrane distillation*. Journal of Membrane Science. 2001; 187(1-2): 193-201.

[164] Al-Sharif, S., Albeirutty, M., Cipollina, A., Micale, G. *Modelling flow and heat transfer in spacer-filled membrane distillation channels using open source CFD code*. Desalination. 2013; 311: 103-112.

[165] Chernyshov, M., Meindersma, G., De Haan, A. *Comparison of spacers for temperature polarization reduction in air gap membrane distillation*. Desalination. 2005; 183(1-3): 363-374.

[166] Shakaib, M., Hasani, S., Ahmed, I., Yunus, R.M. *A CFD study on the effect of spacer orientation on temperature polarization in membrane distillation modules*. Desalination. 2012; 284: 332-340.

[167] Teoh, M.M., Bonyadi, S., Chung, T.-S. *Investigation of different hollow fiber module designs for flux enhancement in the membrane distillation process*. Journal of Membrane Science. 2008; 311(1-2): 371-379.

[168] Chen, G., Yang, X., Wang, R., Fane, A.G. *Performance enhancement and scaling control with gas bubbling in direct contact membrane distillation*. Desalination. 2013; 308: 47-55.

[169] Ding, Z., Liu, L., Liu, Z., Ma, R. *The use of intermittent gas bubbling to control membrane fouling in concentrating TCM extract by membrane distillation*. Journal of Membrane Science. 2011; 372(1-2): 172-181.

[170] Chen, G., Yang, X., Lu, Y., Wang, R., Fane, A.G. *Heat transfer intensification and scaling mitigation in bubbling-enhanced membrane distillation for brine concentration*. Journal of Membrane Science. 2014; 470: 60-69.

[171] Wu, C., Li, Z., Zhang, J., Jia, Y., Gao, Q., Lu, X. *Study on the heat and mass transfer in air-bubbling enhanced vacuum membrane distillation*. Desalination. 2015; 373: 16-26.

[172] Warsinger, D.M., Servi, A., Van Belleghem, S., Gonzalez, J., Swaminathan, J., Kharraz, J., Chung, H.W., Arafat, H.A., Gleason, K.K. *Combining air recharging and membrane superhydrophobicity for fouling prevention in membrane distillation*. Journal of Membrane Science. 2016; 505: 241-252.

[173] Chunrui, W., Yue, J., Huayan, C., Xuan, W., Qijun, G., Xiaolong, L. *Study on air-bubbling strengthened membrane distillation process*. Desalination and Water Treatment. 2011; 34(1-3): 2-5.

[174] Pan, J., Xiao, C., Huang, Q., Liu, H., Hu, J. *ECTFE porous membranes with conveniently controlled microstructures for vacuum membrane distillation*. Journal of Materials Chemistry A. 2015; 3(46): 23549-23559.

[175] Gryta, M. *The study of performance of polyethylene chlorinetrifluoroethylene membranes used for brine desalination by membrane distillation*. Desalination. 2016; 398: 52-63.

[176] Feng, C., Shi, B., Li, G., Wu, Y. *Preparation and properties of microporous membrane from poly (vinylidene fluoride-co-tetrafluoroethylene)(F2. 4) for membrane distillation*. Journal of Membrane Science. 2004; 237(1-2): 15-24.

[177] Zheng, L., Wu, Z., Wei, Y., Zhang, Y., Yuan, Y., Wang, J. *Preparation of PVDF-CTFE hydrophobic membranes for MD application: Effect of LiCl-based mixed additives*. Journal of Membrane Science. 2016; 506: 71-85.

[178] Tijing, L.D., Woo, Y.C., Shim, W.-G., He, T., Choi, J.-S., Kim, S.-H., Shon, H.K. *Superhydrophobic nanofiber membrane containing carbon nanotubes for high-performance direct contact membrane distillation*. Journal of Membrane Science. 2016; 502: 158-170.

[179] Dumée, L.F., Sears, K., Schütz, J., Finn, N., Huynh, C., Hawkins, S., Duke, M., Gray, S. *Characterization and evaluation of carbon nanotube Bucky-Paper membranes for direct contact membrane distillation*. Journal of Membrane Science. 2010; 351(1-2): 36-43.

[180] Jung, J., Shin, Y., Choi, Y.-J., Sohn, J., Lee, S., An, K. *Hydrophobic surface modification of membrane distillation (MD) membranes using water-repelling polymer based on urethane rubber*. Desalination and Water Treatment. 2016; 57(22): 10031-10041.

[181] Yang, X., Wang, R., Shi, L., Fane, A.G., Debowski, M. *Performance improvement of PVDF hollow fiber-based membrane distillation process*. Journal of Membrane Science. 2011; 369(1-2): 437-447.

[182] Razmjou, A., Arifin, E., Dong, G., Mansouri, J., Chen, V. *Superhydrophobic modification of TiO2 nanocomposite PVDF membranes for applications in membrane distillation*. Journal of Membrane Science. 2012; 415: 850-863.

[183] Wu, Y., Kong, Y., Lin, X., Liu, W., Xu, J. *Surface-modified hydrophilic membranes in membrane distillation*. Journal of Membrane Science. 1992; 72(2): 189-196.

[184] Wei, X., Zhao, B., Li, X.-M., Wang, Z., He, B.-Q., He, T., Jiang, B. *CF4 plasma surface modification of asymmetric hydrophilic polyethersulfone membranes for direct contact membrane distillation*. Journal of Membrane Science. 2012; 407: 164-175.

[185] Tian, M., Yin, Y., Yang, C., Zhao, B., Song, J., Liu, J., Li, X.-M., He, T. *CF4 plasma modified highly interconnective porous polysulfone membranes for direct contact membrane distillation (DCMD)*. Desalination. 2015; 369: 105-114.

[186] Essalhi, M., Khayet, M. *Surface segregation of fluorinated modifying macromolecule for hydrophobic/hydrophilic membrane preparation and application in air gap and direct contact membrane distillation*. Journal of Membrane Science. 2012; 417: 163-173.

[187] Qtaishat, M., Khayet, M., Matsuura, T. *Novel porous composite hydrophobic/hydrophilic polysulfone membranes for desalination by direct contact membrane distillation*. Journal of Membrane science. 2009; 341(1-2): 139-148.

[188] Zhang, X., Gao, B., Creamer, A.E., Cao, C., Li, Y. *Adsorption of VOCs onto engineered carbon materials: A review*. Journal of Hazardous Materials. 2017; 338: 102-123.

[189] Roy, S., Bhadra, M., Mitra, S. *Enhanced desalination via functionalized carbon nanotube immobilized membrane in direct contact membrane distillation*. Separation and Purification Technology. 2014; 136: 58-65.

[190] Bhadra, M., Roy, S., Mitra, S. *A bilayered structure comprised of functionalized carbon nanotubes for desalination by membrane distillation*. ACS Applied Materials and Interfaces. 2016; 8(30): 19507-19513.

[191] Bhadra, M., Roy, S., Mitra, S. *Desalination across a graphene oxide membrane via direct contact membrane distillation*. Desalination. 2016; 378: 37-43.

[192] Gethard, K., Sae-Khow, O., Mitra, S. *Carbon nanotube enhanced membrane distillation for simultaneous generation of pure water and concentrating pharmaceutical waste*. Separation and Purification Technology. 2012; 90: 239-245.

[193] Curry, E. *Water scarcity and the recognition of the human right to safe freshwater*. Northwestern Journal of International Rights. 2010; 9: 103.

[194] Thorne, V.T., Thomas, W.L. *Issues of Water Scarcity and Rights for Multinational Companies*. Natural Resources & Environment. 2003; 18: 31.

[195] Nicolaï, A., Sumpter, B.G., Meunier, V. *Tunable water desalination across graphene oxide framework membranes*. Physical Chemistry Chemical Physics. 2014; 16(18): 8646-8654.

[196] Wade, N.M. *Distillation plant development and cost update*. Desalination. 2001; 136(1-3): 3-12.

[197] Shirazi, A., Mahdi, M., Kargari, A. *A review on applications of membrane distillation (MD) process for wastewater treatment*. Journal of Membrane Science and Research. 2015; 1(3): 101-112.

[198] Bhadra, M., Roy, S., Mitra, S. *Flux enhancement in direct contact membrane distillation by implementing carbon nanotube immobilized PTFE membrane*. Separation and Purification Technology. 2016; 161: 136-143.

[199] Zhang, Y., Sivakumar, M., Yang, S., Enever, K., Ramezanianpour, M. *Application of solar energy in water treatment processes: A review*. Desalination. 2018; 428: 116-145.

[200] Kabeel, A., Abdelgaied, M., El-Said, E.M. *Study of a solar-driven membrane distillation system: Evaporative cooling effect on performance enhancement*. Renewable Energy. 2017; 106: 192-200.

[201] Shim, W.G., He, K., Gray, S., Moon, I.S. *Solar energy assisted direct contact membrane distillation (DCMD) process for seawater desalination*. Separationand Purification Technology. 2015; 143: 94-104.

[202] Ragunath, S., Roy, S., Mitra, S. *Selective hydrophilization of the permeate surface to enhance flux in membrane distillation*. Separation and Purification Technology. 2016; 170: 427-433.

[203] Bhadra, M., Roy, S., Mitra, S. *Enhanced desalination using carboxylated carbon nanotube immobilized membranes*. Separation and Purification Technology. 2013; 120: 373-377.

[204] Roy, S., Ragunath, S., Mitra, S. *Effect of module configuration on the overall mass recovery in membrane distillation*. Desalination and Water Treatment. 2017; 95: 74-79.

[205] Daer, S., Kharraz, J., Giwa, A., Hasan, S.W. *Recent applications of nanomaterials in water desalination: a critical review and future opportunities*. Desalination. 2015; 367: 37-48.

[206] Agbaje, T.A., Al-Gharabli, S., Mavukkandy, M.O., Kujawa, J., Arafat, H.A. *PVDF/magnetite blend membranes for enhanced flux and salt rejection in membrane distillation*. Desalination. 2018; 436: 69-80.

[207] Zheng, R., Chen, Y., Wang, J., Song, J., Li, X.-M., He, T. *Preparation of omniphobic PVDF membrane with hierarchical structure for treating saline oily wastewater using direct contact membrane distillation*. Journal of Membrane Science. 2018; 555: 197-205.

[208] Li, K., Hou, D., Fu, C., Wang, K., Wang, J. *Fabrication of PVDF nanofibrous hydrophobic composite membranes reinforced with fabric substrates via electrospinning for membrane distillation desalination*. Journal of Environmental Sciences. 2019; 75: 277-288.

[209] Zhao, J., Shi, L., Loh, C.H., Wang, R. *Preparation of PVDF/PTFE hollow fiber membranes for direct contact membrane distillation via thermally induced phase separation method*. Desalination. 2018; 430: 86-97.

[210] Chen, Y., Zheng, R., Wang, J., Liu, Y., Wang, Y., Li, X.-M., He, T. *Laminated PTFE membranes to enhance the performance in direct contact membrane distillation for high salinity solution*. Desalination. 2017; 424: 140-148.

[211] Woo, Y.C., Tijing, L.D., Park, M.J., Yao, M., Choi, J.-S., Lee, S., Kim, S.-H., An, K.-J., Shon, H.K. *Electrospun dual-layer nonwoven membrane for desalination by air gap membrane distillation*. Desalination. 2017; 403: 187-198.

[212] Munirasu, S., Banat, F., Durrani, A.A., Haija, M.A. *Intrinsically superhydrophobic PVDF membrane by phase inversion for membrane distillation*. Desalination. 2017; 417: 77-86.

[213] Eykens, L., De Sitter, K., Dotremont, C., Pinoy, L., Van der Bruggen, B. *Coating techniques for membrane distillation: An experimental assessment*. Separation and Purification Technology. 2018; 193: 38-48.

[214] Leaper, S., Abdel-Karim, A., Faki, B., Luque-Alled, J.M., Alberto, M., Vijayaraghavan, A., Holmes, S.M., Szekely, G., Badawy, M.I., Shokri, N. *Flux-enhanced PVDF mixed matrix membranes incorporating APTS-functionalized graphene oxide for membrane distillation*. Journal of Membrane Science. 2018; 554: 309-323.

[215] Li, Y., Dong, S., Zhu, L. *Preparation of novel poly (vinylidene fluoride)/TiO 2 photocatalysis membranes for use in direct contact membrane distillation*. Journal of Nanoparticle Research. 2018; 20(3): 63.

[216] Okiel, K., El-Aassar, A.H.M., Temraz, T., El-Etriby, S., Shawky, H.A. *Performance assessment of synthesized CNT/polypropylene composite membrane distillation for oil field produced water desalination*. Desalination and Water Treatment. 2016; 57(24): 10995-11007.

[217] Ragunath, S., Roy, S., Mitra, S. *Carbon nanotube immobilized membrane with controlled nanotube incorporation via phase inversion polymerization for membrane distillation based desalination*. Separation and Purification Technology. 2018; 194: 249-255.

[218] Roy, S., Singha, N.R. *Polymeric nanocomposite membranes for next generation pervaporation process: Strategies, challenges and future prospects*. Membranes. 2017; 7(3): 53.

[219] Roy, S., Hussain, C.M., Mitra, S. *Carbon nanotube-immobilized super-absorbent membrane for harvesting water from the atmosphere*. Environmental Science: Water Research & Technology. 2015; 1(6): 753-760.

[220] Roy, S., Ntim, S.A., Mitra, S., Sirkar, K.K. *Facile fabrication of superior nanofiltration membranes from interfacially polymerized CNT-polymer composites*. Journal of Membrane Science. 2011; 375(1-2): 81-87.

[221] Zhang, H., Li, B., Sun, D., Miao, X., Gu, Y. *SiO2-PDMS-PVDF hollow fiber membrane with high flux for vacuum membrane distillation*. Desalination. 2018; 429: 33-43.

[222] Bhadra, M., Roy, S., Mitra, S. *Nanodiamond immobilized membranes for enhanced desalination via membrane distillation*. Desalination. 2014; 341: 115-119.

[223] Ma, J., Ping, D., Dong, X. *Recent developments of graphene oxide-based membranes: a review*. Membranes. 2017; 7(3): 52.

[224] Thebo, K.H., Qian, X., Zhang, Q., Chen, L., Cheng, H.-M., Ren, W. *Highly stable graphene-oxide-based membranes with superior permeability*. Nature Communications. 2018; 9(1): 1-8.

[225] Yoon, H.W., Cho, Y.H., Park, H.B. *Graphene-based membranes: status and prospects*. Philosophical Transactions of the Royal Society A: Mathematical, Physical and Engineering Sciences. 2016; 374(2060): 20150024.

[226] Xu, Z., Zhang, J., Shan, M., Li, Y., Li, B., Niu, J., Zhou, B., Qian, X. *Organosilane-functionalized graphene oxide for enhanced antifouling and mechanical properties of polyvinylidene fluoride ultrafiltration membranes*. Journal of Membrane Science. 2014; 458: 1-13.

[227] Hegab, H.M., Zou, L. *Graphene oxide-assisted membranes: fabrication and potential applications in desalination and water purification*. Journal of Membrane Science. 2015; 484: 95-106.

[228] Zahirifar, J., Karimi-Sabet, J., Moosavian, S.M.A., Hadi, A., Khadiv-Parsi, P. *Fabrication of a novel octadecylamine functionalized graphene oxide/PVDF dual-layer flat sheet membrane for desalination via air gap membrane distillation*. Desalination. 2018; 428: 227-239.

[229] Ahmad, S.R., Young, R.J., Kinloch, I.A. *Raman spectra and mechanical properties of graphene/polypropylene nanocomposites*. International Journal of Chemical Engineering and Applications. 2015; 6(1): 1.

[230] Saito, R., Hofmann, M., Dresselhaus, G., Jorio, A., Dresselhaus, M. *Raman spectroscopy of graphene and carbon nanotubes*. Advances in Physics. 2011; 60(3): 413-550.

[231] Nguyen, B.D., Ngo, T.K., Bui, T.H., Pham, D.K., Dinh, X.L., Nguyen, P.T. *The impact of graphene oxide particles on viscosity stabilization for diluted polymer solutions using in enhanced oil recovery at HTHP offshore reservoirs*. Advances in Natural Sciences: Nanoscience and Nanotechnology. 2014; 6(1): 015012.

[232] Mengual, J., Khayet, M., Godino, M. *Heat and mass transfer in vacuum membrane distillation*. International Journal of Heat and Mass Transfer. 2004; 47(4): 865-875.

[233] Gryta, M. *Concentration of NaCl solution by membrane distillation integrated with crystallization*. Separation Science and Technology. 2002; 37(15): 3535-3558.

[234] Wirth, D., Cabassud, C. *Water desalination using membrane distillation: comparison between inside/out and outside/in permeation*. Desalination. 2002; 147(1): 139-145.

[235] Cath, T.Y., Adams, V.D., Childress, A.E. *Experimental study of desalination using direct contact membrane distillation: a new approach to flux enhancement*. Journal of Membrane Science. 2004; 228(1): 5-16.

[236] Krishnamoorthy, K., Veerapandian, M., Yun, K., Kim, S.J. *The chemical and structural analysis of graphene oxide with different degrees of oxidation*. Carbon. 2013; 53: 38-49.

[237] Xie, T., Liu, C., Zhang, X. *Molecular dynamics simulation in the application of direct air dehumidification by electrodialysis method*. Procedia Engineering. 2017; 205: 116-122.

[238] Fletcher, A.J., Uygur, Y., Thomas, K.M. *Role of surface functional groups in the adsorption kinetics of water vapor on microporous activated carbons*. The Journal of Physical Chemistry C. 2007; 111(23): 8349-8359.

[239] Dumée, L.F., Gray, S., Duke, M., Sears, K., Schütz, J., Finn, N. *The role of membrane surface energy on direct contact membrane distillation performance*. Desalination. 2013; 323: 22-30.

[240] Khayet, M., Mengual, J., Matsuura, T. *Porous hydrophobic/hydrophilic composite membranes: application in desalination using direct contact membrane distillation*. Journal of Membrane Science. 2005; 252(1-2): 101-113.

[241] Shahroie, B., Rajabi, L., Derakhshan, A.A. *Short review on membrane distillation techniques for removal of dissolved ammonia*. Journal of Applied Research in Water and Wastewater. 2016; 3(2): 277-280.

[242] Kän-man, E., Jönsson, H. *Including oxidisation of ammonia in the eutrophication impact category*. The International Journal of Life Cycle Assessment. 2001; 6(1): 29.

[243] Halim, A.A., Aziz, H.A., Johari, M.A.M., Ariffin, K.S. *Comparison study of ammonia and COD adsorption on zeolite, activated carbon and composite materials in landfill leachate treatment*. Desalination. 2010; 262(1-3): 31-35.

[244] Başakçilardan-Kabakci, S., İpekoğlu, A.N., Talinli, I. *Recovery of ammonia from human urine by stripping and absorption*. Environmental Engineering Science. 2007; 24(5): 615-624.

[245] Du, Q., Liu, S., Cao, Z., Wang, Y. *Ammonia removal from aqueous solution using natural Chinese clinoptilolite*. Separation and Purification Technology. 2005; 44(3): 229-234.

[246] Jorgensen, T., Weatherley, L. *Ammonia removal from wastewater by ion exchange in the presence of organic contaminants*. Water Research. 2003; 37(8): 1723-1728.

[247] Ilies, P., Mavinic, D. *The effect of decreased ambient temperature on the biological nitrification and denitrification of a high ammonia landfill leachate*. Water Research. 2001; 35(8): 2065-2072.

[248] Campos, J.L., Mosquera-Corral, A., Sanchez, M., Méndez, R., Lema, J.M. *Nitrification in saline wastewater with high ammonia concentration in an activated sludge unit*. Water Research. 2002; 36(10): 2555-2560.

[249] Yin, S., Chen, K., Srinivasakannan, C., Guo, S., Li, S., Peng, J., Zhang, L. *Enhancing recovery of ammonia from rare earth wastewater by air stripping combination of microwave heating and high gravity technology*. Chemical Engineering Journal. 2018; 337: 515-521.

[250] Qu, D., Sun, D., Wang, H., Yun, Y. *Experimental study of ammonia removal from water by modified direct contact membrane distillation*. Desalination. 2013; 326: 135-140.

[251] Duong, T., Xie, Z., Ng, D., Hoang, M. *Ammonia removal from aqueous solution by membrane distillation*. Water and Environment Journal. 2013; 27(3): 425-434.

[252] Roy, S., Humoud, M.S., Intrchom, W., Mitra, S. *Microwave-induced desalination via direct contact membrane distillation*. ACS Sustainable Chemistry & Engineering. 2017; 6(1): 626-632.

[253] Roy, S., Ragunath, S. *Emerging membrane technologies for water and energy sustainability: Future prospects, constraints and challenges*. Energies. 2018; 11(11): 2997.

[254] Intrchom, W., Roy, S., Humoud, M., Mitra, S. *Immobilization of Graphene Oxide on the Permeate Side of a Membrane Distillation Membrane to Enhance Flux*. Membranes. 2018; 8(3): 63.

[255] Gethard, K., Sae-Khow, O., Mitra, S. *Water desalination using carbon-nanotube-enhanced membrane distillation*. ACS Applied Materials & Interfaces. 2011; 3(2): 110-114.

[256] Intrchom, W., Mitra, S. *Analytical sample preparation, preconcentration and chromatographic separation on carbon nanotubes*. Current Opinion in Chemical Engineering. 2017; 16: 102-114.

[257] Hylton, K., Chen, Y., Mitra, S. *Carbon nanotube mediated microscale membrane extraction*. Journal of Chromatography A. 2008; 1211(1-2): 43-48.

[258] Sae-Khow, O., Mitra, S. *Carbon nanotube immobilized composite hollow fiber membranes for pervaporative removal of volatile organics from water*. The Journal of Physical Chemistry C. 2010; 114(39): 16351-16356.

[259] Sae-Khow, O., Mitra, S. *Simultaneous extraction and concentration in carbon nanotube immobilized hollow fiber membranes*. Analytical Chemistry. 2010; 82(13): 5561-5567.

[260] Gethard, K., Sae-Khow, O., Mitra, S. *Water desalination using carbon-nanotube-enhanced membrane distillation*. ACS applied materials & interfaces. 2010; 3(2): 110-114.

[261] Bhadra, M., Roy, S., Mitra, S. *A bilayered structure comprised of functionalized carbon nanotubes for desalination by membrane distillation*. ACS Applied Materials & Interfaces. 2016; 8(30): 19507-19513.

[262] Humoud, M.S., Intrchom, W., Roy, S., Mitra, S. *Reduction of Scaling in Microwave Induced Membrane Distillation on Carbon Nanotube Immobilized Membrane*. Environmental Science: Water Research & Technology. 2019.

[263] Chen, Y., Mitra, S. *Fast microwave-assisted purification, functionalization and dispersion of multi-walled carbon nanotubes*. Journal of Nanoscience and Nanotechnology. 2008; 8(11): 5770-5775.

[264] Li, L., Sirkar, K.K. *Studies in vacuum membrane distillation with flat membranes*. Journal of Membrane Science. 2017; 523: 225-234.

[265] Wang, D., Li, K., Teo, W. *Preparation and characterization of polyvinylidene fluoride (PVDF) hollow fiber membranes*. Journal of Membrane Science. 1999; 163(2): 211-220.

[266] Wepasnick, K.A., Smith, B.A., Bitter, J.L., Fairbrother, D.H. *Chemical and structural characterization of carbon nanotube surfaces*. Analytical and Bioanalytical Chemistry. 2010; 396(3): 1003-1014.

[267] Abuilaiwi, F.A., Laoui, T., Al-Harthi, M., Atieh, M.A. *Modification and functionalization of multiwalled carbon nanotube (MWCNT) via fischer esterification*. The Arabian Journal for Science and Engineering. 2010; 35(1): 37-48.

[268] Wu, Z., Mitra, S. *Microwave induced reactive base wash for the removal of oxidation debris from carboxylated carbon nanotubes*. Carbon. 2015; 88: 233-238.

[269] Paul, S., Chandra, A. *Liquid-vapor interfacial properties of water-ammonia mixtures: Dependence on ammonia concentration*. The Journal of Chemical Physics. 2005; 123(17): 174712.

[270] Golebiewski, J., Galeski, A. *Thermal stability of nanoclay polypropylene composites by simultaneous DSC and TGA*. Composites Science and Technology. 2007; 67(15-16): 3442-3447.

[271] Zhao, Y., Yu, H., Xing, D., Lu, W., Shao, Z., Yi, B. *Preparation and characterization of PTFE based composite anion exchange membranes for alkaline fuel cells*. Journal of Membrane Science. 2012; 421: 311-317.

[272] Kombarakkaran, J., Clewett, C., Pietraß, T. *Ammonia adsorption on multi-walled carbon nanotubes*. Chemical Physics Letters. 2007; 441(4-6): 282-285.

[273] Feng, X., Irle, S., Witek, H., Morokuma, K., Vidic, R., Borguet, E. *Sensitivity of ammonia interaction with single-walled carbon nanotube bundles to the presence of defect sites and functionalities*. Journal of the American Chemical Society. 2005; 127(30): 10533-10538.

[274] Ham, C.W., Brown, H.A., Tykociner, J.T., Wilson, T.A., Keener, C.A., Huckert, J.W., *The total and partial vapor pressures of aqueous ammonia solutions*:University of Illinois, 1925.

[275] Hussain, C.M., Saridara, C., Mitra, S. *Modifying the sorption properties of multi-walled carbon nanotubesvia covalent functionalization*. Analyst. 2009; 134(9): 1928-1933.

[276] Ren, X., Chen, C., Nagatsu, M., Wang, X. *Carbon nanotubes as adsorbents in environmental pollution management: a review*. Chemical Engineering Journal. 2011; 170(2-3): 395-410.

[277] Saridara, C., Ragunath, S., Pu, Y., Mitra, S. *Methane preconcentration in a microtrap using multiwalled carbon nanotubes as sorbents*. Analytica Chimica Acta. 2010; 677(1): 50-54.

[278] Kauffman, D.R., Star, A. *Carbon nanotube gas and vapor sensors*. Angewandte Chemie International Edition. 2008; 47(35): 6550-6570.

[279] Ragunath, S., Mitra, S. *Carbon nanotube immobilized composite hollow fiber membranes for extraction of volatile organics from air*. The Journal of Physical Chemistry C. 2015; 119(23): 13231-13237.

[280] Danmaliki, G.I., Shamsuddeen, A.A., Usman, B.J. *The effect of temperature, turbulence, and Ph on the solubility of MTBE*. European Journal of Earth and Environment Vol. 2016; 3(2).

[281] Rosell, M., Lacorte, S., Barceló, D. *Analysis, occurrence and fate of MTBE in the aquatic environment over the past decade*. TrAC Trends in Analytical Chemistry. 2006; 25(10): 1016-1029.

[282] Dale, M.S., Koch, B., Losee, R.F., Crofts, E.W., Davis, M.K. *MTBE in Southern California water*. Journal-American Water Works Association. 2000; 92(8): 42-51.

[283] Gullick, R.W., LeChevallier, M.W. *Occurrence of MTBE in drinking water sources*. Journal-American Water Works Association. 2000; 92(1): 100-113.

[284] Toran, L., Lipka, C., Baehr, A., Reilly, T., Baker, R. *Seasonal and daily variations in concentrations of methyl-tertiary-butyl ether (MTBE) at Cranberry Lake, New Jersey*. Water Research. 2003; 37(15): 3756-3766.

[285] Facetti, J.F., Nunez, R., Gomez, L., Ojeda, J., Bernal, C., Leon-Ovelar, R., Carvallo, F. *Methyl tert-butyl ether (MtBE) in deep wells of the Patiño Aquifer, Paraguay: A preliminary characterization*. The Science of the Total Environment. 2019; 647: 1640.

[286] Schmidt, T.C., Haderlein, S.B., Pfister, R., Forster, R. *Occurrence and fate modeling of MTBE and BTEX compounds in a Swiss Lake used as drinking water supply*. Water Research. 2004; 38(6): 1520-1529.

[287] Morgenroth, E., Arvin, E., *The European Perspective of MTBE as an Oxygenate in Fuels*, Managing for Healthy Ecosystems: ROUTLEDGE in association with GSE Research, 2003: 1447-1458.

[288] Qin, J., Zhang, Z., Li, Q., Huang, J., Peng, X., Qing, L., Liang, G., Liang, L., Huang, Y., Yang, X. *Concentrations and potential health risks of methyl tertiary-butyl ether (MTBE) in air and drinking water from Nanning, South China*. Science of the Total Environment. 2016; 541: 1348-1354.

[289] Levchuk, I., Bhatnagar, A., Sillanpää, M. *Overview of technologies for removal of methyl tert-butyl ether (MTBE) from water*. Science of the Total Environment. 2014; 476: 415-433.

[290] Kujawa, J., Cerneaux, S., Kujawski, W. *Removal of hazardous volatile organic compounds from water by vacuum pervaporation with hydrophobic ceramic membranes*. Journal of Membrane Science. 2015; 474: 11-19.

[291] Gao, R., Zhang, Q., Lv, R., Soyekwo, F., Zhu, A., Liu, Q. *Highly efficient polymer–MOF nanocomposite membrane for pervaporation separation of water/methanol/MTBE ternary mixture*. Chemical Engineering Research and Design. 2017; 117: 688-697.

[292] Keller, A.A., Sandall, O.C., Rinker, R.G., Mitani, M.M., Bierwagen, B., Snodgrass, M.J. *Cost and performance evaluation of treatment technologies for MTBE-contaminated water*. UC TSR&TP Report to the Governor of California. 1998.

[293] Hung, H.-W., Lin, T.-F. *Adsorption of MTBE from contaminated water by carbonaceous resins and mordenite zeolite*. Journal of Hazardous Materials. 2006; 135(1-3): 210-217.

[294] Sutherland, J., Adams, C., Kekobad, J. *Treatment of MTBE by air stripping, carbon adsorption, and advanced oxidation: technical and economic comparison for five groundwaters*. Water Research. 2004; 38(1): 193-205.

[295] Vane, L.M., Alvarez, F.R., Mullins, B. *Removal of methyl tert-butyl ether from water by pervaporation: bench-and pilot-scale evaluations*. Environmental Science & Technology. 2001; 35(2): 391-397.

[296] Yoshida, W., Cohen, Y. *Removal of methyl tert-butyl ether from water by pervaporation using ceramic-supported polymer membranes*. Journal of Membrane Science. 2004; 229(1-2): 27-32.

[297] Karp, J.R., Hamerski, F., Silva, V.R. *Supported silk fibroin/poly (vinyl alcohol) membrane blends: Structure, properties, and ethanol dehydration by pervaporation*. Polymer Engineering & Science. 2018; 58(10): 1879-1887.

[298] Intrchom, W., Roy, S., Mitra, S. *Functionalized carbon nanotube immobilized membrane for low temperature ammonia removal via membrane distillation*. Separation and Purification Technology. 2020; 235: 116188.

[299] Darling, S.B. *Perspective: Interfacial materials at the interface of energy and water*. Journal of Applied Physics. 2018; 124(3): 030901.

[300] Intrchom, W., Roy, S., Humoud, M.S., Mitra, S. *Immobilization of graphene oxide on the permeate side of a membrane distillation membrane to enhance flux*. Membranes. 2018; 8(3): 63.

[301] Sarti, G., Gostoli, C., Bandini, S. *Extraction of organic components from aqueous streams by vacuum membrane distillation*. Journal of Membrane Science. 1993; 80(1): 21-33.

[302] Owens, D.K., Wendt, R. *Estimation of the surface free energy of polymers*. Journal of Applied Polymer Science. 1969; 13(8): 1741-1747.

[303] Vicente, C., André, P., Ferreira, R. *Simple measurement of surface free energy using a web cam*. Revista Brasileira de Ensino de Física. 2012; 34(3): 1-5.

[304] Firsov, S., Zhbankov, G., Bakhramov, M., Abdukadyrov, A., Gafurov, A. *Raman spectra and structure of polytetrafluoroethylene subjected to elastic deformation grinding*. Journal of Applied Spectroscopy. 1993; 59: 644-647.

[305] Dresselhaus, M., Jorio, A., Saito, R. *Characterizing graphene, graphite, and carbon nanotubes by Raman spectroscopy*. Annual Review of Condensed Matter Physics. 2010; 1(1): 89-108.

[306] Su, S., Xu, Y., Wilkie, C., *Thermal degradation of polymer–carbon nanotube composites*, Polymer–Carbon Nanotube Composites: Elsevier, 2011: 482-510.

[307] Kavinkumar, T., Manivannan, S. *Synthesis, characterization and gas sensing properties of graphene oxide-multiwalled carbon nanotube composite*. Journal of Materials Science & Technology. 2016; 32(7): 626-632.

[308] Saffarini, R.B., Mansoor, B., Thomas, R., Arafat, H.A. *Effect of temperature-dependent microstructure evolution on pore wetting in PTFE membranes under membrane distillation conditions*. Journal of Membrane Science. 2013; 429: 282-294.

[309] Street, A., Sustich, R., Duncan, J., Savage, N., *Nanotechnology applications for clean water: solutions for improving water quality*:William Andrew, 2014.

[310] Lee, C.H., Hong, W.H. *Effect of operating variables on the flux and selectivity in sweep gas membrane distillation for dilute aqueous isopropanol*. Journal of Membrane Science. 2001; 188(1): 79-86.

[311] Charfi, K., Khayet, M., Safi, M.J. *Numerical simulation and experimental studies on heat and mass transfer using sweeping gas membrane distillation*. Desalination. 2010; 259(1-3): 84-96.

[312] Feng, X., Huang, R.Y. *Estimation of activation energy for permeation in pervaporation processes*. Journal of Membrane Science. 1996; 118(1): 127-131.

[313] Kujawa, J., Cerneaux, S., Koter, S., Kujawski, W. *Highly efficient hydrophobic titania ceramic membranes for water desalination*. ACS Applied Materials & Interfaces. 2014; 6(16): 14223-14230.

[314] Feng, C., Khulbe, K., Tabe, S. *Volatile organic compound removal by membrane gas stripping using electro-spun nanofiber membrane*. Desalination. 2012; 287: 98-102.

[315] Wang, Y., Qiu, B., Fan, S., Liu, J., Qin, Y., Jian, S., Wang, Y., Xiao, Z. *Membrane distillation of butanol from aqueous solution with polytetrafluoroethylene membrane*. Chemical Engineering & Technology.

[316] Ray, S., Singha, N., Ray, S. *Removal of tetrahydrofuran (THF) from water by pervaporation using homo and blend polymeric membranes*. Chemical Engineering Journal. 2009; 149(1-3): 153-161.

[317] Ray, S., Ray, S. *Synthesis of highly methanol selective membranes for separation of methyl tertiary butyl ether (MTBE)–methanol mixtures by pervaporation*. Journal of Membrane Science. 2006; 278(1-2): 279-289.

[318] Sweetman, M.J., May, S., Mebberson, N., Pendleton, P., Vasilev, K., Plush, S.E., Hayball, J.D. *Activated carbon, carbon nanotubes and graphene: materials and composites for advanced water purification*. C—Journal of Carbon Research. 2017; 3(2): 18.

[319] You, Y., Sahajwalla, V., Yoshimura, M., Joshi, R.K. *Graphene and graphene oxide for desalination*. Nanoscale. 2016; 8(1): 117-119.

[320] APHA, *Standard Methods for the Examination of Water and Wastewater, 14th Edition, Method 418A and 418B*, 1975,410.

[321] ASTM, *Annual Book of ASTM Standards, Part 31, "Water", Standard D1426-74, Method A*, 1976,237.